UNIVERSITY OF CALIFORNIA, SAN DIEGO

Adaptive OFDM-based UWB

A dissertation submitted in partial satisfaction
of the requirements for the degree
Doctor of Philosophy

in

Electrical Engineering
(Communication Theory and Systems)

by

Juan I. Montojo-Bennassar

Committee in charge:

Laurence B. Milstein, Chair
William S. Hodgkiss
Bhaskar D. Rao
Lance W. Small
James R. Zeidler

2009

The dissertation of Juan I. Montojo-Bennassar is approved, and it is acceptable in quality and form for publication on microfilm and electronically:

_____

_____

_____

_____

_____

Chair

University of California, San Diego

2009

To my mother

TABLE OF CONTENTS

Signature Page . . . iii
Dedication . . . iv
Table of Contents . . . vii
List of Figures . . . ix
List of Tables . . . x
Acknowledgments . . . xii
Vita . . . xiii
Abstract of the Dissertation . . . xv

Chapter 1 Introduction . . . 1
1.1 OFDM Systems with Imperfections . . . 2
1.2 Channel Estimation in OFDM Systems . . . 3
1.3 Cognitive OFDM . . . 4
1.4 Outline of the Dissertation . . . 4

Chapter 2 Effects of Imperfections on the Performance of OFDM Systems . . . 6
2.1 Introduction . . . 6
2.2 OFDM System Model . . . 9
2.2.1 OFDM Transmitter and Channel . . . 9
2.2.2 OFDM Receiver . . . 10
2.3 Data Detection . . . 21
2.3.1 Data Detection with Single-Tap Equalizer (ST) . . . 23
2.3.2 Data Detection with Zero-Forcing Equalizer (ZF) . . . 24
2.3.3 Data Detection with MMSE Equalizer . . . 25
2.4 Performance Characterization . . . 26
2.5 Concluding Remarks . . . 34
2.6 Acknowledgements . . . 35

Chapter 3 Channel Estimation for Non-Ideal OFDM Systems . . . 36
3.1 Introduction . . . 36
3.2 System Model . . . 37
3.3 Channel Estimation . . . 41
3.3.1 Frequency Domain Least Squares Channel Estimation . . . 45

3.3.2 Linear Channel Estimator - General Case . . . 47
3.3.3 DFT-based Channel Estimation . . . 48
3.4 Data Detection . . . 50
3.5 Performance Characterization . . . 53
3.6 Concluding Remarks . . . 58
3.7 Acknowledgements . . . 59

Chapter 4 Cognitive Aspects of OFDM-based UWB and How to Enable Them 60
4.1 Introduction . . . 60
4.2 OFDM System Parameters . . . 61
4.3 Cognitive OFDM . . . 63
4.3.1 Symbol duration . . . 64
4.3.2 CP duration . . . 64
4.3.3 Pilot structure . . . 65
4.4 System Description . . . 65
4.4.1 CP discarding and modeling of residual frequency error . . . 67
4.4.2 DFT output . . . 69
4.4.3 Channel estimation . . . 73
4.4.4 Data detection . . . 76
4.5 Optimization Process . . . 76
4.5.1 SINR derivation . . . 77
4.5.2 Capacity Estimation . . . 78
4.6 Analyses and Simulations . . . 79
4.6.1 DFT window . . . 80
4.6.2 Pilot structure . . . 83
4.6.3 CP duration . . . 86
4.6.4 OFDM symbol duration . . . 91
4.7 Conclusions . . . 96
4.8 Acknowledgements . . . 97

Chapter 5 Conclusions . . . 98

Appendix A Cross-covariance between channel estimates and DFT outputs . 101
A.1 Case $n_2 = n_1 = n$ . . . 103
A.2 Case $n_1 = n$ and $n_2 = (n-1)$ . . . 104

Appendix B Partial CP discarding **106**
B.1 Effect of partial CP discarding 106
B.2 Channel estimation with partial partial CP discarding 110

References **114**

LIST OF FIGURES

Figure 2.1 Block diagram of OFDM receiver 10
Figure 2.2 BER performance using test statistic, simulation and Gaussian approximation of ICI and ISI 28
Figure 2.3 BER sensitivity to CP duration for CM1 29
Figure 2.4 BER sensitivity to CP duration for CM2 29
Figure 2.5 BER sensitivity to CP duration for CM3 30
Figure 2.6 BER sensitivity to CP duration for CM4 30
Figure 2.7 BER sensitivity to residual frequency error (analysis and simulation) 32
Figure 2.8 BER sensitivity to timing error (analysis and simulation) 32
Figure 2.9 ISI impact of transmit/receive timing error 33
Figure 2.10 Receiver type sensitivity (analysis and simulation) 33

Figure 3.1 Block diagram of OFDM receiver 39
Figure 3.2 TDM vs. FDM pilot 41
Figure 3.3 BER performance vs. pilot density for CM1, FD-LS 54
Figure 3.4 BER performance vs. pilot density for CM1, DFT-based 55
Figure 3.5 BER performance vs. pilot density for CM4, FD-LS 56
Figure 3.6 BER performance vs. pilot density for CM4, DFT-based 57
Figure 3.7 BER sensitivity to residual frequency error with DFT-based channel estimator 57
Figure 3.8 BER sensitivity to transmit/receive timing errors with FD-LS channel estimator 58

Figure 4.1 Block diagram of OFDM system model 65
Figure 4.2 Illustration of construction of channel matrices 67
Figure 4.3 Illustration of pilot and data transmission (FDM) 71
Figure 4.4 DFT window placement example 81
Figure 4.5 $\hat{d}$ optimization for CM4 channel realization with a channel span of 91 samples and CP=32 82
Figure 4.6 $\hat{d}$ optimization for CM2 channel realization with a channel span of 39 samples and CP=32 83
Figure 4.7 Average estimated capacity vs. SNR for different pilot densities with channel estimation type I: CM1 channel realizations 85

Figure 4.8 Average estimated capacity vs. SNR for different pilot densities with channel estimation type II: CM1 channel realizations 86
Figure 4.9 Average estimated capacity vs. SNR for different pilot densities with channel estimation type III: CM1 channel realizations 87
Figure 4.10 Average estimated capacity vs. SNR for different pilot densities with channel estimation type III: CM2 channel realizations 88
Figure 4.11 Average estimated capacity vs. SNR for different pilot densities with channel estimation type III: CM3 channel realizations 89
Figure 4.12 Average estimated capacity vs. SNR for different pilot densities with channel estimation type III: CM4 channel realizations 90
Figure 4.13 Effect in channel matrices of CP insertion and full CP discarding . 90
Figure 4.14 Effect in channel matrices of CP insertion and partial CP discarding 91
Figure 4.15 Average estimated capacity of UWB channel models CM1, CM2, CM3, and CM4 vs. CP duration 92
Figure 4.16 Average estimated capacity of UWB channel model CM1 vs. CP duration for different SNR levels 93
Figure 4.17 Average estimated capacity for CM1 realizations vs. N: 200kHz residual frequency error 93
Figure 4.18 Average estimated capacity for CM2 realizations vs. N: 200kHz residual frequency error 94
Figure 4.19 Average estimated capacity for CM3 realizations vs. N: 200kHz residual frequency error 95
Figure 4.20 Average estimated capacity for CM4 realizations vs. N: 200kHz residual frequency error 95
Figure 4.21 Average estimated capacity for CM4 realizations vs. N: 50kHz residual frequency error 96

LIST OF TABLES

Table B.1 Effect of phase ramping into channel interpolator 111

ACKNOWLEDGMENTS

I would like to express my deepest gratitude to my advisor Prof. Laurence Milstein. His priceless guidance and advice have been present throughout my stay in the program and has made of it a very memorable chapter of my life. His tremendous insights, the way he manages time, his accessability, his immense dedication to research, the attention to detail, and the high standards for research quality have marked not only my research work but also my personality and I take a lot of it with me.

I would also like to thank Profs James Zeidler, Bhaskar Rao, William Hodgkiss, and Lance Small for serving on my committee.

During my stay at UCSD I have met a number of people that have helped me in different ways throughout my research work. I would like to thank Claudio da Silva and Ramesh Annavajjala for their valuable help.

The perseverance of keeping up with the research throughout the years while keeping a full-time position at Qualcomm would have not been possible without the boundless support of my wife, Maria, and my parents. This dissertation is dedicated to my Mom, who suddenly passed away after being diagnosed with cancer; she had just turned 59. All the long nights and early mornings spent on this research were possible thanks to you and to your help from Heaven. My Dad, a role model, for my entire life, has always been there for me and once more I am so happy to make him proud of me. I would like to thank especially my wife, whose infinite patience, boundless love and deep understanding have made out of a very hectic life a very enjoyable journey. I am really looking forward to start enjoying together our daughter baby-Maria (coming in about a month) who has been pushing me really hard to finishing my dissertation before her arrival!

Finally, to all my family, friends and colleagues at Qualcomm, thank you for being there for me!

Chapter 2 of this dissertation, in full, is a reprint of the material as it appears in J.

I. Montojo and L. B. Milstein, "Effects of Imperfections on the Performance of OFDM Systems," accepted for publication in *IEEE Transactions on Communications*. Chapter 3 of this dissertation, in full, is a reprint of the material as it appears in J. I. Montojo and L. B. Milstein, "Channel Estimation for Non-Ideal OFDM Systems," accepted for publication in *IEEE Transactions on Communications*. The material in Chapter 4, in part, will be submitted for publication by J. I. Montojo and L. B. Milstein in *IEEE Transactions on Communications*. The dissertation author was the primary author and Prof. Laurence B. Milstein directed and supervised the research which forms the basis for these chapters.

VITA

1997	Degree in Telecommunications engineering from Escola Tècnica Superior d'Enginyeria de Telecomunicacions de Barcelona at the Universitat Politècnica de Catalunya, Barcelona, Spain
1997	Certificate in Communication Systems engineering from Institut Eurecom, Sophia Antipolis, France
1999	Master of Science in Electrical Engineering, University of Southern California, Los Angeles, CA.
2009	Doctor of Philosophy in Electrical Engineering (Communication Theory and Systems), University of California, San Diego
1997-present	Principal Engineer and Manager at the Corporate R&D systems engineering department of Qualcomm Inc., San Diego, CA.

PUBLICATIONS

- Non-ideal OFDM Systems and OFDM-based UWB performance

  J1. J. I. Montojo and L. B. Milstein, "Effects of Imperfections on the Performance of OFDM Systems," accepted for publication in *IEEE Trans. Commun*.

  C1. J. I. Montojo and L. B. Milstein, "Effects of Imperfections on the Performance of OFDM-based UWB Systems," in *Proc. IEEE Asilomar Conference on Signals, Systems & Computers*, Pacific Grove, CA, Oct. 2008, pp. 1985-1989

- Channel estimation and receive diversity for OFDM Systems

  J1. J. I. Montojo and L. B. Milstein, "Channel Estimation for Non-Ideal OFDM Systems," accepted for publication in *IEEE Trans. Commun*.

  J2. J. I. Montojo and L. B. Milstein, "Error rate for PSK and QAM modulations for Non-Ideal OFDM Systems with noisy channel estimates and receive diversity," to be submitted to *IEEE Trans. Commun*.

- Cognitive OFDM-based UWB

  J1. J. I. Montojo and L. B. Milstein, "Cognitive Aspects of OFDM-based UWB and How to Enable Them," to be submitted to *IEEE Trans. Commun*.

ABSTRACT OF THE DISSERTATION

Adaptive OFDM-based UWB

by

Juan I. Montojo-Bennassar

Doctor of Philosophy in Electrical Engineering
(Communication Theory and Systems)

University of California, San Diego, 2009

Professor Laurence B. Milstein, Chair

The use of wireless communications is increasing and will continue growing, not only for personal communications but also for machine-to-machine applications. Therefore, the use of physical resources for wireless communications, i.e., time and frequency, need to be optimized to maximize the communication link efficiency and to reduce the "cost" of moving bits over the air.

The joint use of ultra wideband (UWB) and cognitive radio (CR) has been identified as a solution to maximize the use of physical resources for wireless communications and to minimize the cost associated with its transfer. UWB and CR, in conjunction with software defined radio receivers, open up a whole new spectrum of possibilities to re-think the design and implementation of wireless communications. In that sense, the setting of the system parameters can become less rigid and can attempt to adapt to different scenar-

ios with the goal to maximize the communication link efficiency.

This dissertation presents a study on how to realize a cognitive Orthogonal Frequency Division Multiplexing (OFDM) wireless system with the goal of maximizing the utilization of physical resources. We first parameterize the OFDM system to a limited set of degrees of freedom, and then we identify the performance of a non-ideal OFDM system. The non-idealities that we consider are imperfections at the receiver, such as timing errors, residual frequency error and imperfect channel estimation, as well as channel perturbations such as inter-symbol interference (ISI) from a channel delay spread larger than the cyclic prefix (CP) or Doppler stemming from the motion of the transmitter and/or receiver.

With the parameterization of the OFDM system and the performance characterization as a function of different parameters, we present how the cognitive OFDM receiver will select the set of parameters that maximize the communication link efficiency. These parameters are the position, at the receiver, of the DFT window, the pilot structure, the CP duration, and the OFDM symbol duration.

CHAPTER 1

Introduction

The use of wireless communications is increasing and will continue growing, not only for personal communications, but also for machine-to-machine applications. Therefore, the use of physical resources for wireless communications, i.e., time and frequency, need to be optimized to maximize the communication link efficiency and to reduce the "cost" of moving bits over the air.

The joint use of UWB and CR has been identified as a promising combination to maximize the use of physical resources for wireless communications and to minimize the cost associated with its transfer. UWB and CR, in conjunction with software defined radio receivers, open up a whole new spectrum of possibilities to re-think the design and implementation of wireless communications. In that sense, the setting of the system parameters can become less rigid and can attempt to adapt to different scenarios with the goal of maximizing the communication link efficiency.

At the same time, OFDM has been widely adopted for advanced wireless communication systems with usage ranging from Wireless Local Access Networks (WLAN) to Wide Area Networks (WAN) and UWB applications. OFDM systems have the main characteristics of being very scalable in frequency, resilient to frequency selective fading at the expense of a fixed overhead incurred by the CP, and enabling the use of simple receivers based on the FFT operation.

This dissertation presents a study on how to realize a cognitive OFDM wireless system with the goal of maximizing the utilization of physical resources. We first param-

eterize the OFDM system to a limited set of degrees of freedom, and then we identify the performance of a non-ideal OFDM system. The non-idealities that we consider are imperfections at the receiver, such as timing errors, residual frequency error and imperfect channel estimation, as well as channel perturbations, such as ISI from a channel delay spread larger than the CP or Doppler stemming from the motion of the transmitter and/or receiver.

With the parameterization of the OFDM system and the performance characterization as a function of different parameters, we present how a cognitive OFDM receiver will select the set of system parameters that maximize the communication link efficiency. These parameters are the position, at the receiver, of the DFT window, the pilot structure, the CP duration, and the OFDM symbol duration.

The parameter optimization will yield an adaptation of the wireless communications system to different environments, while maximizing the communication link efficiency.

1.1 OFDM Systems with Imperfections

This dissertation starts with the characterization of OFDM systems with imperfections. Indeed, most OFDM analyses assume idealized conditions when it comes to the waveform at the receiver in terms of time and frequency synchronization. In addition, often a CP longer than the channel delay spread is assumed, and thus the impact of the possible ISI from adjacent OFDM symbols is not considered.

Chapter 2 provides a consolidated framework for study and analysis of OFDM systems with imperfections. The imperfections include time and frequency synchronization errors, and channel delay spread beyond the CP duration. Transmit as well as receive filtering operations are explicitly modeled, and different receiver detection criteria are considered.

The use of an OFDM waveform for UWB applications is known to be a promising choice to simplify the receiver design and to maximize the bandwidth scalability, as well as the adaptation to various spectrum allocations. Chapter 2 presents bit error rate (BER) sensitivity analyses to key system parameters for OFDM-based UWB applications. From these sensitivity analyses, we see graceful performance degradation with decreasing CP length and increasing residual frequency error. The performance degradation can be much more critical for timing synchronization errors.

1.2 Channel Estimation in OFDM Systems

Studies of channel estimation techniques for OFDM systems also assume often idealized conditions such as a CP long enough to absorb the entire channel delay spread, or perfect time and frequency synchronization at the receiver. Chapter 3 studies the impact of removing these assumptions. The mean square error (MSE) of various linear channel estimation methods are characterized, and analytical expressions for the BER performance are derived.

The derivations in Chapter 3 are kept generic, so that they apply to both time-division and frequency-division multiplexing of the pilot signal and the data subcarriers. The analysis is specialized to the BER performance characterization of OFDM-based UWB systems for different realistic channel estimation methods with residual time and frequency errors.

The effect of intercarrier interference (ICI) on channel estimation is shown to be small. However, ISI severely impacts the quality of the channel estimates and hence can yield a large ($>$2dB) data demodulation performance degradation.

1.3 Cognitive OFDM

As discussed above, after having parameterized the OFDM system and having characterized the performance for different parameter settings, Chapter 4 presents a cognitive OFDM receiver that seeks maximizing the communication link efficiency by selecting the optimal OFDM parameter settings.

For the parameter optimization problem at the cognitive receiver, we look at an estimated capacity function conditioned on the channel realization. Results in Chapter 4 show how the DFT window placement, the pilot structure and the CP duration can be optimized without the need of a waveform change. However, the optimization of the OFDM symbol duration requires transmission of symbols with multiple lengths for the receiver to select the one optimizing the link efficiency.

1.4 Outline of the Dissertation

In Chapter 2, we present the OFDM system model that will be used in the rest of the dissertation. Chapter 2 introduces much of the notation and the parameterization of the OFDM system. The channel is assumed to be slowly varying, i.e., constant over the duration of an OFDM symbol, for the results in Chapters 2 and 3. Different receiver types are discussed in Chapter 2 although most of the rest of the dissertation will focus on the single tap OFDM receiver. This chapter will present sensitivity analyses vs. some imperfections, e.g., ISI, residual timing error, residual frequency error.

In Chapter 3, different channel estimators are studied for OFDM. This chapter assesses the performance impact of realistic channel estimation on an OFDM system with imperfections as introduced in Chapter 2. Analysis vs. simulation results are presented for BPSK modulation and single receive antenna using the quadratic Gaussian forms in Appendix B of [1].

In Chapter 4, we use the OFDM parameterization and performance characteri-

zations of previous chapters to study a cognitive OFDM receiver capable of identifying system parameters that maximize the communication link efficiency. This chapter builds from the results in all previous chapters.

Finally, Chapter 5 concludes the dissertation with summary remarks.

CHAPTER 2

Effects of Imperfections on the Performance of OFDM Systems

2.1 Introduction

OFDM systems have the advantage of being able to operate as a set of N (number of subcarriers in the system) parallel flat fading channels. However, this desirable property comes at the price of provisioning a fixed overhead, the CP, of duration greater than or equal to the channel delay spread, to maintain the channel orthogonality at the receiver after channel dispersion. Other impairments, such as timing errors, frequency errors, or a channel varying within the OFDM symbol span, will also destroy the orthogonality of these parallel channels.

Research in the area of OFDM systems very often assumes ideal orthogonality conditions. In particular, in analyses of OFDM-based UWB systems [34], a CP long enough to avoid ISI is usually assumed [38]-[42], despite the fact that a large number of path components could be beyond the CP. The assumption of a CP longer than the channel delay spread is used in studies ranging from multi-antenna techniques [38], [40], [41], to channel estimation [39].

Performance of OFDM systems with various imperfections have been considered in references such as [3], [4], [6], [11]-[13], [15], [17], [19], [20], [23], [25], [30], [33], [35], [36], [43], [49]. References [3], [17], [36], [43] analyze the impact of inter-carrier

interference (ICI) due to a time-varying channel within the OFDM symbol time span, while [19] studies the impact of ICI due to frequency error. The impact of a channel delay spread longer than the CP has been studied in [4], [6], [11]-[13], [15], [20], [23], [25], [30], [33], [35], [49].

Reference [4] derives the carrier-to-interference ratio (C/I) at each subcarrier, accounting for the effects of ICI and ISI due to a channel delay spread longer than the CP and to residual frequency error. The authors of [4] advocate the use of channel coding and adaptive equalization to compensate the effects of ICI/ISI. In [6], the power of the ICI/ISI term is derived, and a sensitivity analysis of the CP length is performed for a channel model corresponding to a hilly environment. In [11], a method to cancel the residual ISI is presented to alleviate the performance degradation at demodulation. Reference [12] studies the combined impact of the channel variation within the OFDM symbol time span and the delay spread of the channel. In [13], the optimum timing offset, number of subcarriers and CP duration that minimize the signal-to-noise ratio (SNR) degradation due to ICI/ISI is studied. Reference [15] discusses the loss of orthogonality caused by ICI and ISI when the OFDM system is used for low earth orbit (LEO) satellite channels. Reference [20] derives the power spectral density (PSD) of ISI to optimize the Time Of Reference (TOR) for optimal placing of the Discrete Fourier Transform (DFT) window at the OFDM receiver. References [23] and [25] present expressions for ICI/ISI due to channel delay spread beyond the CP length, and [25] derives the ICI and ISI terms due to a channel delay spread greater than the CP for a time-invariant channel. Reference [33] builds on [25] to obtain expressions for the ICI/ISI terms for a rapidly time-varying channel, i.e., when the channel changes over the OFDM symbol duration. Reference [30] provides good insights on the impact of ICI and ISI due to channel delay spread beyond the CP and residual frequency error for Rayleigh fading. Reference [35] provides sensitivity analysis of capacity vs. OFDM symbol and CP length, and the choice of TOR.

Perfect time and frequency synchronization are assumed in [6], [11], [12], [15], [23], [25], [33]. Perfect time synchronization is assumed in [4], [30], and therefore ISI

from only the previous OFDM symbol is considered. Perfect frequency synchronization is assumed in [13], [20], [35].

To the best of our knowledge, the only publication that characterizes the ICI and ISI terms due to a channel delay spread larger than the CP and imperfect synchronization is [49]. In reference [49], performance analysis for UWB systems with various imperfections is conducted under the Rayleigh fading assumption and assuming a minimum distance receiver.

In this chapter, we also characterize the ICI and ISI terms due to both a channel delay spread larger than the CP and synchronization errors. However, unlike [49], that considers a continuous-time OFDM model, we use a discrete-time OFDM model. The discrete-time OFDM model is more relevant from an implementation perspective, as it enables the efficient utilization of FFT/IFFTs for the generation and processing of the OFDM waveform. Also, [49] does not consider a CP, but rather just uses a guard time between consecutive OFDM symbols with no actual transmission. With this model, the possible ISI from a future OFDM symbol that an OFDM system using an actual CP is subject to is not accounted for in [49]. In this chapter, we model an actual CP and, therefore, are able to quantify the ISI from the next OFDM symbol, which would be incurred with a positive timing error.

Our system model also accounts for transmit and receive filtering operations, which are important as they entail an increase of the effective channel delay spread. Further, we study the performance sensitivity to various types of data detection algorithms with imperfections.

We specialize the generic analysis to conducting sensitivity analyses against various system parameters and/or imperfection levels for UWB channel models. We show BER performance as a function of CP duration for various types of fading environments, and also show BER performance as a function of residual time and frequency errors.

The structure of the chapter is as follows. In Section 2.2, first we present the sys-

tem model, and then we characterize the DFT output at the OFDM receiver for the most general case of ICI and ISI. Section 2.3 covers data demodulation for several different detection criteria and characterizes the SINR at the data demodulator output. Section 2.4 presents performance results comparing analysis, simulations, and a Gaussian approximation of the interference terms. The chapter finishes with some concluding remarks in Section 2.5.

2.2 OFDM System Model

2.2.1 OFDM Transmitter and Channel

The discrete-time OFDM transmit waveform at baseband is given by

$$u[n,k] = \frac{1}{\sqrt{N}} \sum_{m=-N/2}^{N/2-1} s[n,m] \cdot e^{j2\pi m(k-CP)/N} \cdot \Pi_s[\frac{k}{N_T}] \tag{2.1}$$

where N is the number of subcarriers, CP is the duration in samples of the CP, $N_T \triangleq (N + CP)$, and $s[n,m]$ are the information symbols, in general complex. The index n is used as a time index and refers to a particular OFDM symbol, the index m is used as a subcarrier index within the OFDM symbol, and the index k is used as a time index for samples within a given OFDM block. The OFDM symbol duration in seconds is $T \triangleq NT_c$, and the OFDM block duration is $T_f \triangleq N_T T_c$, where T_c is the symbol duration prior to the OFDM modulation. Finally, $\Pi_s[k/N_T]$ is the shifted rectangular function with unit amplitude and spanning the interval $k \in [0, N_T - 1]$.

The transmitter gives an analog support to the discrete-time signal $u[n,k]$ by way of a digital-to-analog conversion (DAC) or pulse shaping filter that we denote by $h^{tx}(t)$, yielding

$$x_{lp}(t) = \sum_{n} \sum_{k}^{N_T-1} u[n,k] h^{tx}(t - kT_c - nT_f), \tag{2.2}$$

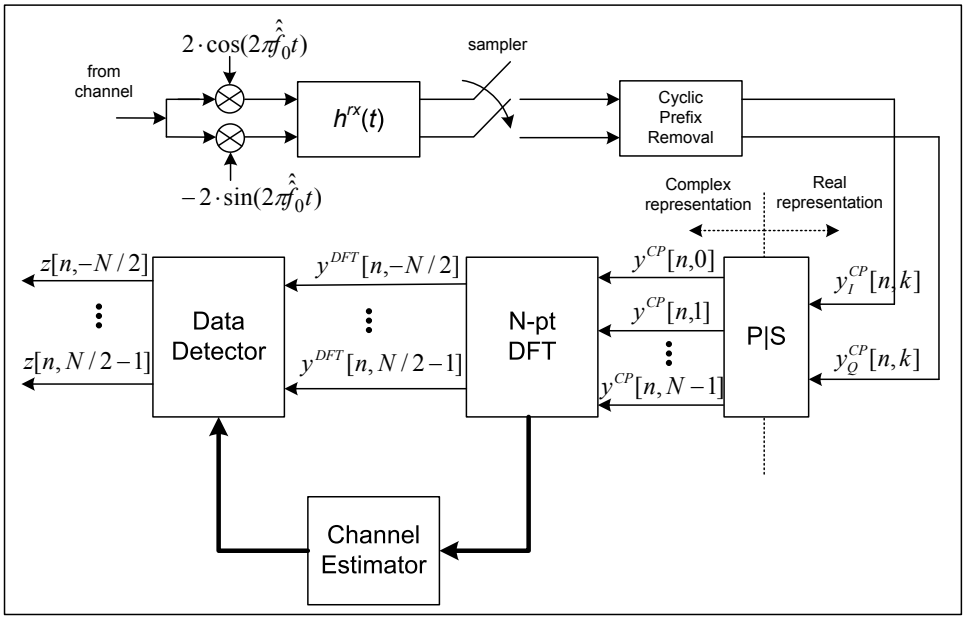

Figure 2.1 *Block diagram of OFDM receiver*

which will be up-converted to the carrier frequency, f_0. Note that we will denote the locally generated carrier frequency at the OFDM transmitter by $\hat{f}_0$.

The channel lowpass equivalent's impulse response is denoted by $h_{lp}^{ch}(t)$ and can be expressed as $h_{lp}^{ch}(t) \triangleq \sum_{p=0}^{P-1} \lambda_p \cdot \delta(t - D_p)$, where P is the number of multi-path components and $\{\lambda_p\}$ represent the taps of the channel's lowpass equivalent. The channel is considered to be slowly varying and, therefore, constant during an OFDM symbol duration. The lowpass equivalent of the channel noise, $n_{lp}(t)$, is assumed to be complex circular white Gaussian (AWGN) with zero mean and two-sided PSD N_0.

2.2.2 OFDM Receiver

Figure 2.1 is a block diagram of the OFDM receiver. The receiver performs, first, passband filtering and down-conversion to baseband using the locally generated carrier frequency denoted by $\hat{\hat{f}}_0$. The CP is discarded and then a DFT is performed.

After receive filtering and down-conversion, the signal part of the incoming signal

may be written as

$$y_{signal}^{RxF}(t) = \underbrace{\{(x_{lp}(t) * h_{lp}^{ch}(t)) \cdot e^{j2\pi\Delta ft}\}}_{\Xi(t)} * h^{rx}(t), \tag{2.3}$$

where '$*$' represents convolution and we have introduced the frequency error $\Delta f \triangleq (\hat{f}_0 - \hat{\hat{f}}_0)$.

Using (2.2), we can write $\Xi(t)$, defined in (2.3), as

$$\Xi(t) = e^{j2\pi\Delta ft} \cdot \sum_n \sum_{k=0}^{N_T-1} u[n,k] \cdot \underbrace{(h_{lp}^{ch}(t) * h^{tx}(t - kT_c - nT_f))}_{h_{lp}^{tx-ch}(t-kT_c-nT_f)} \tag{2.4}$$

where we have introduced $h_{lp}^{tx-ch}(t) \triangleq h_{lp}^{ch}(t) * h^{tx}(t)$ as the convolution of the channel impulse response, $h_{lp}^{ch}(t)$, and the transmit pulse shape filter or DAC, $h^{tx}(t)$. Now, we can manipulate (2.3) to yield

$$\begin{aligned} y_{signal}^{RxF}(t) &= e^{j2\pi\Delta ft} \sum_n \sum_{k=0}^{N_T-1} u[n,k] \cdot \int_{-\infty}^{\infty} h^{rx}(u) \cdot e^{-j2\pi\Delta fu} \\ &\cdot \quad h_{lp}^{tx-ch}(t - u - kT_c - nT_f) \cdot du. \end{aligned} \tag{2.5}$$

Given that the receive filter has a bandwidth in the order of $N/T = 1/T_c = BW_{signal}$, then the relevant range for u in (2.5) is $|u| \leq \vartheta T_c$, where ϑ is an integer number meant to capture the number of T_c intervals so that $\int_{-\infty}^{\infty} h^{rx}(u)e^{-j2\pi\Delta fu}h_{lp}^{tx-ch}(t - u - kT_c - nT_f)du \cong \int_{-\vartheta T_c}^{\vartheta T_c} h^{rx}(u)e^{-j2\pi\Delta fu}h_{lp}^{tx-ch}(t - u - kT_c - nT_f)du$. Looking at the product (Δfu), we see that $(\Delta f\vartheta T_c) = (\Delta f\vartheta/BW_{signal})$. Since, for all practical purposes, $BW_{signal} >> (\Delta f\vartheta)$, we have $(\Delta f\vartheta)/BW_{signal} << 1$, and thus $e^{-j2\pi\Delta fu} \cong 1$ for the values of u that are relevant to the integral. Note that the same approximation is

made in [3]. Therefore,

$$y_{signal}^{RxF}(t) \cong e^{j2\pi\Delta ft} \sum_{n} \sum_{k=0}^{N_T-1} u[n,k] \underbrace{\int_{-\infty}^{\infty} h^{rx}(u) \cdot h_{lp}^{tx-ch}(t-u-kT_c-nT_f) \cdot du}_{h(t-kT_c-nT_f)} \quad (2.6)$$

where we have introduced the effective channel impulse response (incorporating the transmit and receive filtering operations), defined as $h(t) \triangleq h^{rx}(t) * h_{lp}^{tx-ch}(t) = h^{rx}(t) * h_{lp}^{ch}(t) * h^{tx}(t)$.

Similarly, the noise component at the output of the front-end receive filter, $y_{noise}^{RxF}(t)$, may be written as

$$y_{noise}^{RxF}(t) = \{n_{lp}(t) * e^{j2\pi\Delta ft}\} * h^{rx}(t) \cong e^{j2\pi\Delta ft} \int_{-\infty}^{\infty} h_{rx}(u) \cdot n_{lp}(t-u) \cdot du. \quad (2.7)$$

Note that, since $n_{lp}(t)$ is complex circular white Gaussian noise, the rotating phasor $e^{j2\pi\Delta ft}$ will not change the statistics of the noise and therefore can be dropped from the analysis.

We denote the overall waveform after receive filtering and down-conversion by $y^{RxF}(t) \triangleq y_{signal}^{RxF}(t) + y_{noise}^{RxF}(t)$. This signal is sampled at a rate $1/T_c = N/T$ Hz. If the effective channel impulse response, $h(t)$, spans the continuous time interval $[D_{\text{min}}, D_{\text{max}}]$, then its sampled version, $h(kT_c)$, spans the sample interval $[\lceil D_{\text{min}}/T_c \rceil, \lfloor D_{\text{max}}/T_c \rfloor]$. Considering a possible transmit/receive timing error, τ, the signal $h(t+\tau)$ spans the time interval $[D_{\text{min}} - \tau, D_{\text{max}} - \tau]$ and its sampled version, $h(kT_c + \tau)$, spans the sample interval $[\lceil (D_{\text{min}} - \tau)/T_c \rceil, \lfloor (D_{\text{max}} - \tau)/T_c \rfloor]$. Note that, in general, the transmit/receive timing error, τ, is much smaller than the channel delay spread, therefore, $\tau << D_{\text{max}}$. Let us denote the sample interval limits for the effective channel impulse response L_L for the lower limit and L_U for the upper limit, i.e.,

$$L_L \triangleq \lceil (D_{\text{min}} - \tau)/T_c \rceil \text{ and } L_U \triangleq \lfloor (D_{\text{max}} - \tau)/T_c \rfloor. \quad (2.8)$$

Therefore, after sampling at $1/T_c$ Hz, with a transmit/receive timing error τ, yields

$$y^{RxF}[n',k'] \triangleq y^{RxF}(t)|_{t=n'T_f+k'T_c+\tau} = e^{j2\pi\Delta f(n'T_f+k'T_c+\tau)} \cdot \sum_{n}\sum_{k=0}^{N_T-1} u[n,k]\cdot h((n'-n)T_f+(k'-k)T_c+\tau) + y^{RxF}_{noise}(n'T_f+k'T_c+\tau) \quad (2.9)$$

where $k' \in [0, N_T-1]$. Note that we use again the discrete representation of signals with two arguments, n and k, representing time indexing OFDM blocks and samples therein, respectively. Since the time span of the effective channel impulse response, $h(t)$, is, by design, much smaller than the OFDM block duration, when receiving the OFDM block with index n', only three blocks can contribute to the final test statistic. These are the block with index n' itself, the block preceding it and the block following it. Therefore, the summation in n above is only relevant for the values $n = n', n = (n'-1), n = (n'+1)$, and hence

$$y^{RxF}[n,k] = y^{RxF,(n)}_{signal}[n,k] + y^{RxF,(n-1)}_{signal}[n,k] + y^{RxF,(n+1)}_{signal}[n,k] + y^{RxF}_{noise}[n,k] \quad (2.10)$$

where we have defined

$$y^{RxF,(n)}_{signal}[n,k] \triangleq e^{j2\pi\Delta f(nT_f+kT_c+\tau)} \sum_{\xi=0}^{N_T-1} u[n,\xi]\cdot h((k-\xi)T_c+\tau), \quad (2.11)$$

$$y^{RxF,(n-1)}_{signal}[n,k] \triangleq e^{j2\pi\Delta f(nT_f+kT_c+\tau)} \sum_{\xi=0}^{N_T-1} u[n-1,\xi]\cdot h(T_f+(k-\xi)T_c+\tau) \quad (2.12)$$

and

$$y^{RxF,(n+1)}_{signal}[n,k] \triangleq e^{j2\pi\Delta f(nT_f+kT_c+\tau)} \sum_{\xi=0}^{N_T-1} u[n+1,\xi]\cdot h(-T_f+(k-\xi)T_c+\tau) \quad (2.13)$$

Note that $y^{RxF,(n)}_{signal}[n,k]$ contains the contribution of the current OFDM symbol after sam-

pling and before discarding the CP. The terms $y_{signal}^{RxF,(n-1)}[n,k]$ and $y_{signal}^{RxF,(n-1)}[n,k]$ constitute the ISI after sampling and before discarding the CP from the previous and next OFDM symbol, respectively.

The sampled noise is given by

$$y_{noise}^{RxF}[n,k] = y_{noise}^{RxF}(nT_f + kT_c + \tau) \tag{2.14}$$

where all the terms in (2.11)-(2.14) are valid for $k = 0 \ldots (N_T - 1)$.

Keeping track of the sample span of $u[n,k]$ and $h(kT_c + \tau)$, (2.11)-(2.13), may be re-written as

$$y_{signal}^{RxF,(n)}[n,k] = e^{j2\pi\Delta f(nT_f + kT_c + \tau)} \cdot \begin{cases} \sum_{\nu=L_L}^{k} u[n,k-\nu] \cdot h(\nu T_c + \tau), \text{ for } k \\ \quad = \max(0, L_L) \ldots L_U - 1 \\ \sum_{\nu=L_L}^{L_U} u[n,k-\nu] \cdot h(\nu T_c + \tau), \text{ for } k \\ \quad = L_U \ldots \min(N_T + L_L - 1, N_T - 1) \\ \sum_{\nu=k-(N_T-1)}^{L_U} u[n,k-\nu] \cdot h(\nu T_c + \tau), \text{ for } k \\ \quad = N_T + L_L \ldots N_T - 1 \text{ and if } L_L < 0 \end{cases} \tag{2.15}$$

$$y_{signal}^{RxF,(n-1)}[n,k] = e^{j2\pi\Delta f(nT_f + kT_c + \tau)} \cdot \begin{cases} \sum_{\nu=L_L}^{L_U} u[n-1,k-\nu+N_T] h(\nu T_c + \tau), \\ \quad \text{for } k = 0 \ldots L_L - 1 \text{ if } L_L > 0 \\ \sum_{\nu=k+1}^{L_U} u[n-1,k-\nu+N_T] h(\nu T_c + \tau), \\ \quad \text{for } k = \max(0, L_L) \ldots L_U - 1 \end{cases} \tag{2.16}$$

and

$$y_{signal}^{RxF,(n+1)}[n,k] = e^{j2\pi\Delta f(nT_f + kT_c + \tau)} \sum_{\nu=L_L}^{k-N} u[n+1,k-\nu-N_T] \cdot h(\nu T_c + \tau) \tag{2.17}$$

for $k = N_T + L_L \ldots N_T - 1$ if $L_L < 0$.

The expressions in (2.15)-(2.17) show the non-zero contributions of the different terms at each sample point within the OFDM symbol (index k). Note that a non-zero contribution of (2.17), which is the term representing the ISI from the next OFDM symbol, requires $L_L < 0$. This is equivalent to $\tau \geq (D_{\text{min}} + T_c)$ and hence a "late sampling". We will see now how some of the contributions in (2.16), which is the term representing ISI from the previous OFDM symbol, vanish after discarding the CP.

After discarding the CP, we obtain the following signal-dependent term depending on the current OFDM symbol:

$$y_{signal}^{CP,(n)}[n,k] = \tag{2.18}$$
$$\begin{cases} \frac{\alpha_n}{\sqrt{N}} \sum_{m=-N/2}^{N/2-1} s[n,m] e^{j2\pi(m+\overline{\Delta f})k/N} \sum_{\nu=L_L}^{k+CP} h(\nu T_c + \tau) e^{-j2\pi m\nu/N}, \\ \quad \text{for } k = 0 \ldots (L_U - CP - 1) \text{ if } L_U > CP \\ \frac{\alpha_n}{\sqrt{N}} \sum_{m=-N/2}^{N/2-1} s[n,m] e^{j2\pi(m+\overline{\Delta f})k/N} H(m), \\ \quad \text{for } k = \max(0, L_U) \ldots \min(N + L_L - 1, N - 1) \\ \frac{\alpha_n}{\sqrt{N}} \sum_{m=-N/2}^{N/2-1} s[n,m] e^{j2\pi(m+\overline{\Delta f})k/N} \sum_{\nu=k-(N_T-1)}^{L_U} h(\nu T_c + \tau) e^{-j2\pi m\nu/N}, \\ \quad \text{for } k = (N + L_L) \ldots (N-1) \text{ and if } L_L < 0 \end{cases}$$

where we have defined $\alpha_n \triangleq e^{j2\pi\Delta f(nT_f + CP \cdot T_c + \tau)}$, the normalized frequency error as $\overline{\Delta f} \triangleq \Delta f/(1/T)$, which is the residual frequency error normalized by the subcarrier spacing, and the channel frequency response $H(m) \triangleq \sum_{i=L_L}^{L_U} h(\tau + iT_c) e^{-j2\pi mi/N}$. Note that the first term in (2.18) is non-zero if $L_U > CP$, or, equivalently, if $(D_{\text{max}} - \tau) > (CP \cdot T_c)$. This is the condition for ISI from the previous OFDM symbol after discarding the CP as can be seen from realizing that it is the condition for the term (2.19) to be non-zero. Similarly, the last term in (2.18) is non-zero if $L_L < 0$, which is equivalent to $\tau \geq (D_{\text{min}} + T_c)$, as seen before. This is the condition for ISI from the next OFDM symbol, as can be seen from realizing that is the condition for the term (2.20) to be non-zero. Further, note that discarding the CP does not remove the contribution from the next OFDM symbol.

Similarly, the signal-dependent terms depending on the previous and next OFDM symbols after discarding the CP can be identified to be

$$\begin{aligned} y_{signal}^{CP,(n-1)}[n,k] &= \frac{\alpha_n}{\sqrt{N}} \sum_{m=-N/2}^{N/2-1} s[n-1,m] e^{j2\pi mCP/N} e^{j2\pi(m+\overline{\Delta f})k/N} \\ &\cdot \sum_{\nu=k+CP+1}^{L_U} h(\nu T_c + \tau) e^{-j2\pi m\nu/N} \end{aligned} \tag{2.19}$$

which is non-zero only if $L_U > CP$ and applies for $k = 0 \ldots (L_U - CP - 1)$, and

$$\begin{aligned} y_{signal}^{CP,(n+1)}[n,k] &= \frac{\alpha_n}{\sqrt{N}} \sum_{m=-N/2}^{N/2-1} s[n+1,m] e^{-j2\pi mCP/N} e^{j2\pi(m+\overline{\Delta f})k/N} \\ &\cdot \sum_{\nu=L_L}^{k-N} h(\nu T_c + \tau) e^{-j2\pi m\nu/N}, \end{aligned} \tag{2.20}$$

which is non-zero only if $L_L < 0$ and applies for $k = (N + L_L) \ldots (N - 1)$, respectively.

The noise term, after discarding the CP, becomes

$$y_{noise}^{CP}[n,k] = y_{noise}^{RxF}[n,k+CP] \text{ for } k = 0 \ldots (N-1). \tag{2.21}$$

Therefore, the overall DFT input is $y^{CP}[n,k] = y_{signal}^{CP,(n)}[n,k] + y_{signal}^{CP,(n-1)}[n,k] + y_{signal}^{CP,(n+1)}[n,k] + y_{noise}^{CP}[n,k]$, and we define the DFT output to be

$$y^{DFT}[n,l] = \frac{1}{\sqrt{N}} \sum_{k=0}^{N-1} y^{CP}[n,k] \cdot e^{-j2\pi lk/N}, \tag{2.22}$$

for $l = -N/2 \ldots (N/2 - 1)$. Since the DFT is a linear operation, we may characterize the DFT output $y^{DFT}[n,l]$ in terms of the DFTs of each of the terms in $y^{CP}[n,k]$. Using the same notation as before, the DFT output dependent on the current OFDM symbol is

given by

$$
\begin{aligned}
y_{signal}^{DFT,(n)}[n,l] &= \frac{\alpha_n}{N}\sum_{m=-N/2}^{N/2-1}\Bigg[s[n,m] \\
&\cdot \Bigg\{\overbrace{\sum_{k=0}^{L_U-CP-1} e^{j2\pi(\overline{\Delta f}+m-l)k/N}\sum_{\nu=L_L}^{k+CP} h(\nu T_c+\tau)e^{-j2\pi m\nu/N}}^{\text{if } L_U>CP} \\
&+ \sum_{k=\max(0,L_U-CP)}^{\min(N-1,N+L_L-1)} e^{j2\pi(\overline{\Delta f}+m-l)k/N}H(m) \\
&+ \underbrace{\sum_{k=N+L_L}^{N-1} e^{j2\pi(\overline{\Delta f}+m-l)k/N}\sum_{\nu=k-(N-1)}^{L_U} h(\nu T_c+\tau)e^{-j2\pi m\nu/N}}_{\text{if } L_L<0}\Bigg\}\Bigg]
\end{aligned}
\tag{2.23}
$$

The DFT output that depends on the previous OFDM symbol is nonzero if the CP duration is smaller than the channel delay spread minus the timing error, i.e., if $CP < L_U$, in which case

$$
\begin{aligned}
y_{signal}^{DFT,(n-1)}[n,l] &= \frac{\alpha_n}{N}\sum_{m=-N/2}^{N/2-1} s[n-1,m]\cdot e^{j2\pi m\cdot CP/N} \\
&\cdot \sum_{k=0}^{L_U-CP-1} e^{j2\pi(\overline{\Delta f}+m-l)k/N}\sum_{\nu=k+CP+1}^{L_U} h(\nu T_c+\tau)e^{-j2\pi m\nu/N}.
\end{aligned}
\tag{2.24}
$$

The DFT output depending on the next OFDM symbol is nonzero if the timing error, $\tau \geq (D_{\min} + T_c)$, in which case

$$
\begin{aligned}
y_{signal}^{DFT,(n+1)}[n,l] &= \frac{\alpha_n}{N}\sum_{m=-N/2}^{N/2-1} s[n+1,m]\cdot e^{-j2\pi m\cdot CP/N} \\
&\cdot \sum_{k=N+L_L}^{N-1} e^{j2\pi(\overline{\Delta f}+m-l)k/N}\sum_{\nu=L_L}^{k-N} h(\nu T_c+\tau)e^{-j2\pi m\nu/N}.
\end{aligned}
\tag{2.25}
$$

The noise component at the DFT output may be written as

$$y_{noise}^{DFT}[n,l] = \frac{1}{\sqrt{N}} \sum_{k=0}^{N-1} y_{noise}^{CP}[n,k] \cdot e^{-j2\pi lk/N} \tag{2.26}$$

where $y_{noise}^{CP}[n,k]$ is defined in (2.21). To shorten notation, we can define the following variables:

$$\zeta_1(l,m) \triangleq \sum_{k=0}^{(L_U-CP-1)} e^{-j2\pi(l-\overline{\Delta f}-m)k/N} \sum_{i=L_L}^{(k+CP)} h(\tau+iT_c)e^{-j2\pi mi/N} \tag{2.27}$$

$$\zeta_2(l,m) \triangleq H(m) \sum_{k=\max(L_U-CP,0)}^{\min(N+L_L-1,N-1)} e^{-j2\pi(l-\overline{\Delta f}-m)k/N} \tag{2.28}$$

$$\zeta_3(l,m) \triangleq \sum_{k=N+L_L}^{N-1} e^{-j2\pi(l-\overline{\Delta f}-m)k/N} \sum_{i=k-N+1}^{L_U} h(\tau+iT_c)e^{-j2\pi mi/N} \tag{2.29}$$

$$\zeta_4(l,m) \triangleq e^{j2\pi mCP/N} \sum_{k=0}^{(L_U-CP-1)} e^{-j2\pi(l-\overline{\Delta f}-m)k/N} \sum_{i=(k+CP+1}^{L_U} h(\tau+iT_c)e^{-j2\pi mi/N} \tag{2.30}$$

$$\zeta_5(l,m) \triangleq e^{-j2\pi mCP/N} \sum_{k=N+L_L}^{N-1} e^{-j2\pi(l-\overline{\Delta f}-m)k/N} \sum_{i=L_L}^{k-N} h(\tau+iT_c)e^{-j2\pi mi/N} \tag{2.31}$$

Therefore, the signal-dependent output of the DFT may be written as

$$y_{signal}^{DFT,(n)}[n,l] = \frac{\alpha_n}{N} \sum_{m=-N/2}^{N/2-1} s[n,m]\Big\{ \overbrace{\zeta_1(l,m)}^{\text{if } L_U>CP} + \zeta_2(l,m) + \overbrace{\zeta_3(l,m)}^{\text{if } L_L<0} \Big\}$$

$$+\frac{\alpha_n}{N}\underbrace{\sum_{m=-N/2}^{N/2-1} s[n-1,m]\cdot\zeta_4(l,m)}_{\text{if } L_U>CP}+\frac{\alpha_n}{N}\underbrace{\sum_{m=-N/2}^{N/2-1} s[n+1,m]\cdot\zeta_5(l,m)}_{\text{if } L_L<0} \tag{2.32}$$

where we can clearly identify the ICI and ISI terms at the DFT output.

For the data detection process, it is convenient to put (2.32) in matrix form. Matrices are represented by boldface capital letters, e.g., $\mathbf{A}$, and vectors are represented by boldface lowercase letters, e.g., $\mathbf{v}$. Therefore, we define the matrices

$$\mathbf{\Psi}_x \triangleq [\zeta_x[l,m]]_{m,l=-N/2,\ldots,(N/2-1)} \tag{2.33}$$

with $x = 1, 2, 3, 4, 5$. Note that, from (2.32), $\mathbf{\Psi}_1$ is non-zero only if there is ISI from the previous OFDM symbol, $\mathbf{\Psi}_2$ is the matrix characterizing the useful signal term as well as the ICI term due to frequency error, and $\mathbf{\Psi}_3$ is non-zero only if there is ISI from the next OFDM symbol. Further, note that $\mathbf{\Psi}_4$ and $\mathbf{\Psi}_5$ fully characterize the ISI from the previous and next OFDM symbol, respectively. With the matrices defined in (2.33), we can write (2.32) in matrix form as follows:

$$\mathbf{y}_{signal}^{DFT}(n) = \overbrace{\frac{\alpha_n}{N}(\mathbf{\Psi}_1+\mathbf{\Psi}_2+\mathbf{\Psi}_3)}^{\mathbf{A}(n)}\cdot\mathbf{s}(n) + \overbrace{\frac{\alpha_n}{N}\mathbf{\Psi}_4}^{\mathbf{A}_{pre}(n)}\cdot\mathbf{s}(n-1) + \overbrace{\frac{\alpha_n}{N}\mathbf{\Psi}_5}^{\mathbf{A}_{next}(n)}\cdot\mathbf{s}(n+1) \tag{2.34}$$

where $\mathbf{s}(n)$, $\mathbf{s}(n-1)$ and $\mathbf{s}(n+1)$ are column vectors of length N with information symbols at the n^{th}, $(n-1)^{th}$ and $(n+1)^{th}$ OFDM symbols, respectively, and where we have defined the channel state information matrices, $\mathbf{A}(n)$, $\mathbf{A}_{pre}(n)$ and $\mathbf{A}_{next}(n)$. Note that there is no "time" dependency in either $\zeta_x(l,m)$ or $\mathbf{\Psi}_x$ because we assume a particular channel realization that remains constant over the OFDM symbol duration. This condition requires a channel coherence time $T_{coh} >> T$ or, equivalently, $1/T_{coh} << 1/T$, which means that the subcarrier spacing $(1/T)$ is much greater than the Doppler spread $(1/T_{coh} \cong f_d)$. The time dependency in the newly defined matrices $\mathbf{A}(n)$, $\mathbf{A}_{pre}(n)$ and $\mathbf{A}_{next}(n)$ comes from the time-varying phasor α_n and we will drop it from the develop-

ment to shorten notation.

Overall, at the DFT output, we have

$$\mathbf{y}^{DFT}(n) = \underbrace{\mathbf{A}\mathbf{s}(n)}_{\mathbf{y}^{DTF}_{useful \text{ and } ICI}(n)} + \underbrace{\mathbf{A}_{pre}\mathbf{s}(n-1) + \mathbf{A}_{next}\mathbf{s}(n+1)}_{\mathbf{y}^{DTF}_{ISI}(n)} + \underbrace{\mathbf{w}(n)}_{\mathbf{y}^{DTF}_{noise}(n)} \tag{2.35}$$

When there is no ISI, the expression in (2.35) reduces to $\mathbf{y}^{DFT}(n) = \mathbf{A}\cdot\mathbf{s}(n)+\mathbf{w}(n)$. The condition for no ISI can be seen from observation of the terms in (2.32), i.e., $L_U \leq CP$ and $L_L \geq 0$. For this case, the matrix $\mathbf{\Psi}_2$ is the only non-zero matrix, and the term $\zeta_2(l,m)$ takes the form $\zeta_2(l,m) = H(m)\sum_{k=0}^{N-1} e^{-j2\pi(l-\overline{\Delta f}-m)k/N}$. Therefore, the matrix $\mathbf{\Psi}_2$ can be written as $\mathbf{\Psi}_2 = \mathbf{\Delta}\cdot\mathbf{D_H}$, where $\mathbf{\Delta}_{m+N/2,l+N/2} \triangleq \sum_{k=0}^{N-1} e^{j2\pi(l-\overline{\Delta f}-m)k/N}$, and

$$\mathbf{D_H} \triangleq \begin{bmatrix} H(-N/2) & 0 & \cdots & 0 \\ 0 & H(-N/2+1) & \cdots & 0 \\ \vdots & \vdots & \ddots & \vdots \\ 0 & 0 & \cdots & H(N/2-1) \end{bmatrix}$$

Since $\mathbf{\Delta}$ is circulant, it can be shown that it can be decomposed as $\mathbf{\Delta} = N\mathbf{F}\cdot\mathbf{M}^{\phi}\cdot\mathbf{F}^{H}$, where

$$\mathbf{M}^{\phi} \triangleq \begin{bmatrix} e^{j2\pi\overline{\Delta f}0/N} & 0 & \cdots & 0 \\ 0 & e^{j2\pi\overline{\Delta f}1/N} & \cdots & 0 \\ \vdots & \vdots & \ddots & \vdots \\ 0 & 0 & \cdots & e^{j2\pi\overline{\Delta f}(N-1)/N} \end{bmatrix}$$

and $\mathbf{F}$ is the Fourier matrix of size $N \times N$. As a result, for the ISI-free case,

$$\mathbf{y}^{DFT}(n) \triangleq \frac{\alpha_n}{N}\cdot\mathbf{\Delta}\cdot\mathbf{D_H}\cdot\mathbf{s}(n) + \mathbf{w}(n). \tag{2.36}$$

Further, if there is no residual frequency error, the matrix $\mathbf{\Delta}$ becomes the identity matrix

multiplied by N and $\alpha_n = 1$. Therefore, (2.36) becomes

$$\mathbf{y}^{DFT}(n) \triangleq \mathbf{D_H} \cdot \mathbf{s}(n) + \mathbf{w}(n) \tag{2.37}$$

which is the traditional set of N parallel flat fading channels that OFDM systems are regularly associated with.

2.3 Data Detection

We assume linear processing at the receiver, so that

$$\mathbf{z}(n) = \mathbf{M} \cdot \mathbf{y}^{DFT}(n) \tag{2.38}$$

where the matrix $\mathbf{M}$ will take different forms depending on the data detector type. Applying (2.35) to (2.38) yields

$$\mathbf{z}(n) = \mathbf{MA}\mathbf{s}(n) + \mathbf{MA}_{pre}\mathbf{s}(n-1) + \mathbf{MA}_{next}\mathbf{s}(n+1) + \mathbf{Mw}(n) \tag{2.39}$$

Denoting $\mathbf{B} \triangleq \mathbf{MA}$, $\mathbf{B}_{pre} \triangleq \mathbf{MA}_{pre}$ and $\mathbf{B}_{next} \triangleq \mathbf{MA}_{next}$, we can re-write (2.39) as

$$\mathbf{z}(n) = \mathbf{B}\mathbf{s}(n) + \mathbf{B}_{pre}\mathbf{s}(n-1) + \mathbf{B}_{next}\mathbf{s}(n+1) + \mathbf{Mw}(n), \tag{2.40}$$

which we can re-write as $\mathbf{z}(n) = \mathbf{z}_{signal}(n) + \mathbf{w}'(n)$, and where $\mathbf{z}_{signal}(n) \triangleq \mathbf{B}\mathbf{s}(n) + \mathbf{B}_{pre}\mathbf{s}(n-1) + \mathbf{B}_{next}\mathbf{s}(n+1)$ and $\mathbf{w}'(n) \triangleq \mathbf{Mw}(n)$. Clearly, the first summand in (2.40) contains the desired term as well as the ICI term, and therefore we can re-write it as

$$\mathbf{z}(n) = \text{Diag}(\mathbf{B})\mathbf{s}(n) + \overline{\text{Diag}}(\mathbf{B})\mathbf{s}(n) + \mathbf{B}_{pre}\mathbf{s}(n-1) + \mathbf{B}_{next}\mathbf{s}(n+1) + \mathbf{Mw}(n) \tag{2.41}$$

where $\text{Diag}(\mathbf{A})$ represents a diagonal matrix containing only the diagonal elements of the matrix $\mathbf{A}$ and $\overline{\text{Diag}}(\mathbf{A}) = \mathbf{A} - \text{Diag}(\mathbf{A})$ represents a matrix with zero diagonal elements

containing all but the diagonal elements of $\mathbf{A}$.

By inspection of (2.41), we can obtain the SINR of the l^{th} subcarrier at the data detector output as

$$\gamma(n,l) \triangleq \frac{E\{|[\text{Diag}(\mathbf{B})\mathbf{s}(n)]_l|^2\}}{d_1(n,l)} \tag{2.42}$$

where

$$\begin{aligned} d_1(n,l) \triangleq E\{|[\overline{\text{Diag}}(\mathbf{B})\mathbf{s}(n)]_l|^2\} + E\{|[\mathbf{B}_{pre}\mathbf{s}(n-1)]_l|^2\} \\ +E\{|[\mathbf{B}_{next}\mathbf{s}(n+1)]_l|^2\} + E\{|[\mathbf{M}\mathbf{w}(n)]_l|^2\} \end{aligned} \tag{2.43}$$

and where the expectations are done over the random noise and the random information symbols. Note that we have assumed independence between the noise and the signal terms, and we have assumed independence of the modulation symbols at different OFDM symbols, and hence, independence among the ICI and the two possible ISI terms.

Defining $\mathbf{R}_s(n) \triangleq E\{\mathbf{s}(n)\mathbf{s}^H(n)\}$ and $\mathbf{R}_w(n) \triangleq E\{\mathbf{w}(n)\mathbf{w}^H(n)\}$, we can re-write the SINR of the l^{th} subcarrier at the data detector output as

$$\gamma(n,l) \triangleq \frac{|[\mathbf{B}]_{l,l}|^2 E\{|\mathbf{s}(n,l)|^2\}}{d_2(n,l)}, \tag{2.44}$$

where

$$\begin{aligned} d_2(n,l) \triangleq [\mathbf{B}\mathbf{R}_s(n)\mathbf{B}^H]_{l,l} - 2\Re\{[\mathbf{B}\mathbf{R}_s(n)]_{l,l}[\mathbf{B}^H]_{l,l}\} \\ +|[\mathbf{B}]_{l,l}|^2 E\{|\mathbf{s}(n,l)|^2\} + [\mathbf{B}_{pre}\mathbf{R}_s(n-1)\mathbf{B}_{pre}^H]_{l,l} \\ +[\mathbf{B}_{next}\mathbf{R}_s(n+1)\mathbf{B}_{next}^H]_{l,l} + [\mathbf{M}\mathbf{R}_w(n)\mathbf{M}^H]_{l,l} \end{aligned} \tag{2.45}$$

Note that the expressions in (2.44) and (2.45) are valid for any linear receiver, and will be specialized below for different receiver criteria.

For the special case of white noise, i.e., $\mathbf{R}_w(n) = \sigma_w^2\mathbf{I}_N$ and $\mathbf{R}_s(n) = \mathbf{R}_s(n-1) =$

$\mathbf{R}_s(n+1) = \mathbf{I}_N$, (2.44) takes the following form:

$$\gamma(n,l) \triangleq \frac{|[\mathbf{B}]_{l,l}|^2}{d_3(n,l)} \tag{2.46}$$

with

$$d_3(n,l) \triangleq [\mathbf{B}\mathbf{B}^H]_{l,l} - |[\mathbf{B}]_{l,l}|^2 + [\mathbf{B}_{pre}\mathbf{B}_{pre}^H]_{l,l} + [\mathbf{B}_{next}\mathbf{B}_{next}^H]_{l,l} + \sigma_w^2[\mathbf{M}\mathbf{M}^H]_{l,l} \tag{2.47}$$

2.3.1 Data Detection with Single-Tap Equalizer (ST)

For the ST receiver, the detection operation is given by

$$\mathbf{z}_{ST}(n) = \text{Diag}(\mathbf{A}^H)\mathbf{y}^{DFT}(n) \tag{2.48}$$

Note that this received does not attempt to equalize the received signal and only the useful part of the received signal, i.e., $\text{Diag}(\mathbf{A})$, is considered while ignoring the ICI, ISI and noise terms. For this case, $\mathbf{B} = \text{Diag}(\mathbf{A}^H)\mathbf{A}$, $\mathbf{B}_{pre} = \text{Diag}(\mathbf{A}^H)\mathbf{A}_{pre}$ and $\mathbf{B}_{next} = \text{Diag}(\mathbf{A}^H)\mathbf{A}_{next}$, and (2.44) and (2.45) take the following forms, respectively:

$$\gamma_{ST}(n,l) \triangleq \frac{|[\text{Diag}(\mathbf{A}^H)\mathbf{A}]_{l,l}|^2 E\{|\mathbf{s}(n,l)|^2\}}{d_{ST}(n,l)}, \tag{2.49}$$

where

$$\begin{aligned} d_{ST}(n,l) \;\triangleq\; & [\text{Diag}(\mathbf{A}^H)\mathbf{A}\mathbf{R}_s(n)\mathbf{A}^H\text{Diag}(\mathbf{A})]_{l,l} \\ - \;& 2\Re\{[\text{Diag}(\mathbf{A}^H)\mathbf{A}\mathbf{R}_s(n)]_{l,l}[\mathbf{A}^H\text{Diag}(\mathbf{A})]_{l,l}\} \\ + \;& |[\text{Diag}(\mathbf{A}^H)\mathbf{A}]_{l,l}|^2 E\{|\mathbf{s}(n,l)|^2\} + [\text{Diag}(\mathbf{A}^H)\mathbf{A}_{pre}\mathbf{R}_s(n-1)\mathbf{A}_{pre}^H\mathbf{A})]_{l,l} \\ + \;& [\text{Diag}(\mathbf{A}^H)\mathbf{A}_{next}\mathbf{R}_s(n+1)\mathbf{A}_{next}^H\mathbf{A})]_{l,l} + [\mathbf{M}\mathbf{R}_w(n)\mathbf{M}^H]_{l,l} \end{aligned} \tag{2.50}$$

2.3.2 Data Detection with Zero-Forcing Equalizer (ZF)

For the ZF receiver, the detection operation is given by

$$\begin{aligned}\mathbf{z}_{ZF}(n) &\triangleq \left(\mathbf{R}_s(n)\mathbf{A}^H\mathbf{A}\mathbf{R}_s(n)\mathbf{A}^H + \mathbf{A}_{pre}\mathbf{R}_s(n-1)\mathbf{A}_{pre}^H + \mathbf{A}_{next}\mathbf{R}_s(n+1)\mathbf{A}_{next}^H\right)^{-1} \\ &\cdot \quad \mathbf{y}^{DFT}(n) \end{aligned} \tag{2.51}$$

This receiver attempts to suppress the signal-dependent interference, i.e., ICI and ISI. Assuming $\mathbf{R}_s(n) = \mathbf{R}_s(n-1) = \mathbf{R}_s(n+1) = \mathbf{I}_N$, (2.51) becomes

$$\mathbf{z}_{ZF}(n) \triangleq \mathbf{A}^H \left(\mathbf{A}\mathbf{A}^H + \mathbf{A}_{pre}\mathbf{A}_{pre}^H + \mathbf{A}_{next}\mathbf{A}_{next}^H\right)^{-1} \cdot \mathbf{y}^{DFT}(n). \tag{2.52}$$

A variant to this ZF detector is given by

$$\mathbf{z}_{modified\ ZF}(n) \triangleq (\mathbf{A}^H\mathbf{A})^{-1}\mathbf{A}^H\mathbf{y}^{DFT}(n) \tag{2.53}$$

This receiver attempts to suppress the ICI interference, while ignoring the ISI and the noise terms. We denote this receiver by "modified ZF", and we have assumed independent modulation symbols of unit energy, i.e., $\mathbf{R}_s(n) = \mathbf{R}_s(n-1) = \mathbf{R}_s(n+1) = \mathbf{I}_N$. For this case, $\mathbf{B} = \mathbf{I}_N$ (perfect suppression of ICI), $\mathbf{B}_{pre} = (\mathbf{A}^H\mathbf{A})^{-1}\mathbf{A}^H\mathbf{A}_{pre}$ and $\mathbf{B}_{next} = (\mathbf{A}^H\mathbf{A})^{-1}\mathbf{A}^H\mathbf{A}_{next}$, and (2.44), (2.45) take the following forms, respectively:

$$\gamma_{modified\ ZF}(n,l) \triangleq \frac{E\{|\mathbf{s}(n,l)|^2\}}{d_{modified\ ZF}(n,l)}, \tag{2.54}$$

where

$$\begin{aligned} d_{modified\ ZF}(n,l) &\triangleq [(\mathbf{A}^H\mathbf{A})^{-1}\mathbf{A}^H\mathbf{A}_{pre}\mathbf{A}_{pre}^H\mathbf{A}(\mathbf{A}^H\mathbf{A})^{-1}]_{l,l} \\ &+ [(\mathbf{A}^H\mathbf{A})^{-1}\mathbf{A}^H\mathbf{A}_{next}\mathbf{A}_{next}^H\mathbf{A}(\mathbf{A}^H\mathbf{A})^{-1}]_{l,l} \\ &+ [(\mathbf{A}^H\mathbf{A})^{-1}\mathbf{A}^H\mathbf{R}_w\mathbf{A}(\mathbf{A}^H\mathbf{A})^{-1}]_{l,l} \end{aligned} \tag{2.55}$$

For the ISI-free case, $\mathbf{A} = \alpha_n/N\mathbf{\Delta D_H}$, as can be seen from Equation (2.36), and therefore $\mathbf{A}^H\mathbf{A} = 1/N^2{\mathbf{D_H}}^H\mathbf{\Delta}^H\mathbf{\Delta D_H}$. Using the expression for Δ derived in Section 2.2, we can further simplify $\mathbf{A}^H\mathbf{A}$ to yield $\mathbf{A}^H\mathbf{A} = {\mathbf{D_H}}^H\mathbf{F}(\mathbf{M}^\phi)^H\mathbf{F}^H\mathbf{F}\mathbf{M}^\phi\mathbf{F}^H\mathbf{D_H} = {\mathbf{D_H}}^H\mathbf{D_H}$, and therefore

$$\mathbf{A}^H\mathbf{A} = \begin{bmatrix} |H(-N/2)|^2 & 0 & \cdots & 0 \\ 0 & |H(-N/2+1)|^2 & \cdots & 0 \\ \vdots & \vdots & \ddots & \vdots \\ 0 & 0 & \cdots & |H(N/2-1)|^2 \end{bmatrix}.$$

As a result, for the ISI-free case with the modified ZF detector, (2.54) reduces to

$$\gamma_{\text{modified ZF-ISI free}}(n,l) = \frac{E\{|s(n,l-N/2)|^2\}}{[(\mathbf{A}^H\mathbf{A})^{-1}\mathbf{A}^H\mathbf{R}_w\mathbf{A}(\mathbf{A}^H\mathbf{A})^{-1}]_{l,l}}$$

which for white noise case becomes, i.e., $\mathbf{R}_w = \sigma_w^2\mathbf{I}_N$

$$\gamma_{\text{modified ZF-ISI free, white noise}}(n,l) = \frac{|H(l-N/2)|^2 \cdot E\{|s(n,l-N/2)|^2\}}{\sigma_w^2}.$$

2.3.3 Data Detection with MMSE Equalizer

For the Minimum-Mean-Square-Error (MMSE) equalizer receiver, the detection operation is given by

$$\begin{aligned} \mathbf{z}_{MMSE}(n) &\triangleq \mathbf{R_s}(n)\mathbf{A}^H\Big(\mathbf{A}\mathbf{R_s}(n)\mathbf{A}^H + \mathbf{A}_{pre}\mathbf{R_s}(n-1)\mathbf{A}_{pre}^H \\ &+ \mathbf{A}_{next}\mathbf{R_s}(n+1)\mathbf{A}_{next}^H + \mathbf{R}_w\Big)^{-1} \cdot \mathbf{y}^{DFT}(n) \end{aligned} \tag{2.56}$$

This receiver attempts to jointly minimize the ICI, ISI and noise contributions.

2.4 Performance Characterization

Let us express the detector output for the l^{th} subcarrier from (2.40) as

$$\begin{aligned} z(n,l) &= [\mathbf{B}]_{l,l} \cdot s(n,l) + \sum_{m=-N/2, m\neq l}^{N/2-1} [\mathbf{B}]_{l,m} \cdot s(n,m) + \sum_{m=-N/2}^{N/2-1} [\mathbf{M}]_{l,m} \cdot w(n,m) \\ &+ \sum_{m=-N/2}^{N/2-1} [\mathbf{B}_{pre}]_{l,m} \cdot s(n-1,m) + \sum_{m=-N/2}^{N/2-1} [\mathbf{B}_{next}]_{l,m} \cdot s(n+1,m). \end{aligned} \quad (2.57)$$

Denote the modulation symbols contributing to ICI in the detection of the l^{th} subcarrier by $\bar{\mathbf{s}}_l(n)$. Assuming BPSK modulation with equal probability of $s(n,l) = +1$ and $s(n,l) = -1$, we can assume that $s(n,l) = +1$ without loss of generality, to yield

$$\begin{aligned} z(n,l) &= [\mathbf{B}]_{l,l} + \sum_{m=-N/2, m\neq l}^{N/2-1} [\mathbf{B}]_{l,m} \cdot s(n,m) + \sum_{m=-N/2}^{N/2-1} [\mathbf{B}_{pre}]_{l,m} \cdot s(n-1,m) \\ &+ \sum_{m=-N/2}^{N/2-1} [\mathbf{B}_{next}]_{l,m} \cdot s(n+1,m) + w'(n,l) \end{aligned} \quad (2.58)$$

which constitutes the test statistic for a given receiver. Defining the signal amplitude as

$$\begin{aligned} &\alpha_{(n,l)}^{RxType}(\mathbf{A}, \mathbf{A_{pre}}, \mathbf{A_{next}}, \bar{\mathbf{s}}_l(n), \mathbf{s}(n-1), \mathbf{s}(n+1)) \triangleq [\mathbf{B}]_{l,l} \\ &+ \sum_{m=-N/2, m\neq l}^{N/2-1} [\mathbf{B}]_{l,m} \cdot s(n,m) + \sum_{m=-N/2}^{N/2-1} [\mathbf{B}_{pre}]_{l,m} \cdot s(n-1,m) \\ &+ \sum_{m=-N/2}^{N/2-1} [\mathbf{B}_{next}]_{l,m} \cdot s(n+1,m), \end{aligned} \quad (2.59)$$

for BPSK modulation, conditioned on the channel, $\mathbf{A}, \mathbf{A_{pre}}, \mathbf{A_{next}}$, the ICI, $\bar{\mathbf{s}}_l(n)$, and the ISI, $\mathbf{s}(n-1), \mathbf{s}(n+1)$, the BER is given by

$$p_{(n,l)}^{BPSK}(error|\mathbf{A}, \mathbf{A}_{pre}, \mathbf{A}_{next}, \bar{\mathbf{s}}_l(n), \mathbf{s}(n-1), \mathbf{s}(n+1))$$

$$= Q\left(\alpha_{(n,l)}^{RxType}(\cdot)\sqrt{2/\sigma_{w'}^2(n,l)}\right). \tag{2.60}$$

The vector $\bar{\mathbf{s}}_l(n)$ can take 2^{N-1} different values, while the vectors $\mathbf{s}(n-1)$ and $\mathbf{s}(n+1)$ can take 2^N different values. Hence, we can average the BER in (2.60) over these to yield

$$p_{(n,l)}^{BPSK}(error|\mathbf{A}, \mathbf{A}_{pre}, \mathbf{A}_{next}) = \frac{1}{2^{3N-1}} \sum_{i_n=0}^{2^{N-1}-1} \sum_{i_{n-1}=0}^{2^N-1} \sum_{i_{n+1}=0}^{2^{N-1}} Q\left(\alpha_{(n,l)}^{RxType}(\cdot)\sqrt{2/\sigma_{w'}^2(n,l)}\right). \tag{2.61}$$

We can further average the BER across subcarriers yielding

$$\overline{p}_n^{BPSK}(error|\mathbf{A}, \mathbf{A}_{pre}, \mathbf{A}_{next}) = \frac{1}{N} \sum_{l=-N/2}^{N/2-1} p_{(n,l)}^{BPSK}(error|\mathbf{A}, \mathbf{A}_{pre}, \mathbf{A}_{next}). \tag{2.62}$$

Figure 2.2 shows the average BER, $\overline{p}_n^{BPSK}(error|\mathbf{A}, \mathbf{A}_{pre}, \mathbf{A}_{next})$ for two channel realizations, one incurring ISI and the other not incurring ISI. A residual frequency error of 5% of the subcarrier frequency spacing producing ICI is assumed in both cases. We further assume perfect timing, i.e., $\tau = 0$, and data detection using the ST receiver. The average BER is obtained from the test statistics (Equation (2.62)), from simulations and from approximating the interference component of the final test statistic as a Gaussian random variable. The BER assuming Gaussian interference uses the SINR expressions in Section 2.3 and $p_e = Q(\sqrt{2\gamma})$ is plotted. Note that the number of subcarriers for the channel realization not incurring ISI was chosen to be *N*=16, and for the channel realization incurring ISI was chosen to be *N*=8. Further, note that, despite the low value of *N* chosen, the Gaussian approximation, as also found in [17], provides a good match with simulations and the exact prediction using the test statistic, and therefore, will be made in the sequel.

Similar to other studies [4], [15], [17] for certain channel models, Figure 2.3

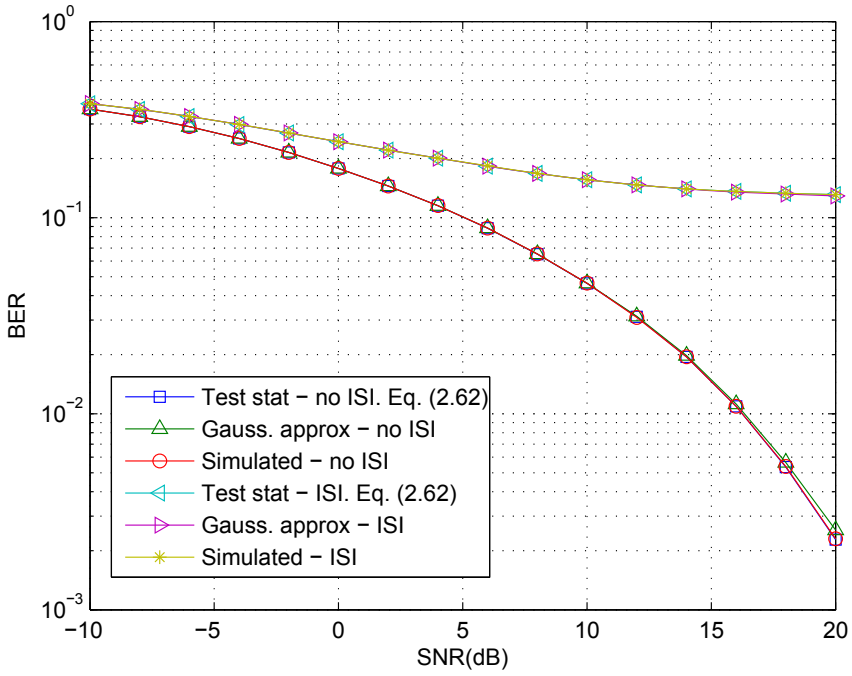

Figure 2.2 *BER performance using test statistic, simulation and Gaussian approximation of ICI and ISI*

through Figure 2.6 show the sensitivity to the CP duration of an ensemble of 1000 channel realizations for the UWB channel models CM1, CM2, CM3, and CM4 defined in [29]. CM1 is based on (0-4m) line-of-sight (LOS) channel measurements with a root-mean-square (RMS) delay spread of 5ns. CM2 is based on (0-4m) non-line-of-sight (NLOS) channel measurements with an RMS delay spread of 8ns. CM3 is based on (4-10m) NLOS channel measurements with an RMS delay spread of 15ns. Finally, CM4 was generated to fit a 25ns RMS delay spread.

All the results assume a system with a subcarrier spacing of 4.125MHz, N=128 subcarriers [34], and a Nyquist filter with 0% roll-off and bandwidth 528MHz. Note that CP durations of 0, 16, 32, 48, 64, and 80 samples constitute 0%, 11.11%, 20%, 27.27%, 33.33%, and 38.46% fixed overhead. The results shown in Figure 2.3 through Figure 2.6 assume perfect time and frequency synchronization, an ST receiver, and result from averaging the performance over 1000 channel realizations. Note that for each of the

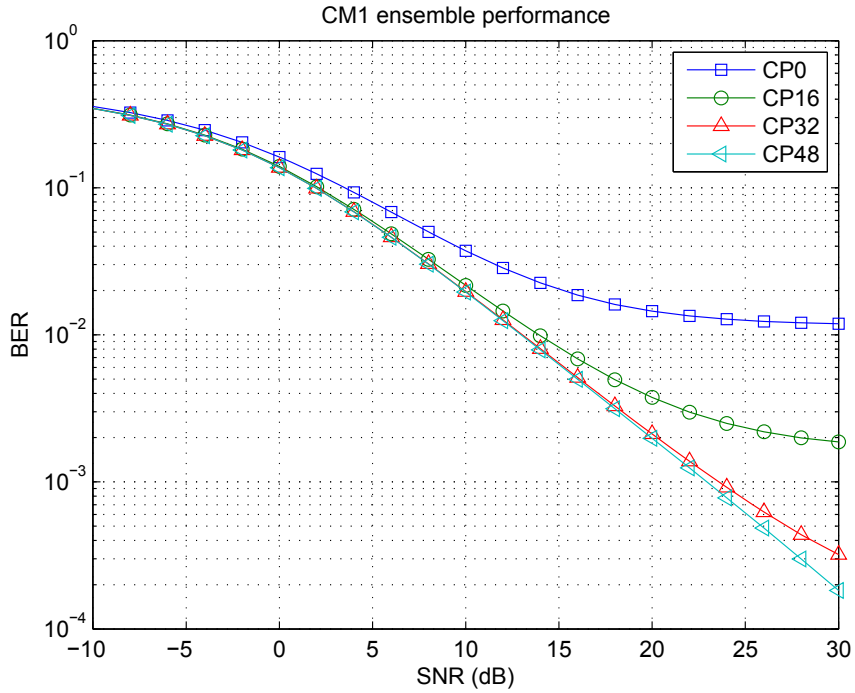

Figure 2.3 *BER sensitivity to CP duration for CM1*

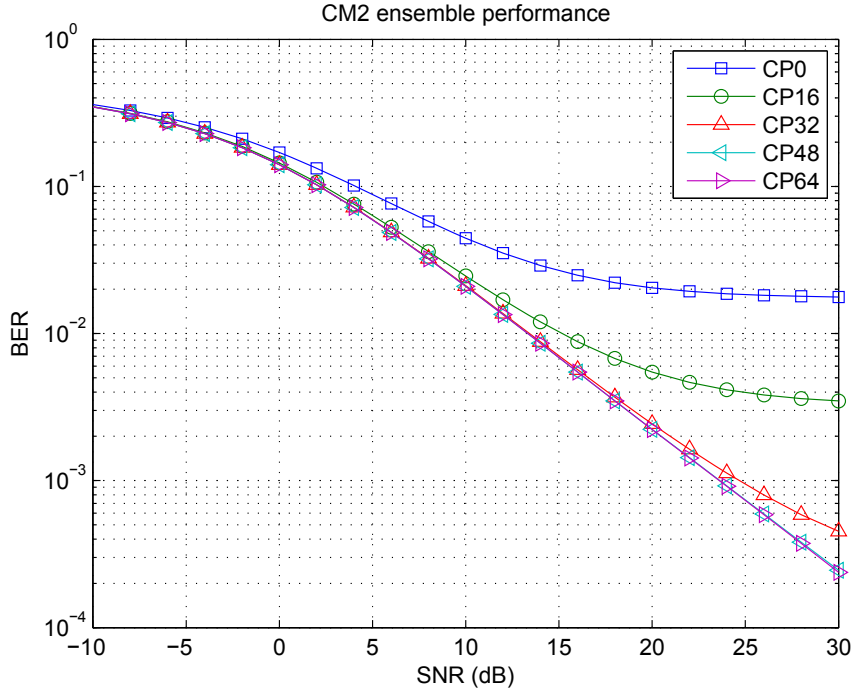

Figure 2.4 *BER sensitivity to CP duration for CM2*

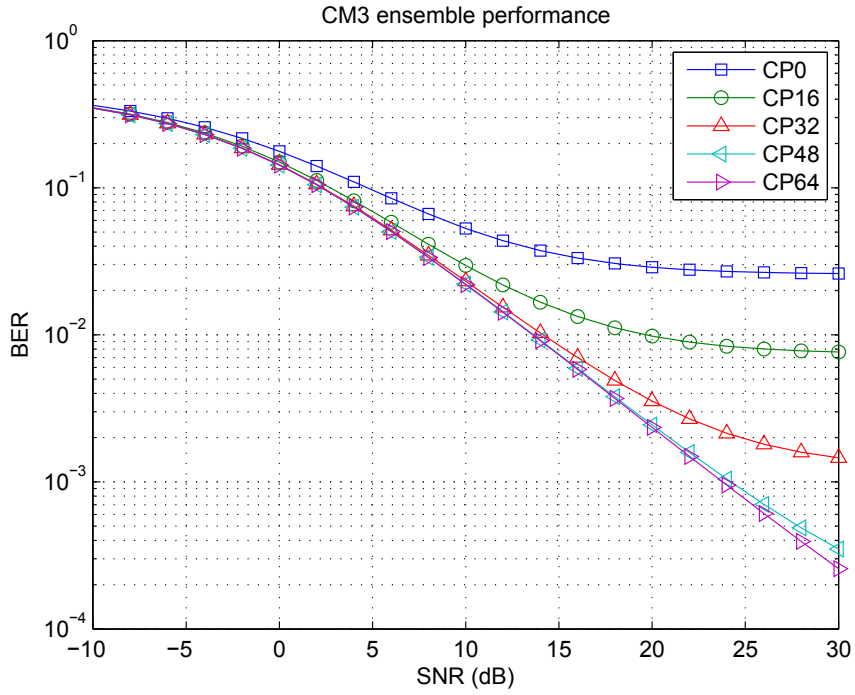

Figure 2.5 *BER sensitivity to CP duration for CM3*

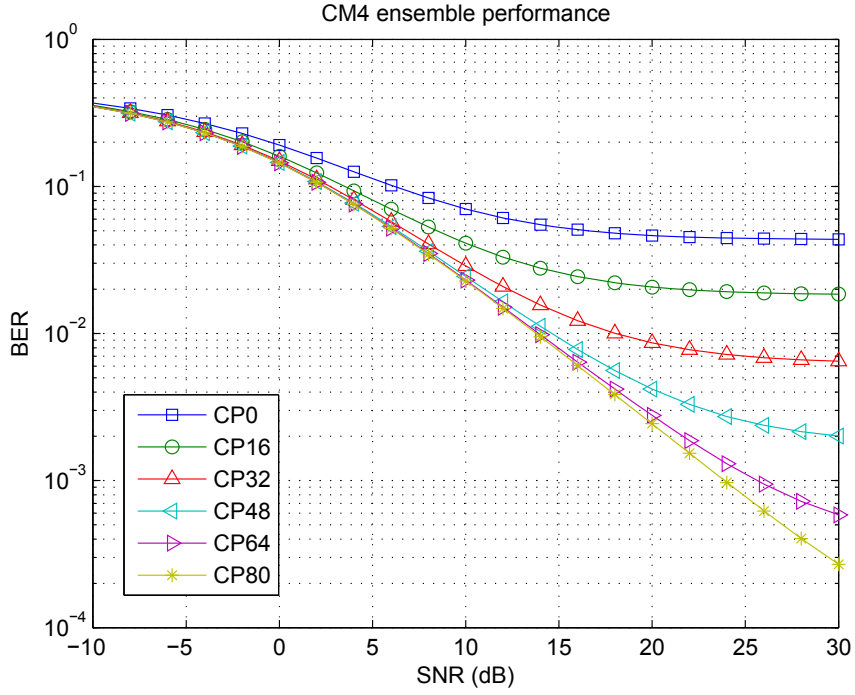

Figure 2.6 *BER sensitivity to CP duration for CM4*

channel models, at some point a longer CP does not improve the performance; this is the point where the ISI is not significant.

Figure 2.7 shows the sensitivity to frequency errors for a given CM1 channel realization. The results are obtained assuming a system with N=128, 20% CP overhead, perfect time synchronization, a Nyquist filter with 0% roll-off and a bandwidth of 528MHz, and an ST receiver. This figure contains analytical (distinguished by lines with inserted characters, e.g., '-*-') and simulation based (distinguished by just characters, e.g., '*') results for frequency errors ranging from 0 to 5% of the subcarrier frequency spacing. Assuming a $\pm$20ppm frequency tolerance at the transmitter and at the receiver, the maximum frequency error incurred would be $\pm$40ppm, which for a 5GHz carrier frequency and 4.125MHz subcarrier spacing equates to a frequency error of 5% of the subcarrier spacing. Note that the frequency error in actual systems would typically be compensated by some frequency compensation mechanism, so that these results show the performance at different levels of residual frequency error. From the results, we can see a graceful performance degradation as frequency errors increase.

Figure 2.8 shows the sensitivity to timing errors for a given CM1 channel realization. The same assumptions as for the results in Figure 2.7 are made, with the exception that now we assume perfect frequency synchronization in order to concentrate on the performance impact of varying the transmit/receive timing error, τ. A positive value of τ means that the OFDM symbol boundary at the receiver is late with respect to the actual symbol boundary, and therefore inevitably there will be ISI from the next OFDM symbol. A negative value of τ advances the OFDM symbol boundary, but since the CP is preceding the OFDM symbol, the actual effect is equivalent to that of a shortened CP. Unlike the frequency errors, the performance degradation for a positive timing error may be quite abrupt, as seen in Figure 2.8. The performance degradation of a negative timing error is much more graceful, as it is equivalent to a shortened CP. Figure 2.9 illustrates this fact graphically, showing the impact of timing error as it affects ISI.

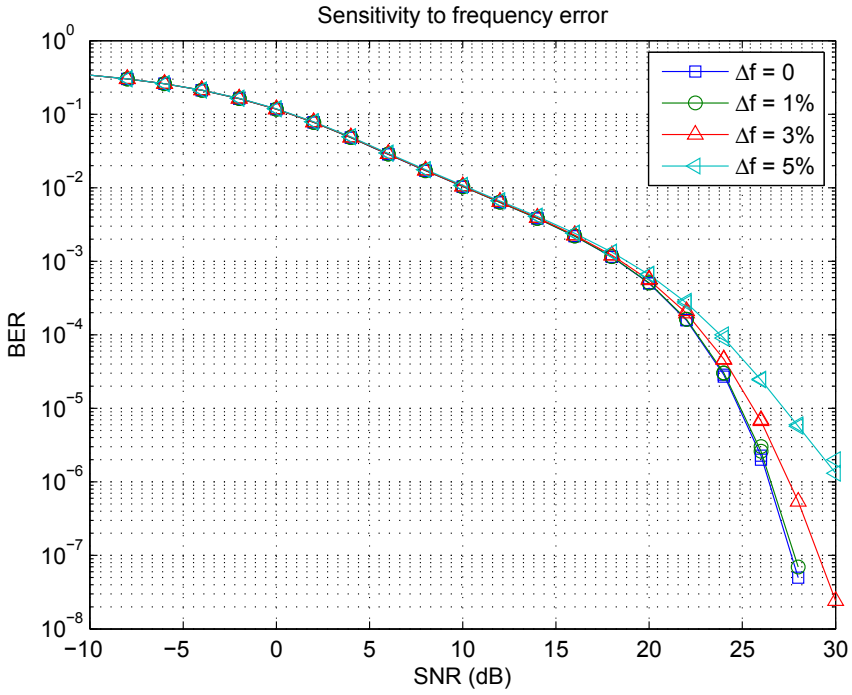

Figure 2.7 *BER sensitivity to residual frequency error (analysis and simulation)*

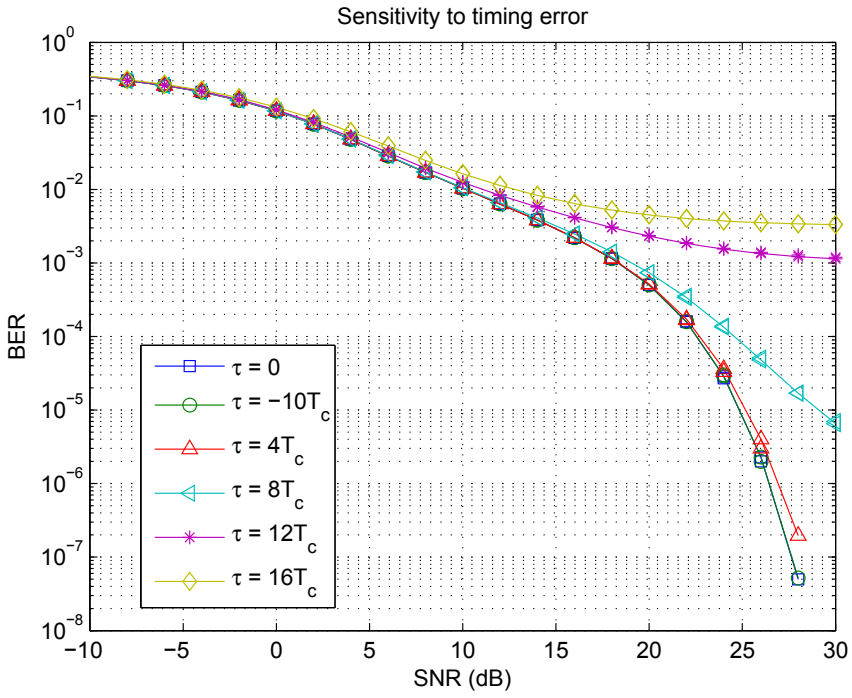

Figure 2.8 *BER sensitivity to timing error (analysis and simulation)*

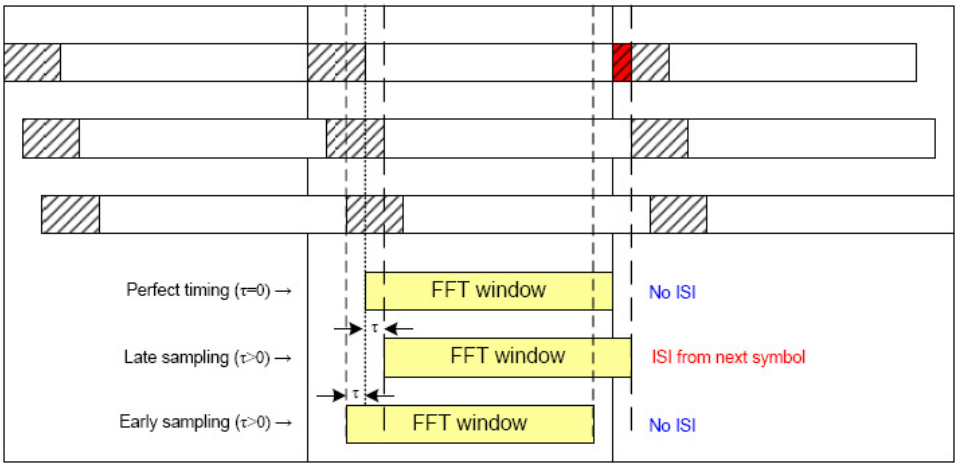

Figure 2.9 *ISI impact of transmit/receive timing error*

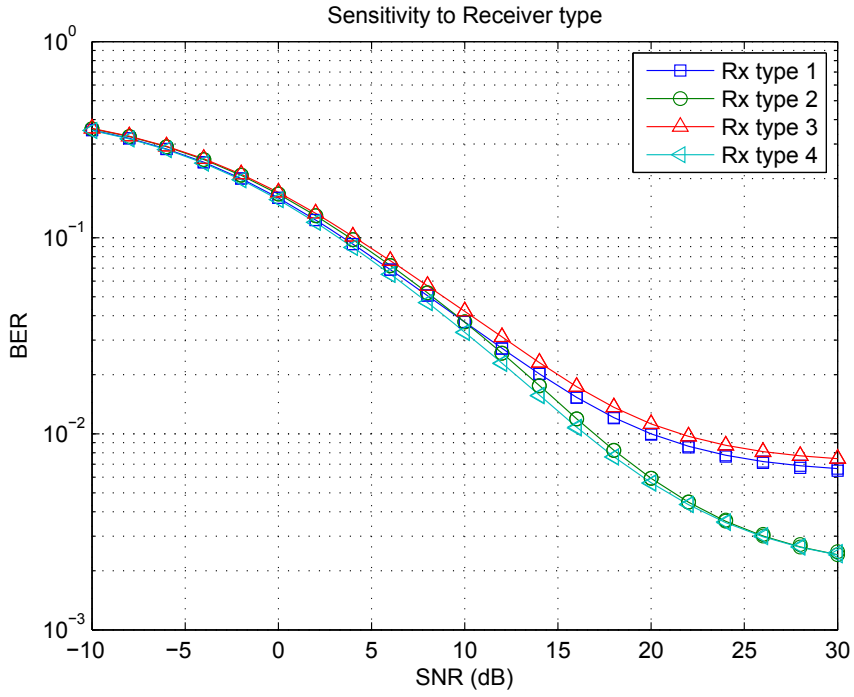

Figure 2.10 *Receiver type sensitivity (analysis and simulation)*

Figure 2.10 shows the sensitivity to the data detection criterion (receiver type) for a given CM4 channel realization incurring ISI. We keep the same hypothesis as for Figure 2.7 and Figure 2.8 in terms of number of subcarriers, subcarrier spacing, filtering, and CP overhead. The results shown assume a 1% frequency error. However, the interference is dominated by the ISI/ICI incurred from a channel delay spread larger than the CP duration. We compare the BER for the data detection criteria presented in Section 2.3. The receiver type 1 (ST) ignores the ICI, ISI and noise terms, however, there is no interference or noise enhancement at the detector output. The receiver type 2 (ZF) tries to minimize the signal-dependent interference, while ignoring the noise term. As we can see, the performance at high SNR matches that of receiver type 4 (MMSE). The receiver type 3 (modified ZF accounting for ICI only) cancels perfectly the ICI, but ignores the ISI and noise terms, and hence enhances their impact. The net effect is a performance close to that of the single tap equalizer receiver which does not attempt to suppress ICI or ISI. The receiver type 4 (MMSE) takes into account the statistics of the ICI, ISI and noise, and achieves the best noise-and-interference suppression. This receiver requires, in addition to the channel state information, knowledge of the noise and interference statistics. However, adaptive techniques such as LMS or RLS implementations can be used without the need of an explicit characterization of the noise and interference statistics.

2.5 Concluding Remarks

An OFDM model thoroughly characterizing the ISI and ICI terms has been presented. Different data detectors have been formulated, and performance comparisons were presented. Section 2.4 specialized the model to UWB systems, and results in Section 2.3 were used to characterize the sensitivity of an OFDM-based UWB system to key system parameters. However, the model introduced in this chapter can be used for other OFDM systems in conjunction with studies of channel estimation, time and frequency correction, and multi-antenna techniques.

2.6 Acknowledgements

This chapter is a reprint of the material as it appears in "Effects of Imperfections on the Performance of OFDM Systems," accepted for publication in *IEEE Transactions on Communications*. The dissertation author was the primary author and Prof. Laurence B. Milstein directed and supervised the research which forms the basis for this chapter.

CHAPTER 3

Channel Estimation for Non-Ideal OFDM Systems

3.1 Introduction

Channel estimation plays an integral role in systems relying on coherent demodulation. The receiver generates the channel estimates from the processing of a training signal of known values (also referred to as a pilot signal). This estimate can be further improved by the use of data symbols by way of decision feedback mechanisms. In OFDM systems, channel estimation consists of estimating the channel gain at each of the frequency subcarriers. In case of no inter-carrier interference (ICI) and no inter-symbol interference (ISI), the channel gain at each of the subcarriers is simply the channel frequency response evaluated at the corresponding subcarrier. However, in the case of ICI and/or ISI, the channel gain for each of the subcarriers is a distorted version of the channel frequency response at the corresponding subcarrier, as derived in [47], [49], [51].

Channel estimation in the context of OFDM systems has primarily focused on the algorithm performance/complexity trade-off. However, the cyclic prefix has been widely assumed to be longer than the channel delay spread [2], [5], [7]-[10], [14], [16], [18], [21], [22], [24], [26]-[28], [32], [37], [44], [46] and hence, the focus has been on the ISI-free case. Reference [31] indicated the importance of considering ISI in channel estimation, but only presented numerical evaluations. This chapter studies the impact of ISI/ICI on the channel estimation of OFDM systems. We look into several channel estimation criteria

focusing on robustness and performance aspects. The channel estimates are applied to the DFT output of the OFDM receiver in order to enable coherent detection of the received symbols. This operation changes the statistics of the DFT output, conditioned on the channel realization, from complex Gaussian to a special case of a Gaussian quadratic form. We derive analytical expressions for the BER performance and compare it with Monte Carlo simulations.

The chapter is structured as follows: Section 3.2 presents the system model and characterizes the DFT output of the OFDM receiver. Different channel estimation methods for OFDM systems are analyzed in Section 3.3. We focus on linear estimators and, in particular, on the simple frequency domain least squares algorithm and on DFT-based channel estimation algorithms. Section 3.4 characterizes the data detector output and provides an analytical bit-error rate (BER) characterization for OFDM systems with realistic channel estimation. Section 3.5 presents numerical results for the channel estimation methods introduced in Section 3.3 using as example different ultra-wideband (UWB) channel models with various imperfections. Finally, Section 3.6 provides some concluding remarks.

3.2 System Model

The system model is the same as that used in [51], where the discrete-time OFDM transmit waveform at baseband is given by

$$u_{n,k} = \frac{1}{\sqrt{N}} \sum_{m=-N/2}^{N/2-1} s_{n,m} \cdot e^{j2\pi m(k-CP)/N} \cdot \Pi_s \left[\frac{k}{N_T} \right] \tag{3.1}$$

and where N is the number of subcarriers, CP is the duration of the cyclic prefix in samples, $N_T = N + CP$, and $s_{n,m}$ are the information symbols, in general complex-valued. The index n is used as a time index throughout the chapter and refers to a particular OFDM symbol. The index m, in turn, is used as a subcarrier index within the OFDM

symbol, and the index k is used as a time index for samples within a given OFDM block. The OFDM symbol duration is $T \triangleq NT_c$, and the OFDM block duration is $T_f \triangleq N_T T_c$, where T_c is the symbol duration prior to OFDM modulation. Finally, $\Pi_s[k/N_T]$ is the shifted rectangular function with unit amplitude and spanning the interval $k \in [0, N_T - 1]$.

The transmitter gives analog support to the discrete-time signal $u_{n,k}$ by way of either a digital-to-analog conversion (DAC) or a pulse shaping filter that we denote by $h^{tx}(t)$. After up-conversion to the carrier frequency, f_0, the transmitter output signal becomes

$$x(t) = \Re\left\{\sum_n \sum_{k=0}^{N_T-1} u_{n,k} \cdot h^{tx}(t - kT_c - nT_f) \cdot e^{j2\pi \hat{f}_0 t}\right\} \tag{3.2}$$

where $\hat{f}_0$ is the locally generated carrier frequency at the OFDM transmitter.

The channel low pass equivalent's impulse response is denoted by $h_{lp}^{ch}(t)$ and can be expressed as $h_{lp}^{ch}(t) \triangleq \sum_{p=0}^{P-1} \lambda_p \cdot \delta(t - D_p)$. Therefore, the channel output may be expressed as

$$r(t) = \Re\left\{\sum_{p=0}^{P-1} \lambda_p \sum_n \sum_{k=0}^{N_T-1} u_{n,k} \cdot h^{tx}(t - D_p - kT_c - nT_f) \cdot e^{j2\pi \hat{f}_0 t}\right\} + n(t) \tag{3.3}$$

where $\{\lambda_p\}$ represent the taps of the channel's lowpass equivalent impulse response. The channel is considered to be slowly varying and, in particular, constant during an OFDM symbol duration. The lowpass equivalent of the channel noise, $n_{lp}(t)$, is assumed to be complex circular white Gaussian (AWGN) with zero mean and two-sided power spectral density N_0.

Figure 3.1 is a block diagram of the OFDM receiver. The receiver performs, first, a down-conversion to baseband using the locally generated carrier frequency denoted by $\hat{\hat{f}}_0$. The down-conversion is followed by a lowpass filtering operation and subsequent sampling. The lowpass filtering is performed using a filter with impulse response $h^{rx}(t)$. The CP is discarded and then a DFT is performed.

The effective channel impulse response, $h(t)$, is the convolution of the transmit

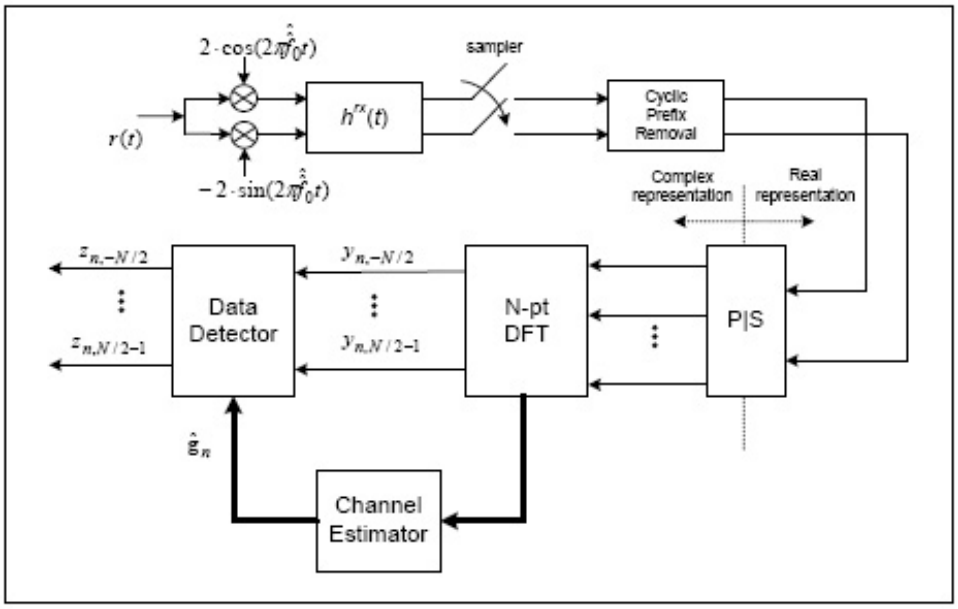

Figure 3.1 *Block diagram of OFDM receiver*

filter, receive filter and low-pass equivalent channel impulse response, i.e., $h(t) \triangleq h^{tx}(t) * h_{lp}^{ch}(t) * h^{rx}(t)$. Assuming that $h(t)$ spans the continuous time interval $[D_{\min}, D_{\max}]$, then its sampled version, $h(kT_c)$, spans the sample interval $[\lceil D_{\min}/T_c \rceil, \lfloor D_{\max}/T_c \rfloor]$. Considering a possible transmit/receive timing error, τ, the signal $h(t+\tau)$ spans the time interval $[D_{\min} - \tau, D_{\max} - \tau]$ and its sampled version, $h(kT_c + \tau)$, spans the sample interval $[\lceil (D_{\min} - \tau)/T_c \rceil, \lfloor (D_{\max} - \tau)/T_c \rfloor]$. Note that, in general, the transmit/receive timing error, τ, is much smaller than the channel delay spread, therefore, $\tau << D_{\max}$. Let us denote the sample interval limits for the effective channel impulse response as L_L for the lower limit and L_U for the upper limit, i.e.,

$$L_L \triangleq \lceil (D_{\min} - \tau)/T_c \rceil \text{ and } L_U \triangleq \lfloor (D_{\max} - \tau)/T_c \rfloor. \tag{3.4}$$

The DFT output at the *l*th subcarrier of the *n*th OFDM symbol was characterized in [51] to be

$$y_{n,l} = \sum_{m=-N/2}^{N/2-1} A_{l,m} \cdot s_{n,m} + \sum_{m=-N/2}^{N/2-1} B_{l,m}^{pre} \cdot s_{n-1,m} + \sum_{m=-N/2}^{N/2-1} B_{l,m}^{next} \cdot s_{n+1,m} + y_{n,l}^{noise} \tag{3.5}$$

where

$$
\begin{aligned}
A_{l,m} \triangleq \frac{\alpha_n}{N}\Bigg(& \sum_{k=\max(0,L_U-CP)}^{\min(N-1,N+L_L-1)} e^{j2\pi(\overline{\Delta f}+m-l)k/N}\cdot H(m) \\
& + \underbrace{\sum_{k=0}^{L_U-CP-1} e^{j2\pi(\overline{\Delta f}+m-l)k/N} \sum_{\nu=L_L}^{k+CP} h(\nu T_c+\tau)\cdot e^{-j2\pi m\nu/N}}_{\text{if } L_U>CP} \\
& + \underbrace{\sum_{k=N+L_L}^{N-1} e^{j2\pi(\overline{\Delta f}+m-l)k/N} \sum_{\nu=k-(N-1)}^{L_U} h(\nu T_c+\tau)\cdot e^{-j2\pi m\nu/N}}_{\text{if } L_L<0}\Bigg).
\end{aligned} \tag{3.6}
$$

If $L_U > CP$

$$
B_{l,m}^{pre} \triangleq \frac{\alpha_n}{N}\cdot e^{j2\pi mCP/N} \sum_{k=0}^{L_U-CP-1} e^{j2\pi(\overline{\Delta f}+m-l)k/N} \sum_{\nu=k+CP+1}^{L_U} h(\nu T_c+\tau)\cdot e^{-j2\pi m\nu/N}, \tag{3.7}
$$

and $B_{l,m}^{pre} \triangleq 0$ if $L_U \leq CP$. Finally, if $L_L < 0$

$$
B_{l,m}^{next} \triangleq \frac{\alpha_n}{N}\cdot e^{-j2\pi mCP/N} \sum_{k=N+L_L}^{N-1} e^{j2\pi(\overline{\Delta f}+m-l)k/N} \sum_{\nu=L_L}^{k-N} h(\nu T_c+\tau)\cdot e^{-j2\pi m\nu/N}, \tag{3.8}
$$

and $B_{l,m}^{next} \triangleq 0$ if $L_L \geq 0$. Note that there is no time-dependency in (3.6), (3.7) and (3.8) because the analysis assumes the channel realization remains constant over the OFDM symbol span. The effective channel frequency response at the *l*th subcarrier is defined to be $H(l) \triangleq \sum_{\nu=L_L}^{L_U} h(\nu T_c+\tau)\cdot e^{-j2\pi l\nu/N}$. The residual frequency error at the receiver is defined by $\Delta f \triangleq (\hat{f}_0 - \hat{\hat{f}}_0)$ and its normalized version by $\overline{\Delta f} \triangleq \frac{\Delta f}{1/T}$, where $1/T$ is the subcarrier frequency spacing. Finally, $\alpha_n \triangleq e^{j2\pi\overline{\Delta f}(nN_T+CP+\tau)/N}$ provides the initial phase at the *n*th OFDM symbol.

The noise component, $y_{n,l}^{noise}$, in (3.5) is a complex Gaussian with zero mean and covariance $K_{y^{noise}}(n_1,l_1;n_2,l_2) = 1/2\cdot E\{y_{n_1,l_1}^{noise}\cdot y_{n_2,l_2}^{noise*}\} = N_0\cdot\delta_K(n_2-n_1)\cdot\delta_K(l_2-l_1)$ provided that the autocorrelation of the receive front-end filter satisfies the following

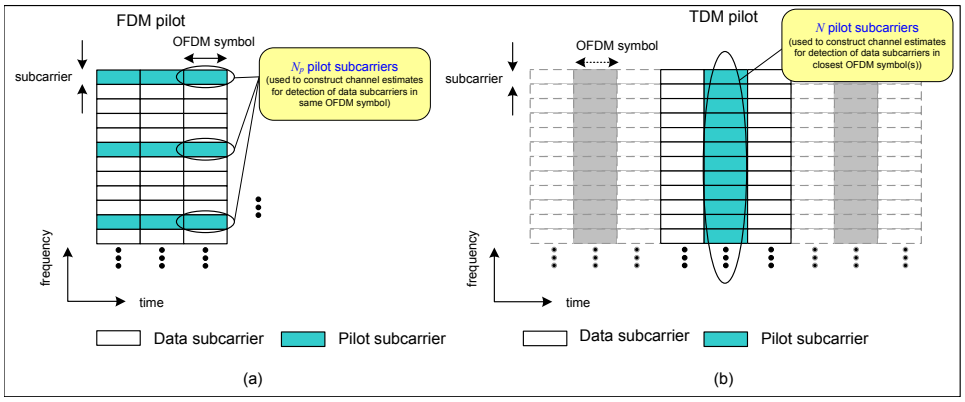

Figure 3.2 *TDM vs. FDM pilot*

condition: $R_{h_{rx}}(kT_c) = \delta_K(k)$, where $\delta_K(k)$ represents the Kronecker delta function defined as $\delta_K(k) \triangleq \begin{cases} 1 \text{ if } k = 0 \\ 0 \text{ else} \end{cases}$.

This chapter focuses on the channel estimation problem in the presence of both residual frequency and timing errors. The residual frequency error, Δf, and the transmit-receive timing error, τ, are assumed to be constant for the time span of the channel estimation process.

3.3 Channel Estimation

In order to perform coherent demodulation at the receiver, reference signals known at the transmitter and the receiver need to be transmitted within the OFDM waveform. Different ways to transmit the reference or pilot signal exist as shown in Figure 3.2.

In plot (a) of Figure 3.2, the pilot subcarriers are placed in every OFDM symbol multiplexed with the data subcarriers in the frequency domain (FDM). In this case, there is one pilot subcarrier every several subcarriers (note that in the illustration there is one pilot subcarrier every five subcarriers). We will refer to this structure as an FDM pilot. In plot (b) of Figure 3.2, the pilot is time-division multiplexed (TDM) with the data. In this case, there is one OFDM symbol with pilot signal every several OFDM symbols (note

that in the illustration there is one OFDM symbol with pilot signal every three OFDM symbols). When the pilot is present in an OFDM symbol it occupies all the subcarriers in that symbol and the channel estimates from the pilot signal are used in the closest OFDM symbols with data subcarriers (data subcarriers with solid lines in the illustration). We will refer to this structure as a TDM pilot. The channel estimation problem, however, is the same for either method and therefore we will keep a generic notation that applies to both techniques. Later in the development, we will specialize to a specific pilot transmission strategy and channel estimation criterion.

If we want to discriminate between contributions of the data and pilot subcarriers at the output of the DFT, we can re-write (3.5) as

$$y_{n,l} = \sum_{m\in\{D(n)\}} A_{l,m}s_{n,m} + \sum_{m\in\{P(n)\}} A_{l,m}s_{n,m} + \sum_{m\in\{D(n-1)\}} B^{pre}_{l,m}s_{n-1,m} \tag{3.9}$$
$$+ \sum_{m\in\{P(n-1)\}} B^{pre}_{l,m}s_{n-1,m} + \sum_{m\in\{D(n+1)\}} B^{next}_{l,m}s_{n+1,m} + \sum_{m\in\{P(n+1)\}} B^{next}_{l,m}s_{n+1,m} + y^{noise}_{n,l}$$

where we have defined $\{P(n)\}$ as the set of pilot subcarriers, and $\{D(n)\}$ as the set of data subcarriers in the *n*th OFDM symbol. Also, we start denoting the modulation symbols for the pilot subcarriers as $p_{n,m}$ to distinguish them from the data symbols, $s_{n,m}$.

For a data subcarrier, i.e., if $l \in \{D(n)\}$, we can re-write (3.9) as

$$y_{n,l} = A_{l,l}s_{n,l} + \sum_{m\in\{D(n)\backslash l\}} A_{l,m}s_{n,m} + \sum_{m\in\{P(n)\}} A_{l,m}p_{n,m} + \sum_{m\in\{D(n-1)\}} B^{pre}_{l,m}s_{n-1,m}$$
$$+ \sum_{m\in\{P(n-1)\}} B^{pre}_{l,m}p_{n-1,m} + \sum_{m\in\{D(n+1)\}} B^{next}_{l,m}s_{n+1,m} + \sum_{m\in\{P(n+1)\}} B^{next}_{l,m}p_{n+1,m}$$
$$+ y^{noise}_{n,l} \tag{3.10}$$

and for a pilot subcarrier, i.e., if $l \in \{P(n)\}$

$$y_{n,l} = A_{l,l}p_{n,l} + \sum_{m\in\{D(n)\}} A_{l,m}s_{n,m} + \sum_{m\in\{P(n)\backslash l\}} A_{l,m}p_{n,m} + \sum_{m\in\{D(n-1)\}} B^{pre}_{l,m}s_{n-1,m}$$

$$+ \sum_{m\in\{P(n-1)\}} B_{l,m}^{pre} p_{n-1,m} + \sum_{m\in\{D(n+1)\}} B_{l,m}^{next} s_{n+1,m} + \sum_{m\in\{P(n+1)\}} B_{l,m}^{next} p_{n+1,m} + y_{n,l}^{noise} \tag{3.11}$$

where the set of subcarriers $\{D(n)\backslash l\}$ denotes all the data subcarriers in the *n*th OFDM symbol except the *l*th subcarrier. From (3.10) and (3.11), we can identify the useful term, the interference created by the pilot subcarriers, the interference created by the data subcarriers, and the noise. The useful term at the *l*th subcarrier of the *n*th OFDM symbol is $y_{n,l}^{useful} \triangleq A_{l,l} \cdot s_{n,l}$ for data subcarriers and is $y_{n,l}^{useful} \triangleq A_{l,l} \cdot p_{n,l}$ for pilot subcarriers. We define the channel gain of the useful component at the *l*th subcarrier of the DFT output by $\psi_l \triangleq A_{l,l}$. The interference created by the pilot subcarriers may be expressed as

$$w_{n,l}^{pilot} \triangleq \sum_{m\in\{P(n)\}} A_{l,m} \cdot p_{n,m} + \sum_{m\in\{P(n-1)\}} B_{l,m}^{pre} \cdot p_{n-1,m} + \sum_{m\in\{P(n+1)\}} B_{l,m}^{next} \cdot p_{n+1,m} \tag{3.12}$$

if $l \in \{D(n)\}$, and

$$w_{n,l}^{pilot} \triangleq \sum_{m\in\{P(n)\backslash l\}} A_{l,m} \cdot p_{n,m} + \sum_{m\in\{P(n-1)\}} B_{l,m}^{pre} \cdot p_{n-1,m} + \sum_{m\in\{P(n+1)\}} B_{l,m}^{next} \cdot p_{n+1,m} \tag{3.13}$$

if $l \in \{P(n)\}$. Note that for a given residual frequency and timing error, the interference created by the pilot subcarriers, conditioned on the channel realization, is deterministic, since the pilot subcarriers are, by definition, known at the transmitter and the receiver.

Finally, to shorten notation, we combine the noise and the data interference into a single term in (3.14) and (3.15):

$$w_{n,l} \triangleq \sum_{m\in\{D(n)\backslash l\}} A_{l,m} \cdot s_{n,m} + \sum_{m\in\{D(n-1)\}} B_{l,m}^{pre} \cdot s_{n-1,m} + \sum_{m\in\{D(n+1)\}} B_{l,m}^{next} \cdot s_{n+1,m} + y_{n,l}^{noise} \tag{3.14}$$

if $l \in \{D(n)\}$, and

$$\begin{aligned} w_{n,l} &\triangleq \sum_{m\in\{D(n)\}} A_{l,m}\cdot s_{n,m} + \sum_{m\in\{D(n-1)\}} B^{pre}_{l,m}\cdot s_{n-1,m} + \sum_{m\in\{D(n+1)\}} B^{next}_{l,m}\cdot s_{n+1,m} \\ &+ y^{noise}_{n,l} \end{aligned} \tag{3.15}$$

if $l \in \{P(n)\}$.

The covariance of the noise-and-interference in subcarriers l_1 and l_2 of the *n*th OFDM symbol, conditioned on the channel realization, is denoted by $K_w(n; l_1, l_2)$, and is computed in Appendix A. The variance of the noise-and-interference term in (3.14), conditioned on the channel realization, can be shown to be given by

$$\begin{aligned} \sigma^2_w(n,l) &\triangleq E\{|w_{n,l}|^2\}/2 \\ &= \sum_{m\in\{D(n)\backslash l\}} |A_{l,m}|^2\cdot E\{|s_{n,m}|^2\}/2 + \sum_{m\in\{D(n-1)\}} |B^{pre}_{l,m}|^2\cdot E\{|s_{n-1,m}|^2\}/2 \\ &+ \sum_{m\in\{D(n+1)\}} |B^{next}_{l,m}|^2\cdot E\{|s_{n+1,m}|^2\}/2 + N_0 \end{aligned} \tag{3.16}$$

for data subcarriers, where we have assumed independence of data modulation symbols across subcarriers and OFDM symbols. This variance can be easily computed from (3.15) for pilot subcarriers.

With this newly-introduced notation, we can re-write (3.10) and (3.11) as

$$y_{n,l} = \begin{cases} \psi_l\cdot s_{n,l} + w^{pilot}_{n,l} + w_{n,l} \text{ if } l\in\{D(n)\} \\ \psi_l\cdot p_{n,l} + w^{pilot}_{n,l} + w_{n,l} \text{ if } l\in\{P(n)\} \end{cases}, \tag{3.17}$$

respectively. From the processing of the pilot subcarriers at the DFT output, i.e., the second expression in (3.17), we will derive the channel estimates at all the data subcarriers for coherent demodulation of the data. We denote the channel estimate at the *l*th subcarrier of the *n*th OFDM symbol by $\hat{g}_{n,l}$. In order to measure the quality of the channel estimates, we define its mean value, conditioned on the channel realization, as $\hat{\psi}_{n,l} \triangleq E\{\hat{g}_{n,l}\}$ and its

noise-and-interference as $v_{n,l} \triangleq \hat{g}_{n,l} - E\{\hat{g}_{n,l}\}$. Therefore, the channel estimator output will be expressed as

$$\hat{g}_{n,l} \triangleq \hat{\psi}_{n,l} + v_{n,l}. \tag{3.18}$$

The mean value of the channel estimate, conditioned on the channel realization, will directly determine whether the channel estimate is biased or not. With the channel estimate's mean and variance, we can derive the mean square error (MSE) of the channel estimate, conditioned on the channel realization, as

$$MSE(n,l) \triangleq E\{|\hat{g}_{n,l} - \psi_l|^2\} = E\{|\hat{\psi}_{n,l} - \psi_l + v_{n,l}|^2\} = |\hat{\psi}_{n,l} - \psi_l|^2 + 2\sigma_v^2(n,l) \tag{3.19}$$

which is the sum of the power of the bias and the variance of the estimator.

3.3.1 Frequency Domain Least Squares Channel Estimation

The first step to perform for many channel estimation algorithms is to remove the known data modulation symbols at each of the pilot subcarriers, yielding

$$\hat{g}_{n,l}^{FD-LS} = y_{n,l}/p_{n,l}, l \in \{P(n)\} \tag{3.20}$$

The estimate in (3.20) is the simplest channel estimator. It is called a frequency domain (FD) least-squares (LS) estimator [2], and we will look into it in detail as it is the starting point for the other linear channel estimators in this chapter.

Using (3.17), we can re-write (3.20) as

$$\hat{g}_{n,l}^{FD-LS} = (\psi_l \cdot p_{n,l} + w_{n,l}^{pilot} + w_{n,l})/p_{n,l} = \psi_l + w_{n,l}^{pilot}/p_{n,l} + w_{n,l}/p_{n,l}, l \in \{P(n)\} \tag{3.21}$$

Therefore, the mean value of this estimator, conditioned on the channel realization, is

$$\hat{\psi}_{n,l}^{FD-LS} \triangleq E\{\hat{g}_{n,l}^{FD-LS}\} = \psi_l + w_{n,l}^{pilot}/p_{n,l}, l \in \{P(n)\} \tag{3.22}$$

and the noise-and-interference term is

$$v_{n,l}^{FD-LS} \triangleq \hat{g}_{n,l}^{FD-LS} - E\{\hat{g}_{n,l}^{FD-LS}\} = w_{n,l}/p_{n,l}, l \in \{P(n)\} \tag{3.23}$$

The covariance of the noise-and-interference in subcarriers l_1 and l_2 at the *n*th OFDM symbol, conditioned on the channel realization, is defined to be

$$K_{v_{FD-LS}}(n; l_1, l_2) \triangleq E\{v_{n,l_1}^{FD-LS} \cdot v_{n,l_2}^{FD-LS*}\}/2 = \frac{1}{p_{n,l_1} \cdot p_{n,l_2}^*} E\{w_{n,l_1} \cdot w_{n,l_2}^*\}/2 \tag{3.24}$$

Using the result in Appendix A, and given that l_1 and l_2 are pilot subcarriers, we can re-write (3.24) as

$$\begin{aligned} K_{v_{FD-LS}}(n; l_1, l_2) = \frac{1}{p_{n,l_1} \cdot p_{n,l_2}^*} \Big(& P_d \sum_{m \in \{D(n)\}} A_{l_1,m} \cdot A_{l_2,m}^* \\ & + P_d \sum_{m \in \{D(n-1)\}} B_{l_1,m}^{pre} \cdot B_{l_2,m}^{pre*} + P_d \sum_{m \in \{D(n+1)\}} B_{l_1,m}^{next} \cdot B_{l_2,m}^{next*} + N_0 \cdot \delta_K(l_2 - l_1) \Big) \end{aligned} \tag{3.25}$$

where we have assumed constant average power of the data modulation symbols across the OFDM symbols, i.e., $P_d \triangleq E\{|s_{n,m}|^2\}/2 = E\{|s_{n-1,m}|^2\}/2 = E\{|s_{n+1,m}|^2\}/2$, and independence of the data modulation symbols across both subcarriers and OFDM symbols.

The variance of the channel estimate, conditioned on the channel realization, is easily obtained from (3.25) as

$$\begin{aligned} & \sigma_{v_{FD-LS}}^2(n, l) \triangleq K_{v_{FD-LS}}(n; l, l) \\ & = \frac{P_d}{|p_{n,l}|^2} \Big(\sum_{m \in \{D(n)\}} |A_{l,m}|^2 + \sum_{m \in \{D(n-1)\}} |B_{l,m}^{pre}|^2 + \sum_{m \in \{D(n+1)\}} |B_{l,m}^{next}|^2 + \frac{1}{P_d} N_0 \Big) \end{aligned} \tag{3.26}$$

We can now compute the MSE of the FD-LS estimate at the *l*th subcarrier of the *n*th

OFDM symbol, conditioned on the channel realization, from (3.19) as

$$MSE_{FD-LS}(n,l) = |w_{n,l}^{pilot}/p_{n,l}|^2 + 2\sigma^2_{v_{FD-LS}}(n,l) \tag{3.27}$$

3.3.2 Linear Channel Estimator - General Case

In general, a linear channel estimator can be expressed as a linear combination of the FD-LS channel estimation at the different subcarriers, i.e.,

$$\hat{g}_{n,l} \triangleq \sum_{m\in\{P(n)\}} \Omega_{l,m} \cdot \hat{g}_{n,m}^{FD-LS} \tag{3.28}$$

Therefore, in general, the mean of the linear channel estimator, conditioned on the channel realization, will be

$$\begin{aligned} \hat{\psi}_{n,l} &= E\left\{ \sum_{m\in\{P(n)\}} \Omega_{l,m} \cdot \hat{g}_{n,m}^{FD-LS} \right\} = \sum_{m\in\{P(n)\}} \Omega_{l,m} \cdot E\left\{\hat{g}_{n,m}^{FD-LS}\right\} \\ &= \sum_{m\in\{P(n)\}} \Omega_{l,m} \cdot \psi_m + \sum_{m\in\{P(n)\}} \Omega_{l,m} \cdot w_{n,m}^{pilot}/p_{n,m} \end{aligned} \tag{3.29}$$

and the noise-and-interference $v_{n,l} = \sum_{m\in\{P(n)\}} \Omega_{l,m} \cdot w_{n,m}/p_{n,m}$. Thus,

$$\begin{aligned} K_v(n;l_1,l_2) &= E\{v_{n,l_1} v_{n,l_2}^*\}/2 \\ &= E\{ \sum_{m_1\in\{P(n)\}} \Omega_{l_1,m_1} w_{n,m_1}/p_{n,m_1} \sum_{m_2\in\{P(n)\}} \Omega_{l_2,m_2}^* w_{n,m_2}^*/p_{n,m_2}^*\}/2 \\ &= \sum_{m_1\in\{P(n)\}} \sum_{m_2\in\{P(n)\}} \frac{\Omega_{l_1,m_1}\cdot\Omega_{l_2,m_2}^*}{p_{n,m_1}\cdot p_{n,m_2}^*} \cdot E\{w_{n,m_1} w_{n,m_2}^*\}/2 \end{aligned} \tag{3.30}$$

From the result in Appendix A, and given that l_1, l_2 are pilot subcarriers, we re-write (3.30) as

$$K_v(n;l_1,l_2) = \sum_{m_1\in\{P(n)\}} \sum_{m_2\in\{P(n)\}} \frac{\Omega_{l_1,m_1}\cdot\Omega_{l_2,m_2}^*}{p_{n,m_1}\cdot p_{n,m_2}^*} \Big(P_d \sum_{\vartheta\in\{D(n)\}} A_{m_1,\vartheta} A_{m_2,\vartheta}^*$$

$$+P_d \sum_{\vartheta\in\{D(n-1)\}} B^{pre}_{m_1,\vartheta} B^{pre*}_{m_2,\vartheta} + P_d \sum_{\vartheta\in\{D(n+1)\}} B^{next}_{m_1,\vartheta} B^{next*}_{m_2,\vartheta} + N_0 \cdot \delta_K(m_2 - m_1)\Big) \quad (3.31)$$

where we have assumed again constant average power of data subcarriers across OFDM symbols, and independence of the data modulation symbols across both subcarriers and OFDM symbols. Finally, the variance of the channel estimate at the *l*th subcarrier, conditioned on the channel realization, is given by

$$\sigma_v^2(n,l) \triangleq K_v(n;l,l) = \sum_{m_1\in\{P(n)\}} \sum_{m_2\in\{P(n)\}} \frac{\Omega_{l,m_1} \cdot \Omega^*_{l,m_2}}{p_{n,m_1} \cdot p^*_{n,m_2}} \Big(P_d \sum_{\vartheta\in\{D(n)\}} A_{m_1,\vartheta} A^*_{m_2,\vartheta}$$
$$+P_d \sum_{\vartheta\in\{D(n-1)\}} B^{pre}_{m_1,\vartheta} B^{pre*}_{m_2,\vartheta} + P_d \sum_{\vartheta\in\{D(n+1)\}} B^{next}_{m_1,\vartheta} B^{next*}_{m_2,\vartheta} + N_0 \cdot \delta_K(m_2 - m_1)\Big) \quad (3.32)$$

The MSE of the channel estimate can be computed from the expressions in (3.29) and (3.32), as shown in (3.19).

3.3.3 DFT-based Channel Estimation

A particular example of a linear estimator is one based upon the DFT. Motivated by the fact that, for the ISI-free case, the channel gain at the *l*th subcarrier is simply the channel's frequency response evaluated at that subcarrier, DFT-based channel estimation methods have been widely studied for OFDM systems [2], [14].

In order to simplify the analysis, we use the following matrix representation of the signals at the DFT output:

$$\mathbf{y}(n) = \mathbf{D}_\psi \cdot \mathbf{s}(n) + \mathbf{w}_{pilot}(n) + \mathbf{w}(n) \quad (3.33)$$

where $\mathbf{D}_\psi$ is a diagonal matrix of size $(N \times N)$ with entries corresponding to the channel gain, ψ_l, at each of the subcarriers. The modulation symbols at each of the N subcarriers are represented by the column vector $\mathbf{s}(n)$. Similarly, the interference created by the pilot subcarriers is represented by the column vector $\mathbf{w}_{pilot}(n)$, and the noise and data

interference are represented by the column vector $\mathbf{w}(n)$. The previous Section has defined the FD-LS channel estimate as $\hat{\mathbf{g}}_{FD-LS}(n) = \mathbf{D}_p^{-1}(n) \cdot \mathbf{y}_{pilot}(n)$, where $\mathbf{D}_p^{-1}(n)$ is a diagonal matrix of size $(N_p \times N_p)$ containing the inverse of the known modulation symbols at the pilot subcarriers, and where $\mathbf{y}_{pilot}(n)$ is a column vector with the DFT outputs corresponding to the N_p pilot subcarriers.

We will focus our analysis on the estimator "C" in [14], setting M (the number of coefficients for time-domain processing) to N_h. Therefore, the channel estimate can be written as

$$\hat{\mathbf{g}}_{DFT}(n) = \mathbf{F}_N \cdot \mathbf{X} \cdot \mathbf{Y}^H \cdot \mathbf{F}_{N_p}^H \cdot \hat{\mathbf{g}}_{FD-LS}(n) \tag{3.34}$$

where $\mathbf{F}_N$ is the DFT matrix of size N and therefore $F_N[l,k] = \frac{1}{\sqrt{N}} e^{-j2\pi(l-N/2)k/N}, l = 0, \ldots, (N-1), k = 0, \cdots, (N-1)$. $\mathbf{F}_N^H$ is the IDFT matrix of size N. The matrix X of size $(N \times N_h)$ zero pads an input vector of length N_h to length N and is defined in (3.35). The matrix $\mathbf{Y}^H$ of size $(N_h \times N_p)$ truncates an input vector of length N_p to length N_h and is also defined in (3.35). Note that in (3.34),

$$\mathbf{X} = \begin{bmatrix} \mathbf{I}_{N_h} \\ \mathbf{0}_{(N-N_h)\times N_h} \end{bmatrix} \text{ and } \mathbf{Y} = \begin{bmatrix} \mathbf{I}_{N_h} \\ \mathbf{0}_{(N_p-N_h)\times N_h} \end{bmatrix} \tag{3.35}$$

Therefore, the DFT-based channel estimator takes the N_p FD-LS channel estimates and transforms them to the time domain. Note that we consider the case where the number of pilot subcarriers, N_p, may be different from the number of subcarriers in the system, N, to include the case where, for example, pilot subcarriers are frequency multiplexed with data subcarriers. Therefore, $N_p \leq N$. However, note that N_p will be the upper limit of the number of time-domain samples that we can estimate.

The matrix $\mathbf{Y}^H$ in (3.35) performs time-domain processing. Different techniques can be used to process the channel impulse response taps in the time domain [14], but we consider the truncation operation to retain only the first N_h samples. Note that, unlike N_p, which is a fixed system parameter (number of pilot subcarriers in an OFDM symbol), the

value of N_h can be adapted at the receiver depending on, for example, the actual channel delay spread. These samples are then zero-padded to length N by way of the matrix $\mathbf{X}$. Finally, the DFT provides a channel estimate at the N system subcarriers.

We can re-write (3.28) in matrix form as $\hat{\mathbf{g}}(n) = \mathbf{\Omega} \cdot \hat{\mathbf{g}}_{FD-LS}(n)$, and therefore the DFT-based channel estimator can be characterized as shown in the general case of linear channel estimator by setting $\mathbf{\Omega} = \mathbf{F}_N \cdot \mathbf{X} \cdot \mathbf{Y}^H \cdot \mathbf{F}_{N_p}^H$.

3.4 Data Detection

Different data detection criteria exist. We will focus on the simplest one, consisting of a single-tap equalizer defined as

$$z_{n_1,l} = y_{n_1,l} \cdot \hat{g}_{n_2,l}^* \tag{3.36}$$

where $\hat{g}_{n,l}$ is the channel estimate for the *l*th subcarrier of the *n*th OFDM symbol. In order to keep the derivations generic for FDM and TDM pilots, we use the suffix n_1 for indexing the OFDM symbol for which data detection is performed, and we use the suffix n_2 for indexing the OFDM symbol for which channel estimation for the data detection of the n_1-th OFDM symbol is performed. Substituting (3.17) and (3.18) in (3.36) yields

$$\begin{aligned} z_{n_1,l} &= (\psi_l \cdot s_{n_1,l} + w_{n_1,l}^{pilot} + w_{n_1,l}) \cdot (\hat{\psi}_{n_2,l}^* + v_{n_2,l}^*) \\ &= (\psi_l \cdot \hat{\psi}_{n_2,l}^* \cdot s_{n_1,l} + \hat{\psi}_{n_2,l}^* \cdot w_{n_1,l}^{pilot}) + (\psi_l \cdot s_{n_1,l} + w_{n_1,l}^{pilot}) \cdot v_{n_2,l}^* + w_{n_1,l} \cdot \hat{\psi}_{n_2,l}^* \\ &+ w_{n_1,l} \cdot v_{n_2,l}^* \end{aligned} \tag{3.37}$$

Note that, conditioned on a channel realization, the expression in (3.36) is the result of the product of two complex Gaussian random variables. From Equation (B-1) of [1], the decision variable at the data detector can be expressed as a special case of the following general quadratic form: $D = \sum_{k=1}^{L} (A|X_k|^2 + B|Y_k|^2 + CX_kY_k^* + C^*X_k^*Y_k)$. For our

problem, $L = 1$, $A = B = 0$ and $C = 1/2$, yielding $D = \Re\{XY^*\}$ which is the decision variable at the data detector output for BPSK modulation and the single-tap equalizer receiver. The impact of imperfect channel estimation in CDMA systems with rake receivers has been investigated before, e.g., [45], [48], [50], however, to the best of the authors' knowledge, no such analysis has been published for OFDMA systems.

In the context of our analysis, X is the DFT output that we have denoted by $y_{n,l} = \psi_l + w_{n,l}^{pilot} + w_{n,l}$, assuming $s_{n,l} = 1$, and Y is the channel estimate that we have denoted by $\hat{g}_{n,l} = \hat{\psi}_{n,l} + v_{n,l}$.

From Equation (B-21) in [1], the bit error probability at one subcarrier for BPSK is

$$P_b = Q_1(a, b) - \frac{v_2/v_1}{1 + v_2/v_1} \cdot I_0(ab) \cdot e^{-(a^2+b^2)/2} \tag{3.38}$$

where $Q_1(a, b)$ is the Marcum Q function and $I_0(x)$ is the zeroth order modified Bessel function of the first kind. The parameters v_1 and v_2 are defined in (3.42) and (3.43), respectively, and are a function of the central second order moment and the cross-covariance of $y_{n,l}$ and $\hat{g}_{n,l}$. The variables a and b are defined in (3.45) and are a function of the first and central second order moments, and the cross-covariance of $y_{n,l}$ and $\hat{g}_{n,l}$.

The first order and the central second order moments of $y_{n,l}$ and $\hat{g}_{n,l}$, conditioned on the channel realization, are

$$E\{y_{n,l}|_{\psi_l}\} = \psi_l + w_{n,l}^{pilot}, \qquad E\{\hat{g}_{n,l}|_{\psi_l}\} = \hat{\psi}_{n,l} \tag{3.39}$$

$$Var(y_{n,l}|_{\psi_l}) = \sigma_w^2(n, l), \qquad Var(\hat{g}_{n,l}|_{\psi_l}) = \sigma_v^2(n, l) \tag{3.40}$$

The cross-covariance of $y_{n_1,l}$ and $\hat{g}_{n_2,l}$, conditioned on the channel realization, is

$$\rho_{y\hat{g}}(n_1, n_2; l) = E\{w_{n_1,l} \cdot v_{n_2,l}^*|_{\psi_l}\}/2 \tag{3.41}$$

and is characterized in Appendix A. From here, we drop the subscripts in $y_{n,l}$ and $\hat{g}_{n,l}$ to shorten notation.

The variables v_1 and v_2 for our special case are given by

$$\begin{aligned} v_1 &= \sqrt{w^2 + \frac{1}{(Var(y)\cdot Var(\hat{g}) - |\rho_{y\hat{g}}|^2)\cdot(|C|^2 - AB)}} - w \\ &= \sqrt{\frac{4(\Re\{\rho_{y\hat{g}}\})^2}{(\sigma_w^2\sigma_v^2 - |\rho_{y\hat{g}}|^2)^2} + \frac{4}{\sigma_w^2\sigma_v^2 - |\rho_{y\hat{g}}|^2}} - \frac{2\Re\{\rho_{y\hat{g}}\}}{\sigma_w^2\sigma_v^2 - |\rho_{y\hat{g}}|^2} \\ &= 2\sqrt{\frac{(\Re\{\rho_{y\hat{g}}\})^2 + \sigma_w^2\sigma_v^2 - |\rho_{y\hat{g}}|^2}{(\sigma_w^2\sigma_v^2 - |\rho_{y\hat{g}}|^2)^2}} - \frac{2\Re\{\rho_{y\hat{g}}\}}{\sigma_w^2\sigma_v^2 - |\rho_{y\hat{g}}|^2} \\ &= \frac{2}{\sigma_w^2\sigma_v^2 - |\rho_{y\hat{g}}|^2}\left(\sqrt{(\Re\{\rho_{y\hat{g}}\})^2 + \sigma_w^2\sigma_v^2 - |\rho_{y\hat{g}}|^2} - \Re\{\rho_{y\hat{g}}\}\right) \end{aligned} \tag{3.42}$$

and

$$\begin{aligned} v_2 &= \sqrt{w^2 + \frac{1}{(Var(y)\cdot Var(\hat{g}) - |\rho_{y\hat{g}}|^2)\cdot(|C|^2 - AB)}} + w \\ &= \frac{2}{\sigma_w^2\sigma_v^2 - |\rho_{y\hat{g}}|^2}\left(\sqrt{(\Re\{\rho_{y\hat{g}}\})^2 + \sigma_w^2\sigma_v^2 - |\rho_{y\hat{g}}|^2} + \Re\{\rho_{y\hat{g}}\}\right) \end{aligned} \tag{3.43}$$

where we have used

$$w = \frac{A\cdot Var(y) + B\cdot Var(\hat{g}) + C\cdot\rho_{y\hat{g}}^* + C^*\cdot\rho_{y\hat{g}}}{2(Var(y)\cdot Var(\hat{g}) - |\rho_{y\hat{g}}|^2)\cdot(|C|^2 - AB)} = \frac{2\Re\{\rho_{y\hat{g}}\}}{\sigma_w^2\sigma_v^2 - |\rho_{y\hat{g}}|^2}. \tag{3.44}$$

In addition,

$$a = \left[\frac{2v_1^2v_2(\alpha_1v_2 - \alpha_2)}{(v_1+v_2)^2}\right]^{1/2} \text{ and } b = \left[\frac{2v_1v_2^2(\alpha_1v_1 + \alpha_2)}{(v_1+v_2)^2}\right]^{1/2} \tag{3.45}$$

where

$$\begin{aligned} \alpha_1 = (|C|^2 - AB)\cdot\big(&|E\{y\}|^2Var(\hat{g}) + |E\{\hat{g}\}|^2Var(y) - E^*\{y\}E\{\hat{g}\}\rho_{y\hat{g}} \\ &-E\{y\}E^*\{\hat{g}\}\rho_{y\hat{g}}^*\big) = \frac{1}{4}\left(|\psi + w^{pilot}|^2\cdot\sigma_v^2 + |\hat{\psi}|^2\cdot\sigma_w^2 - 2\Re\{\hat{\psi}\cdot(\psi + w^{pilot})\cdot\rho_{y\hat{g}}\}\right) \end{aligned} \tag{3.46}$$

and

$$\begin{aligned}\alpha_2 &= A \cdot |E\{y\}|^2 + B \cdot |E\{\hat{g}\}|^2 + CE^*\{y\}E\{\hat{g}\} + C^*E\{y\}E^*\{\hat{g}\} \\ &= \Re\{(\psi + w^{pilot}) \cdot \hat{\psi}^*\}. \end{aligned} \tag{3.47}$$

Section 3.5 will evaluate the BER performance for different UWB channel models and with different channel estimation algorithms.

3.5 Performance Characterization

The performance characterizations in this Section will use realizations of the UWB channel model described in [29]. We will use the two extremes in terms of channel delay spread, namely channel model 1 (CM1), based on (0-4m) line-of-sight (LOS) channel measurements, and channel model 4 (CM4), generated to fit a $25ns$ RMS delay to represent the extreme NLOS multipath channel for UWB applications.

All the evaluations assume an OFDM-based UWB system with $N = 128$ subcarriers with a subcarrier spacing of $4.125MHz$ ($T = 242.42ns$). The CP duration is assumed to be $T_{CP} = 60.61ns$, and we assume a single-tap equalizer detector. The BERs shown are the result of averaging the performance over 1000 channel realizations. The analytical results using the derivations in Section 3.4 also are compared to simulation results for all the evaluations (simulation results are distinguished by characters in the plots e.g., '*' and analyses by corresponding solid lines).

Figure 3.3 through Figure 3.6 show the BER sensitivity to the pilot signal density. For these evaluations, we assume 1% residual frequency error and an early sampling at the receiver corresponding to 12.5% of the CP, i.e., $\tau = -4T_c$. Figure 3.3 shows the BER averaged over 1000 CM1 realizations for different pilot densities for the FD-LS channel estimator. The BER is shown for perfect channel estimation, for a TDM pilot (100% pilot density) and for FDM pilots with 50%, 33% and 25% densities. Results for TDM pilots

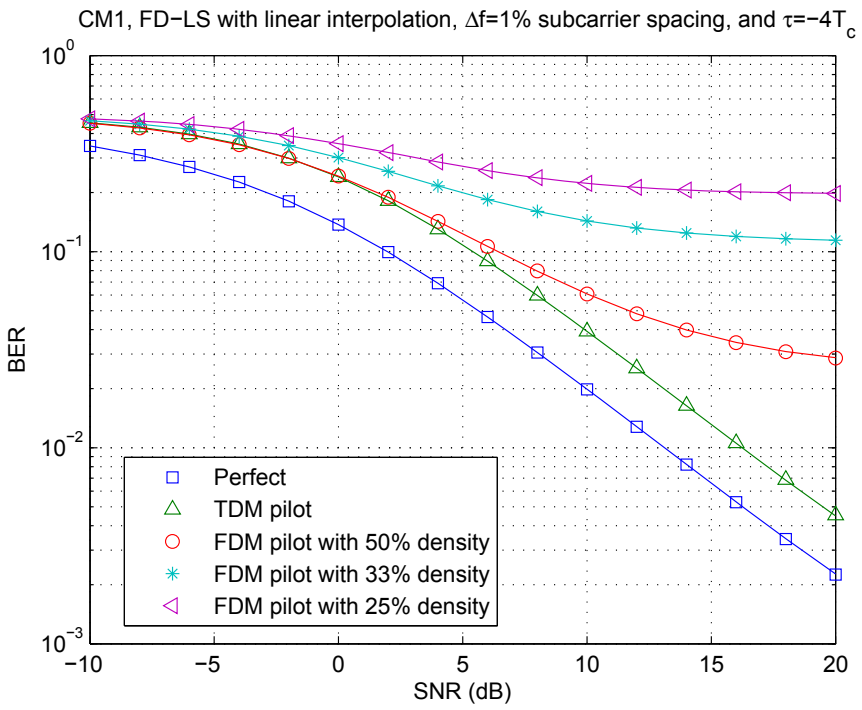

Figure 3.3 *BER performance vs. pilot density for CM1, FD-LS*

assume the channel remains constant for a time interval starting at the OFDM symbol used for channel estimation and ending at the the last OFDM symbol used for data detection. The FD-LS channel estimates for the FDM pilot cases are linearly interpolated to obtain the channel estimates on the data subcarriers. This linear interpolator can be seen as a special realization of the matrix $\mathbf{\Omega}$ in the general linear channel estimator in Subsection 3.3.2. As we can see, the performance worsens as we go to sparser pilot densities.

Figure 3.4 shows the same characterization for a DFT-based channel estimator. The number of time-domain samples to estimate has been set to $N_h = 64$ for both the TDM pilot and the FDM pilot with 50% density. The number of time-domain samples has been set to the number of pilot subcarriers for the other FDM pilot configurations, i.e., $N_h = 43$ and $N_h = 32$ for 33% and 25% pilot densities, respectively. The performance improvement with respect to the FD-LS channel estimator is significant, particularly for the FDM pilots with sparser densities.

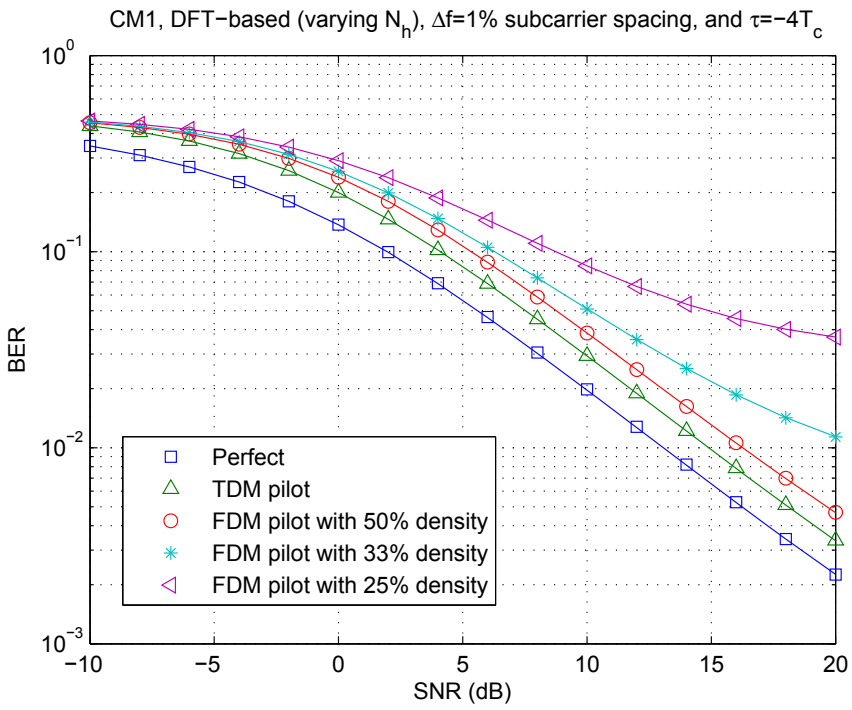

Figure 3.4 *BER performance vs. pilot density for CM1, DFT-based*

Figure 3.5 shows the average performance of the FD-LS channel estimator using 1000 CM4 realizations. This channel model incurs high levels of ISI, and from the results, we can see that there is now a large degradation due to channel estimation. Indeed, the BER for the FDM pilot hits an error floor at very large values. Therefore, these results indicate that the linear interpolator that we use in conjunction with the FD-LS channel estimator is not adequate for this highly frequency selective channel. Also, we can clearly see the very severe impact of ISI into the detection performance.

Figure 3.6, in turn, shows the same performance characterization for a DFT-based channel estimator. The number of time-domain samples to estimate has been set in the same way as for Figure 3.4, i.e., $N_h = 64$ for the TDM pilot and the FDM pilot with 50% density, and $N_h = 43$ and $N_h = 32$ for the 33% and 25% pilot densities, respectively. Note that $N_h = 64$ corresponds to twice the time span of the CP, and this is the case with best BER performance. Further, note that performance of the DFT-based channel estimator is consistently better than that of the FD-LS channel estimator, however the

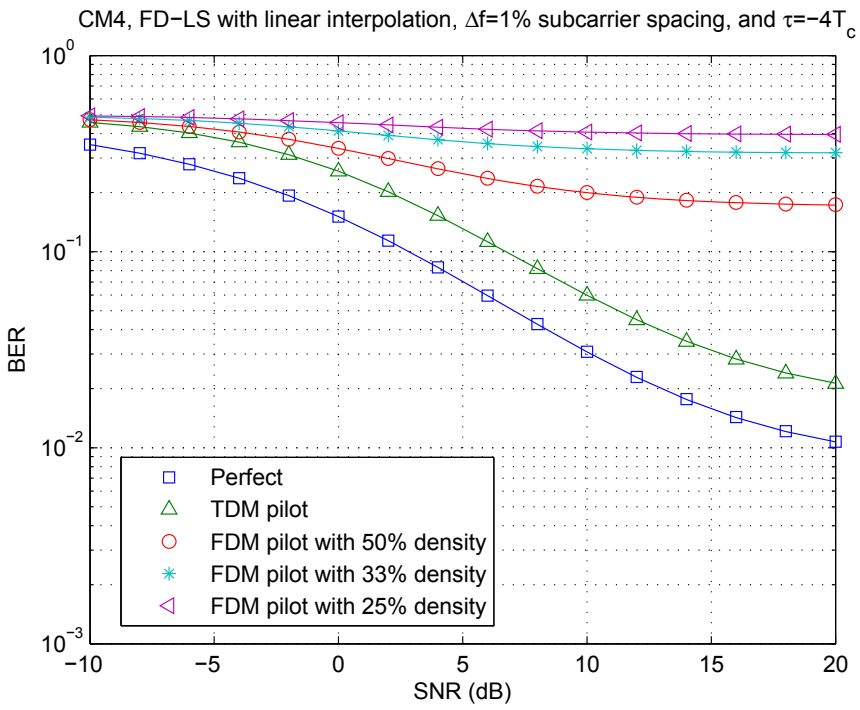

Figure 3.5 *BER performance vs. pilot density for CM4, FD-LS*

performance degradation due to channel estimation is quite considerable in either case.

Figure 3.7 shows the impact on channel estimation at different levels of residual frequency error. The results are obtained using 1000 CM1 realizations and perfect timing synchronization to isolate the impact of the residual frequency error. We choose a TDM pilot and a DFT-based channel estimator. The number of time-domain samples to obtain the estimate has been set to $N_h = 64$. The results show graceful performance degradation as the residual frequency error increases from 0% to 10% of the subcarrier spacing.

Figure 3.8 shows the impact on channel estimation at different levels of residual timing error. The results are obtained using 1000 CM1 realizations, perfect frequency synchronization, an FD-LS channel estimator and a TDM pilot. We can see, for this case, that a negative timing error (early sampling) of 10 samples has little impact in performance compared to perfect timing synchronization. This timing error is absorbed by the CP. However, a positive timing error (late sampling) severely impacts the performance, as

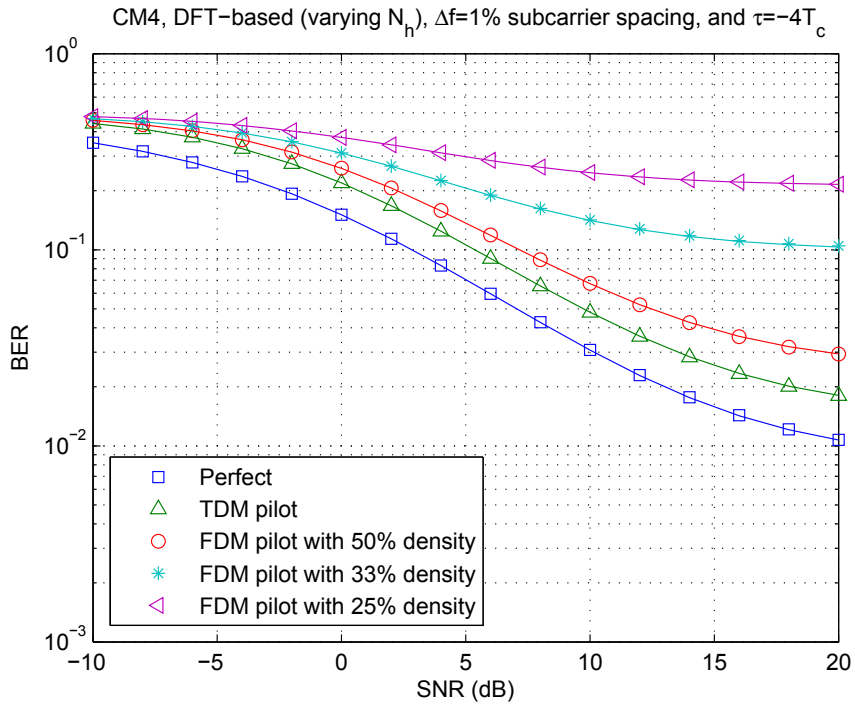

Figure 3.6 *BER performance vs. pilot density for CM4, DFT-based*

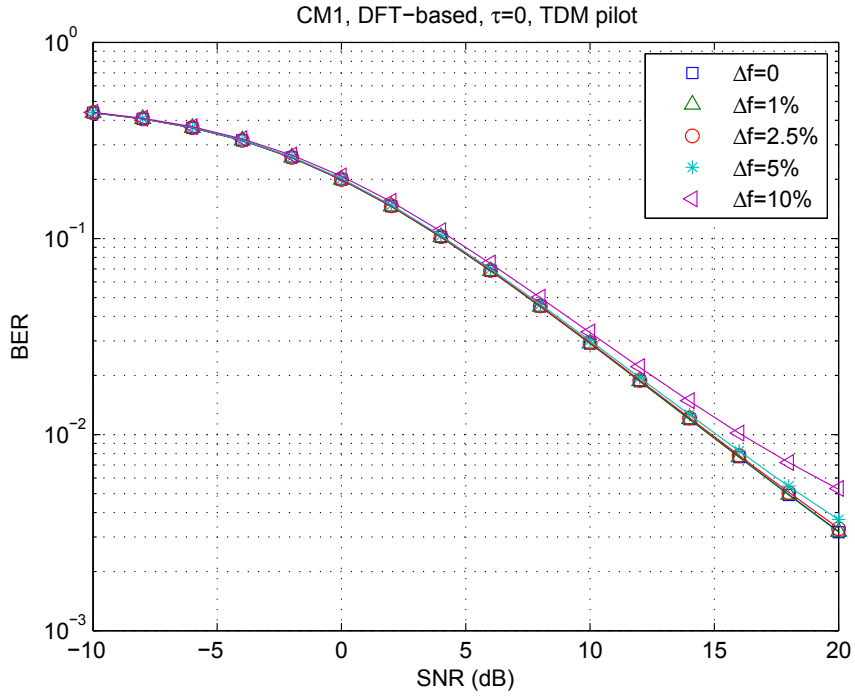

Figure 3.7 *BER sensitivity to residual frequency error with DFT-based channel estimator*

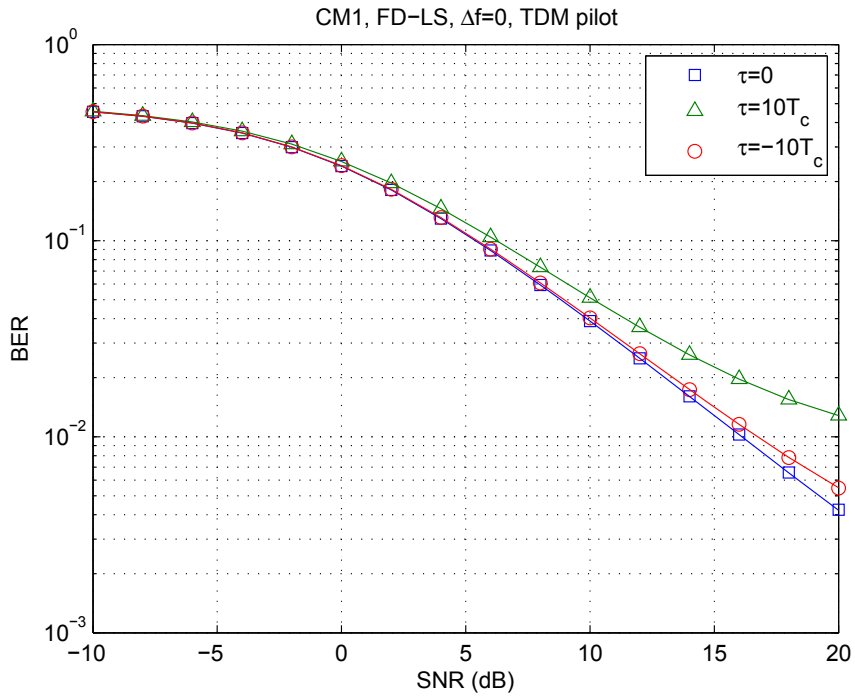

Figure 3.8 *BER sensitivity to transmit/receive timing errors with FD-LS channel estimator*

ISI from the next OFDM symbol is inevitably incurred.

3.6 Concluding Remarks

This chapter has analyzed the impact of realistic channel estimation in OFDM systems accounting for imperfections such as residual time and frequency error, and a channel delay spread larger than the CP. We have also studied the impact of the pilot signal density on the data demodulation performance.

From the performance study at different levels of residual frequency error, the effect of intercarrier interference on channel estimation has been shown to be small. However, intersymbol interference severely impacts the quality of the channel estimates and hence can yield a large (>2dB) data demodulation performance degradation.

The pilot signal density and the associated channel estimation algorithm have been

shown to be critical for the ISI cases. Note that ISI may be incurred by a channel delay spread larger than the CP, or by timing errors at the terminal receiver (late sampling), irrespective of the channel delay spread.

The large degradation in performance due to ISI emphasizes the importance of selecting an adequate CP length in OFDM systems. Further, channel estimation algorithms providing robust performance in the presence of ISI are critical for robust performance of OFDM systems.

3.7 Acknowledgements

This chapter is a reprint of the material as it appears in "Channel Estimation for Non-Ideal OFDM Systems," accepted for publication in *IEEE Transactions on Communications*. The dissertation author was the primary author and Prof. Laurence B. Milstein directed and supervised the research which forms the basis for this chapter.

CHAPTER 4

Cognitive Aspects of OFDM-based UWB and How to Enable Them

4.1 Introduction

Wireless communications systems are characterized by a choice of multiple access scheme and a set of system parameters. These system parameters may be related to the deployment characteristics, e.g., center carrier frequency, system bandwidth; or to the specifics related to the multiple access scheme, e.g., spreading factor for CDMA systems or number of subcarriers for OFDM systems. Traditionally the set of system parameters is fixed or very rigid for a given deployment scenario and is selected with a 'one-size-fits-all' mentality. An example of such design criterion is the LTE system where the subcarrier spacing is 15kHz for all the unicast applications, and is 7.5kHz for dedicated multicast operation for single frequency network (SFN) operation and without return link. The choice of the subcarrier spacing is the same irrespective of the typical terminal speed in a given cell, which could range from static or pedestrian speeds to high speed trains at 350km/h. Similarly, there are two cyclic prefix durations of 4.7μs and 16.66μs for the so-called 'normal CP' and 'extended CP' operation, respectively. The CP duration is not expected to adapt to the channel conditions but is rather semi-statically configured for a given cell or even a given deployment scenario. The same CP duration is used irrespective of whether a cell is a hot-spot with line-of-sight (LOS) or a scattered micro-cell deployment in a big city down-town. Advances in RF and baseband processing enable the use of

software defined radios for operation in wireless systems. This new capability opens up a new range of possibilities when it comes to the operation of wireless systems. It could be no longer required to use a very rigid set of system parameters to operate in a wireless system, but rather one can envision adapting the set of system parameters to the environmental characteristics with the objective to maximize the spectral efficiency and hence the user experience or minimize the 'cost' to move bits over the air. This is particularly true for point-to-point communications where the 'system' parameters can be optimized for that particular set of communicating entities or network nodes. The adaptation to the environment is enabled by a cognitive component at the network nodes that need to establish a communication link. Therefore, there will be a learning/identification process at the receiver followed by the selection of parameters optimizing the link performance, and their subsequent application. This chapter investigates a cognitive OFDM system where the OFDM system parameters are adapted to the environmental conditions. We first discuss the parameters that define an OFDM system. Then, we define cognitive OFDM by listing the system parameters that will be adapted to the environment. We present the system model and describe what receiver operations are generalized to enable the cognitive component of the system operation. We then discuss the adaptation process which has the goal to select the system parameters that are best for the given environment. The chapter continues with the analysis of the proposed operation supported by simulations. We finish the chapter with some concluding remarks.

4.2 OFDM System Parameters

Consider an OFDM system with a bandwidth of B Hz. We define the sample time as $T_s \triangleq 1/B$ seconds and we introduce the following OFDM parameters:

- OFDM symbol duration without CP: T seconds or N samples. Note the following parameter relationships: $T = N \cdot T_s$, also $B = N/T = 1/T_s$. Further note that $1/T$ Hz is the OFDM subcarrier spacing.

- CP duration: T_{CP} seconds or CP samples ($T_{CP} = CP \cdot T_s$)
- Pilot (reference signal) structure

Note that the number of subcarriers is the same as the number of samples without CP in an OFDM symbol, i.e., $N = B/(1/T) = T/T_s$. Further, note that not all the subcarriers need to be used for communication and some subcarriers may be skipped at the transmitter and the receiver to e.g., avoid interfering other users or systems. In an OFDM system, the following conditions need to apply to maintain orthogonality across the different subcarriers:

- The channel is to remain constant over the OFDM symbol duration
- The channel frequency response is to be flat on a subcarrier

Defining T_{coh} as the coherence time of the channel, the first condition implies that

$$T << T_{\text{coh}} \sim 1/f_d \tag{4.1}$$

where f_d is the Doppler frequency. Similarly, defining B_{coh} as the coherence frequency of the channel, the second condition implies that

$$1/T << B_{\text{coh}} \sim 1/\tau_{\text{max}} \tag{4.2}$$

where τ_{max} is the maximum channel path delay. Therefore, putting the inequalities in (4.1) and (4.2) together implies that the symbol duration, T, in the an OFDM system is to satisfy

$$\tau_{\text{max}} << T << 1/f_d \tag{4.3}$$

Additionally, the CP needs to be long enough to avoid severe effect of ISI, and therefore $T_{CP} \sim \tau_{\text{max}}$. The CP enables an ISI-free operation of the OFDM system, however, it incurs and unrecoverable overhead equal to $T_{CP}/(T + T_{CP}) = CP/(N + CP)$ which

should be kept as small as possible. Therefore, since the relative CP overhead should be small, the CP duration should be much smaller than the OFDM symbol duration, i.e., $T_{CP} << T$.

If $T_{CP} \sim \tau_{\text{max}}$, then $T >> T_{CP}$ from the condition on flat frequency response on a subcarrier.

Regarding the pilot structure, it is important to have a time/frequency structure of the pilot signal so that it has an adequate time-density according to T_{coh}, and an adequate frequency-density according to B_{coh} and yet incurring the minimum overhead.

4.3 Cognitive OFDM

In this chapter we investigate an OFDM system that adapts selected system parameters to maximize the system's spectral efficiency. This maximization will improve the user experience and will optimize the use of physical resources (time and frequency) over the air. According to Section 4.2, the system parameters that are adapted are the OFDM symbol duration, the CP duration and the pilot or reference signal structure. In addition, we will consider the optimization of the DFT window placement, which is, indeed, a time tracking algorithm targeting maximization of the spectral efficiency at the receiver node. This optimization is important because the other optimizations build on top of it.

On top of the optimization of these system parameters (pilot structure, CP duration and OFDM symbol duration), the communication system can, and, indeed, should perform link adaptation in the form of power control, modulation-and-coding (MCS) adaptation, and other scheduler operations (e.g., selection of time and frequency resources for the use of the communication link).

4.3.1 Symbol duration

The symbol duration, T seconds, determines the OFDM subcarrier spacing $1/T$ Hz. Therefore, for a given operating system bandwidth, $B = N/T$ Hz, longer OFDM symbols (larger T) yield more subcarriers (larger N) with lower subcarrier spacing (smaller $1/T$). Longer OFDM symbols have the advantaged of having less ISI effect and less CP overhead (for the same CP duration). At the same time, longer OFDM symbols are more prone to ICI due to channel variations over the duration of the symbol, and also yield lower subcarrier spacing, which has the disadvantage of being more prone to frequency errors.

Clearly, the benefits of having a longer OFDM symbol are directly related to the drawbacks of having a shorter OFDM symbol, and vice-versa. Therefore, the cognitive component at the receiver needs to identify the right trade-off balance to minimize the CP overhead while maintaining the orthogonality across subcarriers.

Note that the number of dimensions (time and frequency resources) does not change with different OFDM symbol duration. Longer OFDM symbols yield more subcarriers over a longer time interval, while shorter OFDM symbols yield less subcarriers over a shorter time interval.

4.3.2 CP duration

The CP in OFDM systems enables ISI-free operation while incurring non-recoverable overhead. Therefore, it is desirable to have a CP as small as possible while still maintaining orthogonality across subcarriers and enough robustness against timing errors. It is important to note that it may be beneficial to operate the system with some residual ISI but with smaller CP overhead, rather than with no ISI but with larger CP overhead. This comment will become manifest with the study in Section 4.6.3. The cognitive component at the receiver needs to identify the channel delay spread to accordingly adapt the CP duration to an optimal value. The CP overhead is related to the OFDM symbol duration

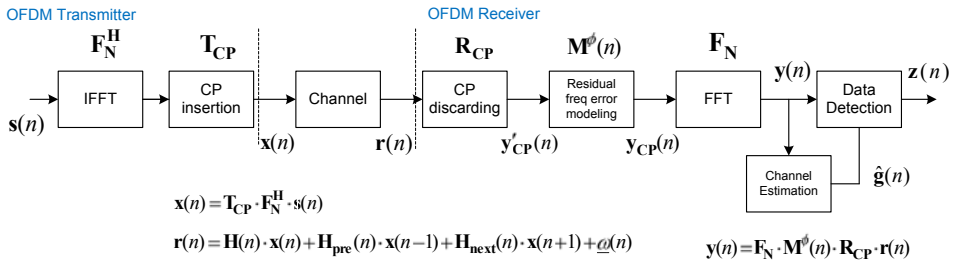

Figure 4.1 *Block diagram of OFDM system model*

and therefore, the CP overhead is effectively reduced having longer OFDM symbols. The OFDM symbol duration is discussed in the previous subsection and has its own selection trade-offs.

4.3.3 Pilot structure

The pilot signal enables channel estimation at the receiver for coherent demodulation of the data. In OFDM systems, the pilot structure consists of the frequency and time placement of pilot symbols in the overall transmission waveform. The sampling frequency provided by the pilot subcarriers needs to be adequate to capture frequency-domain variations of the channel and therefore is related to the channel coherence bandwidth. Note that the channel coherence bandwidth was also relevant for the determination of the CP duration. The sampling in time provided by the pilot needs to capture the time-domain variations of the channel and therefore is related to the channel coherence time. Note that the channel coherence time was also relevant for the determination of the OFDM symbol duration.

4.4 System Description

We consider a regular discrete-time OFDM system [51] with some generalized receiver operations related to the CP discarding and the DFT operation. Figure 4.1 is a block diagram of the OFDM system model.

The transmission of the n^{th} OFDM symbol is described as

$$\mathbf{x}(n) \triangleq \mathbf{T}_{\text{CP}} \cdot \mathbf{F}_N^H \cdot \mathbf{s}(n) \tag{4.4}$$

where, $\mathbf{s}(n)$ is a column vector of size N with the modulation symbols (data and pilot multiplexed in the frequency domain as shown in Figure 4.3) for each of the N subcarriers at the n^{th} OFDM symbol. $\mathbf{F}_N$ is the DFT matrix of size $(N \times N)$ and therefore, $\mathbf{F}_N^H$ is the IDFT matrix of the same size.

$$\mathbf{F}_N \triangleq \frac{1}{\sqrt{N}} \begin{bmatrix} e^{-j2\pi(-\frac{N}{2})\cdot 0/N} & e^{-j2\pi(-\frac{N}{2})\cdot 1/N} & \dots & e^{-j2\pi(-\frac{N}{2})\cdot (N-1)/N} \\ e^{-j2\pi(-\frac{N}{2}+1)\cdot 0/N} & e^{-j2\pi(-\frac{N}{2}+1)\cdot 1/N} & \dots & e^{-j2\pi(-\frac{N}{2}+1)\cdot (N-1)/N} \\ \vdots & \vdots & \ddots & \vdots \\ e^{-j2\pi(\frac{N}{2}-1)\cdot 0/N} & e^{-j2\pi(\frac{N}{2}-1)\cdot 1/N} & \dots & e^{-j2\pi(\frac{N}{2}-1)\cdot (N-1)/N} \end{bmatrix} \tag{4.5}$$

Defining $N_T \triangleq (N + CP)$, the matrix $\mathbf{T}_{\text{CP}}$ is of size $(N_T \times N)$ and inserts the CP of length CP_{tx} samples at the OFDM transmitter. It can be expressed in matrix form as

$$\mathbf{T}_{\text{CP}} = \begin{bmatrix} \mathbf{0}_{CP_{\text{tx}} \times (N - CP_{\text{tx}})} & \mathbf{I}_{CP_{\text{tx}}} \\ & \mathbf{I}_N \end{bmatrix}_{N_T \times N} \tag{4.6}$$

The output of the channel at the n^{th} OFDM symbol is described as [51]

$$\mathbf{r}(n) \triangleq \mathbf{H}(n) \cdot \mathbf{x}(n) + \mathbf{H}_{\text{pre}}(n) \cdot \mathbf{x}(n-1) + \mathbf{H}_{\text{next}}(n) \cdot \mathbf{x}(n+1) + \underline{\omega}(n) \tag{4.7}$$

where $\mathbf{H}(n)$, $\mathbf{H}_{\text{pre}}(n)$ and $\mathbf{H}_{\text{next}}(n)$ represent the channel matrices at the n^{th} OFDM symbol. Note that these channel matrices account for the filtering processes at the OFDM transmitter and receiver. Further, note that we account for possible time-variations of the channel matrices as shown by the use of the argument 'n'. These channel matrices can be illustrated as shown in Figure 4.2.

The channel matrices depend on the placement of the OFDM symbol boundary at

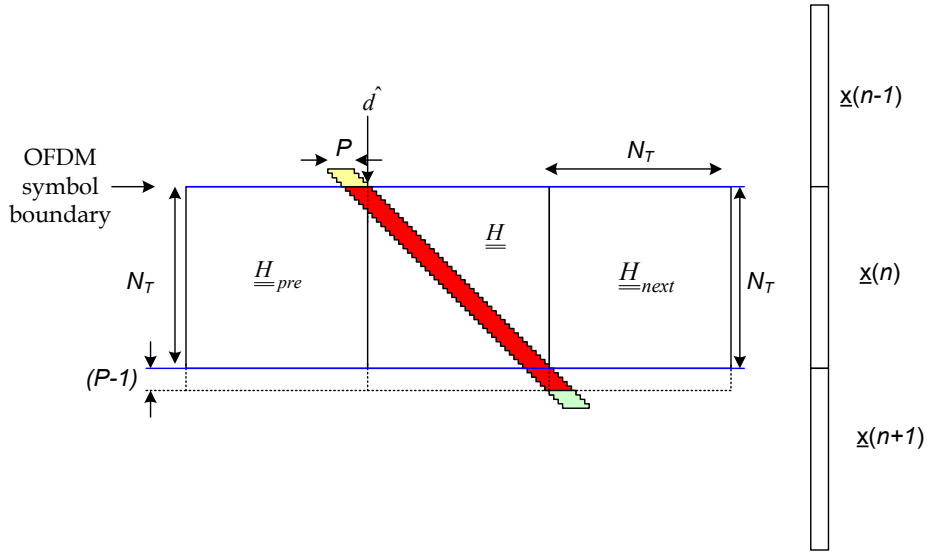

Figure 4.2 *Illustration of construction of channel matrices*

the receiver, in other words, the channel matrices depend on the timing synchronization of the OFDM receiver. We will use the variable $\hat{d}_n$ to indicate the sample that the OFDM receiver deems to be the first sample in the n^{th} OFDM symbol, and that, hence, will determine the DFT window placement for the reception of that symbol. In an actual OFDM receiver, the determination of $\hat{d}_n$ is the result of running a time-synchronization algorithm procedure to determine the OFDM symbol boundaries. This procedure is usually assisted by synchronization signals in the OFDM system to facilitate the task to determine the first sample of a given OFDM symbol. Once the synchronization signals have been used for the determination of the OFDM symbol boundaries, the OFDM receiver may choose to update the symbol boundary to e.g., trade ISI from previous or next OFDM symbol by different placements of the DFT window.

4.4.1 CP discarding and modeling of residual frequency error

At the receiver, the CP discarding operation performs the following operation

$$\mathbf{y}'_{\text{CP}}(n) \triangleq \mathbf{R}_{\text{CP}} \cdot \mathbf{r}(n) \tag{4.8}$$

where $\mathbf{R}_{\text{CP}}$ is a matrix of size $(N \times N_T)$ that discards the CP at the OFDM receiver. While traditional OFDM receivers would discard the first CP samples, this CP discarding operation is more generic and will discard a number of samples, $CP_{\text{rx}} \leq CP_{\text{tx}}$, at the beginning of the OFDM symbol and a number of samples, $(CP_{\text{tx}} - CP_{\text{rx}})$, at the end of the OFDM symbol. We denote this operation by 'partial CP removal' and it will be useful to investigate the effect of having a smaller CP duration with the objective to make the selection of the optimal CP duration. It can be represented as

$$\mathbf{R}_{\text{CP}} \triangleq \begin{bmatrix} \mathbf{0}_{N \times CP_{\text{rx}}} & \mathbf{I}_N & \mathbf{0}_{N \times (CP_{\text{tx}} - CP_{\text{rx}})} \end{bmatrix}_{N \times N_T} \tag{4.9}$$

Note that the traditional CP discarding can be expressed as $\mathbf{R}_{\text{CP}} \triangleq [\mathbf{0}_{N \times CP_{\text{tx}}} \quad \mathbf{I}_N]_{N \times N_T}$.

The residual frequency offset at the receiver is modeled as a time varying diagonal matrix that we denote by $\mathbf{M}^{\phi}(n)$:

$$\mathbf{M}^{\phi}(n) \triangleq \alpha_n \cdot \begin{bmatrix} e^{j2\pi\overline{\Delta f} \cdot 0/N} & 0 & \cdots & 0 \\ 0 & e^{j2\pi\overline{\Delta f} \cdot 1/N} & \cdots & 0 \\ \vdots & \vdots & \ddots & \vdots \\ 0 & 0 & \cdots & e^{j2\pi\overline{\Delta f} \cdot (N-1)/N} \end{bmatrix} \tag{4.10}$$

where $\alpha_n \triangleq e^{j2\pi\overline{\Delta f}(nT_f + T_{CP} + \tau)/T}$ provides the initial phase of each OFDM block [51]. The parameters T_f and T_{CP} represent the OFDM block and CP duration, respectively. Note that $T_f = T + T_{CP}$. Also, the parameter $\overline{\Delta f}$ represents the residual frequency error at the receiver normalized by the subcarrier frequency spacing $1/T$. Finally, the parameter τ denotes the transmit-receive timing difference. A value of $\tau = 0$ implies that the first sample at the OFDM receiver corresponds to the first sample of the OFDM symbol multiplied by the first channel gain.

Therefore, we define

$$\mathbf{y}_{\text{CP}}(n) = \mathbf{M}^{\phi}(n) \cdot \mathbf{y}'_{\text{CP}}(n) \tag{4.11}$$

$$= \mathbf{M}^{\phi}(n)\mathbf{R}_{\text{CP}}\mathbf{H}(n)\mathbf{T}_{\text{CP}}\mathbf{F}_N^H\mathbf{s}(n) + \mathbf{M}^{\phi}(n)\mathbf{R}_{\text{CP}}\mathbf{H}_{\text{pre}}(n)\mathbf{T}_{\text{CP}}\mathbf{F}_N^H\mathbf{s}(n-1)$$
$$+\mathbf{M}^{\phi}(n)\mathbf{R}_{\text{CP}}\mathbf{H}_{\text{next}}(n)\mathbf{T}_{\text{CP}}\mathbf{F}_N^H\mathbf{s}(n+1) + \mathbf{M}^{\phi}(n)\mathbf{R}_{\text{CP}}\underline{\omega}(n)$$

We will ignore the phase rotation of $\underline{\omega}(n)$, since the channel's noise is assumed to be complex circular, and therefore, a phase rotation does not change its statistical characterization.

Defining the following channel matrices

$$\begin{aligned} \widetilde{\mathbf{H}}(n) &\triangleq \mathbf{R}_{\text{CP}} \cdot \mathbf{H}(n) \cdot \mathbf{T}_{\text{CP}} \\ \widetilde{\mathbf{H}}_{\text{pre}}(n) &\triangleq \mathbf{R}_{\text{CP}} \cdot \mathbf{H}_{\text{pre}}(n) \cdot \mathbf{T}_{\text{CP}} \\ \widetilde{\mathbf{H}}_{\text{next}}(n) &\triangleq \mathbf{R}_{\text{CP}} \cdot \mathbf{H}_{\text{next}}(n) \cdot \mathbf{T}_{\text{CP}} \end{aligned} \tag{4.12}$$

we can re-write

$$\begin{aligned} \mathbf{y}_{\text{CP}}(n) &= \mathbf{M}^{\phi}(n) \cdot \widetilde{\mathbf{H}}(n) \cdot \mathbf{F}_N^H \cdot \mathbf{s}(n) + \mathbf{M}^{\phi}(n) \cdot \widetilde{\mathbf{H}}_{\text{pre}}(n) \cdot \mathbf{F}_N^H \cdot \mathbf{s}(n-1) \\ &+ \mathbf{M}^{\phi}(n) \cdot \widetilde{\mathbf{H}}_{\text{next}}(n) \cdot \mathbf{F}_N^H \cdot \mathbf{s}(n+1) + \mathbf{R}_{\text{CP}} \cdot \underline{\omega}(n) \end{aligned} \tag{4.13}$$

4.4.2 DFT output

The DFT output operation at the OFDM receiver yields

$$\mathbf{y}(n) \triangleq \mathbf{F}_N \cdot \mathbf{y}_{\text{CP}}(n) \tag{4.14}$$

Developing the terms in(4.14) yields

$$\begin{aligned} \mathbf{y}(n) &= \mathbf{F}_N \cdot \mathbf{M}^{\phi}(n) \cdot \widetilde{\mathbf{H}}(n) \cdot \mathbf{F}_N^H \cdot \mathbf{s}(n) + \mathbf{F}_N \cdot \mathbf{M}^{\phi}(n) \cdot \widetilde{\mathbf{H}}_{\text{pre}}(n) \cdot \mathbf{F}_N^H \cdot \mathbf{s}(n-1) \\ &+ \mathbf{F}_N \cdot \mathbf{M}^{\phi}(n) \cdot \widetilde{\mathbf{H}}_{\text{next}}(n) \cdot \mathbf{F}_N^H \cdot \mathbf{s}(n+1) + \mathbf{F}_N \cdot \mathbf{R}_{\text{CP}} \cdot \underline{\omega}(n) \end{aligned} \tag{4.15}$$

Defining the following effective channel matrices and the noise at the DFT output as

$$\begin{aligned}
\mathbf{A}(n) &\triangleq \mathbf{F}_N \cdot \mathbf{M}^{\phi}(n) \cdot \widetilde{\mathbf{H}}(n) \cdot \mathbf{F}_N^H && (4.16)\\
\mathbf{B}_{\text{pre}}(n) &\triangleq \mathbf{F}_N \cdot \mathbf{M}^{\phi}(n) \cdot \widetilde{\mathbf{H}}_{\text{pre}}(n) \cdot \mathbf{F}_N^H && (4.17)\\
\mathbf{B}_{\text{next}}(n) &\triangleq \mathbf{F}_N \cdot \mathbf{M}^{\phi}(n) \cdot \widetilde{\mathbf{H}}_{\text{next}}(n) \cdot \mathbf{F}_N^H && (4.18)\\
\mathbf{y}_{\text{noise}}(n) &\triangleq \mathbf{F}_N \cdot \mathbf{R}_{\text{CP}} \cdot \underline{\omega}(n) && (4.19)
\end{aligned}$$

we can re-write (4.15) as

$$\mathbf{y}(n) = \mathbf{A}(n) \cdot \mathbf{s}(n) + \mathbf{B}_{\text{pre}}(n) \cdot \mathbf{s}(n-1) + \mathbf{B}_{\text{next}}(n) \cdot \mathbf{s}(n+1) + \mathbf{y}_{\text{noise}}(n) \qquad (4.20)$$

We can separate the desired term from the ICI term using the following equality $\mathbf{A}(n) \cdot \mathbf{s}(n) = \mathbf{D}_A(n) \cdot \mathbf{s}(n) + \overline{\mathbf{D}}_A(n) \cdot \mathbf{s}(n)$, where $\mathbf{D}_A(n)$ is a diagonal matrix with the entries of the diagonal of $\mathbf{A}$, and $\overline{\mathbf{D}}_A(n) \triangleq \mathbf{A} - \mathbf{D}_A$. Therefore, we can re-write (4.20) as

$$\mathbf{y}(n) = \mathbf{D}_A(n) \cdot \mathbf{s}(n) + \overline{\mathbf{D}}_A(n) \cdot \mathbf{s}(n) + \mathbf{B}_{\text{pre}}(n) \cdot \mathbf{s}(n-1) + \mathbf{B}_{\text{next}}(n) \cdot \mathbf{s}(n+1) + \mathbf{y}_{\text{noise}}(n) \qquad (4.21)$$

Denoting the number of data subcarriers in an OFDM symbol by N_d, we define the matrix $\mathbf{\Lambda}_d$ of size $(N_d \times N)$. $\mathbf{\Lambda}_d$ is a matrix with entries taking values 0 or 1, which extracts the rows of a vector of size $(N \times 1)$ corresponding to data subcarriers. Similarly, denoting the number of pilot subcarriers in an OFDM symbol by N_p, we define the matrix $\mathbf{\Lambda}_p$ of size $(N_p \times N)$. $\mathbf{\Lambda}_p$ is a matrix with entries taking values 0 or 1, which extracts the rows of a vector of size $(N \times 1)$ corresponding to pilot subcarriers. Note that $N = (N_d + N_p)$, further note that $\mathbf{\Lambda}_d^H \cdot \mathbf{\Lambda}_d + \mathbf{\Lambda}_p^H \cdot \mathbf{\Lambda}_p = \mathbf{I}_N$. With these definitions, we can further separate the contribution of the data and pilot subcarriers in (4.21) as

$$\begin{aligned}
\mathbf{y}(n) &= \mathbf{D}_A(n) \cdot \mathbf{s}(n) + \overline{\mathbf{D}}_A(n) \cdot \mathbf{\Lambda}_d^H \cdot \mathbf{\Lambda}_d \cdot \mathbf{s}(n) + \overline{\mathbf{D}}_A(n) \cdot \mathbf{\Lambda}_p^H \cdot \mathbf{\Lambda}_p \cdot \mathbf{s}(n)\\
&+ \mathbf{B}_{\text{pre}}(n) \cdot \mathbf{\Lambda}_d^H \cdot \mathbf{\Lambda}_d \cdot \mathbf{s}(n-1) + \mathbf{B}_{\text{pre}}(n) \cdot \mathbf{\Lambda}_p^H \cdot \mathbf{\Lambda}_p \cdot \mathbf{s}(n-1) && (4.22)
\end{aligned}$$

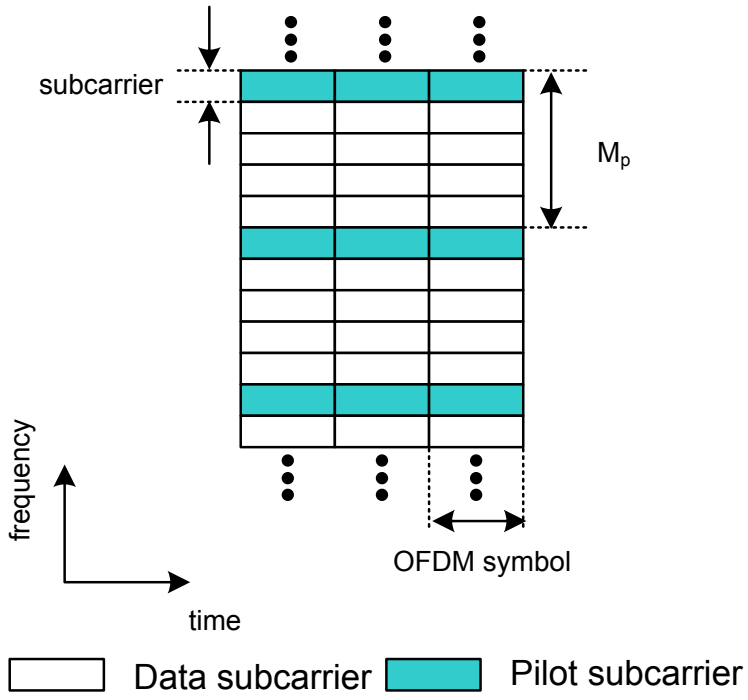

Figure 4.3 *Illustration of pilot and data transmission (FDM)*

$$+ \quad \mathbf{B}_{\text{next}}(n) \cdot \mathbf{\Lambda}_d^H \cdot \mathbf{\Lambda}_d \cdot \mathbf{s}(n+1) + \mathbf{B}_{\text{next}}(n) \cdot \mathbf{\Lambda}_p^H \cdot \mathbf{\Lambda}_p \cdot \mathbf{s}(n+1) + \mathbf{y}_{\text{noise}}(n)$$

We assume a pilot transmission consisting of inserting pilot subcarriers on each OFDM symbol.

The same pilot transmission is assumed on every OFDM symbol to facilitate the optimization process. Indeed, the optimization process will yield a solution with OFDM symbols as long as possible to minimize the CP overhead while retaining orthogonality of the subcarriers to maximize the capacity of the communication link. Note that the parameter M_p characterizes the FDM pilot transmission depicted in Figure 4.3 as there is one pilot subcarrier every M_p subcarriers starting from the first subcarrier.

Defining the interference caused by the pilot subcarriers by

$$\mathbf{w}_{\text{pilot}}(n) \triangleq \overline{\mathbf{D}}_A(n)\mathbf{\Lambda}_p^H\mathbf{\Lambda}_p\mathbf{s}(n) + \mathbf{B}_{\text{pre}}(n)\mathbf{\Lambda}_p^H\mathbf{\Lambda}_p\mathbf{s}(n-1) + \mathbf{B}_{\text{next}}(n)\mathbf{\Lambda}_p^H\mathbf{\Lambda}_p\mathbf{s}(n+1) \quad (4.23)$$

and the total noise-and-interference by

$$\mathbf{w}(n) \triangleq \overline{\mathbf{D}}_A(n)\mathbf{\Lambda}_d^H\mathbf{\Lambda}_d\mathbf{s}(n)+\mathbf{B}_{\text{pre}}(n)\mathbf{\Lambda}_d^H\mathbf{\Lambda}_d\mathbf{s}(n-1)+\mathbf{B}_{\text{next}}(n)\mathbf{\Lambda}_d^H\mathbf{\Lambda}_d\mathbf{s}(n+1)+\mathbf{y}_{\text{noise}}(n), \tag{4.24}$$

we can re-write (4.22), i.e., the DFT output in vector form as

$$\mathbf{y}(n) = \mathbf{D}_A(n)\cdot\mathbf{s}(n) + \mathbf{w}_{\text{pilot}}(n) + \mathbf{w}(n). \tag{4.25}$$

The covariance of the noise-and-interference at the DFT output conditioned on the channel realization is

$$\begin{aligned}\mathbf{K}_w &= \frac{1}{2}E\{\mathbf{w}\cdot\mathbf{w}^H\} \\ &= \overline{\mathbf{D}}_A(n)\mathbf{\Lambda}_d^H\mathbf{\Lambda}_d\mathbf{K}_s(n)\mathbf{\Lambda}_d^H\mathbf{\Lambda}_d\overline{\mathbf{D}}_A^H(n) + \mathbf{B}_{\text{pre}}(n)\mathbf{\Lambda}_d^H\mathbf{\Lambda}_d\mathbf{K}_s(n-1)\mathbf{\Lambda}_d^H\mathbf{\Lambda}_d\mathbf{B}_{\text{pre}}^H(n) \\ &+ \mathbf{B}_{\text{next}}(n)\mathbf{\Lambda}_d^H\mathbf{\Lambda}_d\mathbf{K}_s(n+1)\mathbf{\Lambda}_d^H\mathbf{\Lambda}_d\mathbf{B}_{\text{next}}^H(n) + \mathbf{K}_{\mathbf{y}_{\text{noise}}}(n)\end{aligned} \tag{4.26}$$

where we have assumed independence of the transmit symbols across different OFDM symbols, and where we have introduced the covariance of the transmit symbols $\mathbf{K}_s(n) \triangleq \frac{1}{2}E\{\mathbf{s}(n)\cdot\mathbf{s}^H(n)\}$, and the covariance of the noise at the DFT output $\mathbf{K}_{\mathbf{y}_{\text{noise}}}(n) \triangleq \frac{1}{2}E\{\mathbf{y}_{\text{noise}}(n)\cdot\mathbf{y}_{\text{noise}}^H(n)\}$. Assuming independence of transmit symbols across subcarriers, i.e., $\mathbf{K}_s(n) = \mathbf{K}_s(n-1) = \mathbf{K}_s(n+1) = P_s\mathbf{I}_N$, and uncorrelated noise across subcarriers, i.e., $\mathbf{K}_{\mathbf{y}_{\text{noise}}}(n) = \sigma^2_{\text{noirse}}\mathbf{I}_N$, then we can re-write (4.26) as

$$\begin{aligned}\mathbf{K}_w &= P_s\overline{\mathbf{D}}_A(n)\mathbf{\Lambda}_d^H\mathbf{\Lambda}_d\overline{\mathbf{D}}_A^H(n) + P_s\mathbf{B}_{\text{pre}}(n)\mathbf{\Lambda}_d^H\mathbf{\Lambda}_d\mathbf{B}_{\text{pre}}^H(n) \\ &+ P_s\mathbf{B}_{\text{next}}(n)\mathbf{\Lambda}_d^H\mathbf{\Lambda}_d\mathbf{B}_{\text{next}}^H(n) + \sigma^2_{\text{noise}}\mathbf{I}_N\end{aligned} \tag{4.27}$$

where we have used the fact that $\mathbf{\Lambda}_d\mathbf{\Lambda}_d^H = \mathbf{I}_{N_d}$. We can express the DFT output at the l^{th} subcarrier of the n^{th} OFDM symbol as

$$y_{n,l} = \psi_{n,l}\cdot s_{n,l} + w_{n,l}^{\text{pilot}} + w_{n,l} \tag{4.28}$$

where

$$w_{n,l} = \sum_{m\in\{D(n)\backslash l\}} A_{l,m}s_{n,m} + \sum_{m\in\{D(n-1)\}} B^{\text{pre}}_{l,m}s_{n-1,m} + \sum_{m\in\{D(n+1)\}} B^{\text{next}}_{l,m}s_{n+1,m} + y^{\text{noise}}_{n,l}, \tag{4.29}$$

$$w^{\text{pilot}}_{n,l} = \sum_{m\in\{P(n)\backslash l\}} A_{l,m}s_{n,m} + \sum_{m\in\{P(n-1)\}} B^{\text{pre}}_{l,m}s_{n-1,m} + \sum_{m\in\{P(n+1)\}} B^{\text{next}}_{l,m}s_{n+1,m} \tag{4.30}$$

and

$$\psi_{n,l} = A_{l,l} \tag{4.31}$$

and where $\{D(n)\}$ and $\{P(n)\}$ denote the data and pilot subcarriers in the n^{th} OFDM symbol, respectively, and where $\{D(n) \setminus l\}$ denotes the data subcarriers in the n^{th} OFDM symbol except the l^{th} subcarrier.

4.4.3 Channel estimation

We consider a linear channel estimator where the de-rotated (usually denoted descrambled) pilot subcarriers at the DFT output constitute the input to the channel estimator, i.e., $\mathbf{D}_p^{-1}(n) \cdot \mathbf{\Lambda}_p \cdot \mathbf{y}(n)$, where $\mathbf{D}_p(n)$ is a diagonal matrix of size $(N_p \times N_p)$ with diagonal entries set to the modulation symbols at the pilot subcarriers constituting the scrambling of the pilot sequence.

The de-rotated (descrambled) pilot subcarriers are linearly combined to generate the channel estimates at the N subcarriers. This linear combination can be implemented by the matrix $\mathbf{\Omega}$ of size $(N \times N_p)$, which represents the linear processing according to a given channel estimation criterion, e.g., linear frequency domain interpolator, DFT-based

channel estimator, etc. [52]. Therefore, we express the channel estimates as

$$\hat{\mathbf{g}}(n) \triangleq \mathbf{\Omega} \cdot \mathbf{D}_p^{-1}(n) \cdot \mathbf{\Lambda}_p \cdot \mathbf{y}(n) \tag{4.32}$$

Using (4.25) we can re-write (4.32) as

$$\hat{\mathbf{g}}(n) = \mathbf{\Omega} \cdot \mathbf{D}_p^{-1}(n) \cdot \mathbf{\Lambda}_p \cdot (\mathbf{D}_A(n) \cdot \mathbf{s}(n) + \mathbf{w}_{\text{pilot}}(n) + \mathbf{w}(n)) \tag{4.33}$$

Note that $\mathbf{D}_p^{-1}(n) \cdot \mathbf{\Lambda}_p \cdot \mathbf{D}_A(n) \cdot \mathbf{s}(n)$ is a column vector of length N_p with entries the channel gains $A_{l,l}$ at the pilot subcarriers, i.e., $l \in \{P(n)\}$. Denote by $\underline{\psi}(n)$ the column vector of length N with entries equal to the diagonal of $\mathbf{A}(n)$ as $\underline{\psi}(n) \triangleq \text{diag}(\mathbf{A}(n)) = \text{diag}(\mathbf{D}_{\mathbf{A}}(n))$. Therefore, we can re-write (4.33) as

$$\hat{\mathbf{g}}(n) = \mathbf{\Omega} \cdot \mathbf{\Lambda}_p \cdot \underline{\psi}(n) + \mathbf{\Omega} \cdot \mathbf{D}_p^{-1}(n) \cdot \mathbf{\Lambda}_p \cdot \mathbf{w}_{\text{pilot}}(n) + \mathbf{\Omega} \cdot \mathbf{D}_p^{-1}(n) \cdot \mathbf{\Lambda}_p \cdot \mathbf{w}(n) \tag{4.34}$$

We can now express the vector of channel estimates as

$$\hat{\mathbf{g}}(n) = \hat{\underline{\psi}}(n) + \mathbf{v}(n) \tag{4.35}$$

where we have introduced the mean value conditioned on the channel realization $\hat{\underline{\psi}}(n)$ computed to be

$$\hat{\underline{\psi}}(n) \triangleq E\{\hat{\mathbf{g}}(n)|_{\mathbf{A}(n),\mathbf{B}_{\text{pre}}(n),\mathbf{B}_{\text{next}}(n)}\} = \mathbf{\Omega}\mathbf{\Lambda}_p\underline{\psi}(n) + \mathbf{\Omega}\mathbf{D}_p^{-1}\mathbf{\Lambda}_p\mathbf{w}_{\text{pilot}}(n) \tag{4.36}$$

and the channel estimation noise-and-interference

$$\mathbf{v}(n) \triangleq \hat{\mathbf{g}}(n) - E\{\hat{\mathbf{g}}(n)|_{\mathbf{A}(n),\mathbf{B}_{\text{pre}}(n),\mathbf{B}_{\text{next}}(n)}\} = \mathbf{\Omega}\mathbf{D}_p^{-1}\mathbf{\Lambda}_p\mathbf{w}(n) \tag{4.37}$$

The covariance of the channel estimates conditioned on the channel realization is

$$\mathbf{K}_v \triangleq \frac{1}{2} E\{\mathbf{v}\mathbf{v}^H|_{\mathbf{A},\mathbf{B}_{\text{pre}},\mathbf{B}_{\text{next}}}\} = \mathbf{\Omega}\mathbf{D}_p^{-1}\mathbf{\Lambda}_p\mathbf{K}_w\mathbf{\Lambda}_p^H(\mathbf{D}_p^{-1})^H\mathbf{\Omega}^H \tag{4.38}$$

where $\mathbf{K}_w$ was found in (4.26) and (4.27). Note that the channel estimates at each of the carriers are complex circular Gaussian random variables as we assume the ICI and ISI interference to follow a Gaussian distribution [51]. The channel estimate at the l^{th} subcarrier of the n^{th} OFDM symbol can be expressed as

$$\hat{g}_{n,l} \triangleq \hat{\psi}_{n,l} + v_{n,l} \tag{4.39}$$

where the mean of the channel estimate conditioned on the channel realization can be written as

$$\hat{\psi}_{n,l} = E\{\hat{g}_{n,l}|_{\mathbf{A}(n),\mathbf{B}_{\text{pre}}(n),\mathbf{B}_{\text{next}}(n)}\} = \sum_{m\in\{P(n)\}} \Omega_{l,m}\cdot(\psi_{n,m} + w_{n,m}^{\text{pilot}}/p_{n,m}) \tag{4.40}$$

and the channel estimate noise can be written as

$$v_{n,l} = \hat{g}_{n,l} - E\{\hat{g}_{n,l}|_{\mathbf{A}(n),\mathbf{B}_{\text{pre}}(n),\mathbf{B}_{\text{next}}(n)}\} = \sum_{m\in\{P(n)\}} \Omega_{l,m}\cdot w_{n,m}/p_{n,m} \tag{4.41}$$

Defining the bias of the channel estimate by

$$\Delta\hat{\psi}_{n,l} = (\hat{\psi}_{n,l} - \psi_{n,l}) \tag{4.42}$$

we capture the case where the channel estimate $\hat{g}_{n,l}$ may be biased - this is important for the computation of the desired signal power and the noise-and-interference power.

4.4.4 Data detection

Assuming a single tap equalizer receiver we define the data detection output as

$$\begin{aligned} z_{n,l} &\triangleq \hat{g}_{n,l}^* \cdot y_{n,l} = \hat{g}_{n,l}^* \cdot \left(\psi_{n,l} \cdot s_{n,l} + w_{n,l}^{\text{pilot}} + w_{n,l}\right) \\ &= \hat{g}_{n,l}^* \cdot (\psi_{n,l} \cdot s_{n,l} + w_{n,l}^{\text{pilot}}) + \hat{g}_{n,l}^* \cdot w_{n,l} \end{aligned} \tag{4.43}$$

where we have used the expression for $y_{n,l}$ in (4.28). In the next Section, we will use the fact that conditioned on the channel realization, $\mathbf{A}(n)$, $\mathbf{B}_{\text{pre}}(n)$ and $\mathbf{B}_{\text{next}}(n)$, the channel estimate, $\hat{g}_{n,l}$, and the transmitted symbol, $s_{n,l}$, the output of the data detector is complex circular Gaussian with the following moments:

$$E\{z_{n,l}|_{\mathbf{A}(n),\mathbf{B}_{\text{pre}}(n),\mathbf{B}_{\text{next}}(n),s_{n,l},\hat{g}_{n,l}}\} = \hat{g}_{n,l}^* \cdot (\psi_{n,l} \cdot s_{n,l} + w_{n,l}^{\text{pilot}}) \tag{4.44}$$

and

$$Var\{z_{n,l}|_{\mathbf{A}(n),\mathbf{B}_{\text{pre}}(n),\mathbf{B}_{\text{next}}(n),s_{n,l},\hat{g}_{n,l}}\} = |\hat{g}_{n,l}|^2 \cdot Var\{w_{n,l}\} \tag{4.45}$$

where $Var\{w_{n,l}\}$ can be easily found from the diagonal elements of the covariance matrix $\mathbf{K}_w$ defined in (4.26) or (4.27).

4.5 Optimization Process

The goal of the cognitive receiver is to find a set of parameters so that the capacity of the communication link is maximized. In this Section we will compute the effective capacity for different hypotheses of the OFDM system parameters for the cognitive OFDM receiver to choose the optimal parameter settings.

First, we characterize the SINR at the data detector output conditioned on the channel realization, channel estimate and transmitted symbol. Then, we use this conditional SINR to estimate the capacity of the link for different hypotheses at the cognitive

receiver.

4.5.1 SINR derivation

chap5.5a Using $\hat{g}_{n,l} = \psi_{n,l} + \hat{g}_{n,l} - \psi_{n,l}$, we can re-write the data detector output in (4.43) as

$$\begin{aligned} z_{n,l} &= \hat{g}^*_{n,l} \cdot (\psi_{n,l} \cdot s_{n,l} + w^{\text{pilot}}_{n,l}) + \hat{g}^*_{n,l} \cdot w_{n,l} \\ &= (\psi_{n,l} + \hat{g}_{n,l} - \psi_{n,l})^* \cdot \psi_{n,l} \cdot s_{n,l} + \hat{g}^*_{n,l} \cdot w^{\text{pilot}}_{n,l} + \hat{g}^*_{n,l} \cdot w_{n,l} \\ &= |\psi_{n,l}|^2 \cdot s_{n,l} + (\hat{g}_{n,l} - \psi_{n,l})^* \cdot \psi_{n,l} \cdot s_{n,l} + \hat{g}^*_{n,l} \cdot w^{\text{pilot}}_{n,l} + \hat{g}^*_{n,l} \cdot w_{n,l} \end{aligned} \quad (4.46)$$

from where we see that the signal of interest is $z_{\text{useful}} \triangleq |\psi_{n,l}|^2 \cdot s_{n,l}$ and the contribution to the noise-and interference is $z_{\text{noise and interference}} \triangleq (\hat{g}_{n,l} - \psi_{n,l})^* \cdot \psi_{n,l} \cdot s_{n,l} + \hat{g}^*_{n,l} \cdot w^{\text{pilot}}_{n,l} + \hat{g}^*_{n,l} \cdot w_{n,l}$.

The data detector output SINR at the l^{th} subcarrier of the n^{th} OFDM symbol conditioned on the channel realization, the channel estimate and the transmitted symbol can be computed as follows:

$$\text{SNR}_{n,l}(\hat{g}_{n,l}|_{\mathbf{A},\mathbf{B}_{\text{pre}},\mathbf{B}_{\text{next}},\hat{g}_{n,l},s_{n,l}}) \triangleq \frac{|z_{\text{useful}}|^2}{E\{|z_{\text{noise and interference}}|^2|_{\mathbf{A},\mathbf{B}_{\text{pre}},\mathbf{B}_{\text{next}},\hat{g}_{n,l},s_{n,l}}\}} \quad (4.47)$$

where we drop from now on the OFDM symbol index n to shorten notation and where

$$\begin{aligned} E\{|z_{\text{noise and interference}}|^2|_{\mathbf{A},\mathbf{B}_{\text{pre}},\mathbf{B}_{\text{next}},\hat{g}_{n,l},s_{n,l}}\} &= |(\hat{g}_{n,l} - \psi_{n,l})^* \cdot \psi_{n,l} \cdot s_{n,l} + \hat{g}^*_{n,l} \cdot w^{\text{pilot}}_{n,l}|^2 \\ &+ |\hat{g}_{n,l}|^2 \cdot Var\{w_{n,l}\} \end{aligned} \quad (4.48)$$

where $Var\{w_{n,l}\}$ can be easily found from the diagonal elements of the covariance matrix $\mathbf{K}_w$ defined in (4.26) or (4.27).

Denoting the channel estimate by $\hat{g}_{n,l} = x_{n,l} + jy_{n,l}$ we can re-write (4.47) as

$$\text{SNR}_{n,l}(x_{n,l}, y_{n,l}|_{\mathbf{A},\mathbf{B}_{\text{pre}},\mathbf{B}_{\text{next}},\hat{g}_{n,l},s_{n,l}}) = \frac{|\psi_{n,l}|^4 \cdot |s_{n,l}|^2}{|(x_{n,l} + jy_{n,l} - \psi_{n,l})^* \cdot \psi_{n,l} \cdot s_{n,l} + (x_{n,l} - jy_{n,l}) \cdot w_{n,l}^{\text{pilot}}|^2 + (x_{n,l}^2 + y_{n,l}^2) \cdot Var\{w_{n,l}\}} \tag{4.49}$$

4.5.2 Capacity Estimation

For a given channel realization and a set of parameters $\{\hat{d}, M_p, CP, N\}$, we denote by $C_{n,l}(\hat{d}, M_p, CP, N|_{\mathbf{A},\mathbf{B}_{\text{pre}},\mathbf{B}_{\text{next}}})$ the capacity of the l^{th} data subcarrier of the n^{th} OFDM symbol.

As discussed in Section 4.4.4, we use the fact that the data detector output in (4.43) conditioned on the channel realization, $\mathbf{A}$, $\mathbf{B}_{\text{pre}}$, $\mathbf{B}_{\text{next}}$, the channel estimate, $\hat{g}_{n,l}$, and the transmitted symbol, $s_{n,l}$, is complex circular Gaussian and therefore, we can compute $C_{n,l}(\hat{d}, M_p, CP, N|_{\mathbf{A},\mathbf{B}_{\text{pre}},\mathbf{B}_{\text{next}}})$ averaging over the probability density function of the channel estimate $\hat{g}_{n,l} = x_{n,l} + jy_{n,l}$ as follows

$$\begin{aligned} &C_{n,l}(\hat{d}, M_p, CP, N|_{\mathbf{A},\mathbf{B}_{\text{pre}},\mathbf{B}_{\text{next}}}) \\ &\quad = \int_{-\infty}^{\infty}\int_{-\infty}^{\infty} log_2(1 + \text{SNR}_{n,l}(x_{n,l}, y_{n,l}|_{\mathbf{A},\mathbf{B}_{\text{pre}},\mathbf{B}_{\text{next}},\hat{g}_{n,l},s_{n,l}})) \\ &\quad \cdot f_{\hat{g}}(x_{n,l}, y_{n,l}) \cdot dx_{n,l}dy_{n,l} \end{aligned} \tag{4.50}$$

where $\text{SNR}_{n,l}(x_{n,l}, y_{n,l}|_{\mathbf{A},\mathbf{B}_{\text{pre}},\mathbf{B}_{\text{next}},\hat{g}_{n,l},s_{n,l}})$ is the SINR of the l^{th} data subcarrier of the n^{th} OFDM symbol at the data detector output conditioned on the channel realization, the channel estimate and the transmitted symbol, as characterized in (4.49). The function $f_{\hat{g}}(x_{n,l}, y_{n,l})$ is the probability density function of the channel estimate $\hat{g}_{n,l} = x_{n,l} + jy_{n,l}$, which, conditioned on the channel realization, is, in turn, also complex circular Gaussian, as discussed in Section 4.4.3, and therefore

$$f_{\hat{g}}(x_{n,l}, y_{n,l}) = \frac{1}{\pi\sigma_{v_{n,l}}^2} \cdot e^{-\frac{(x_{n,l} - \Re\{\hat{\psi}_{n,l}\})^2 + (y_{n,l} - \Im\{\hat{\psi}_{n,l}\})^2}{\sigma_{v_{n,l}}^2}} \tag{4.51}$$

where the first order moment, $\hat{\psi}_{n,l}$ is characterized in (4.40) and the second order moment, $\sigma^2_{v_{n,l}}$, can be obtained from the diagonal terns of $\mathbf{K}_v$ in (4.38).

We define the effective capacity averaged across data subcarriers for a given channel realization and set of parameters as

$$C_n^{\text{effective}}(\hat{d}, M_p, CP, N|_{\mathbf{A},\mathbf{B}_{\text{pre}},\mathbf{B}_{\text{next}}}) \triangleq \frac{N_d}{(N_d + N_p + CP_{\text{rx}})} \cdot \Big(\frac{1}{N_d} \sum_{l \in \{D(n)\}} C_{n,l}(\cdot)\Big) \quad (4.52)$$

where we have used $C_{n,l}(\cdot)$ to denote $C_{n,l}(\hat{d}, M_p, CP, N|_{\mathbf{A},\mathbf{B}_{\text{pre}},\mathbf{B}_{\text{next}}})$, where the summation is performed over the N_d data subcarriers, and where the first term in the RHS is the ratio of time-frequency dimensions that contribute to the capacity of the OFDM system. Note that only the data subcarriers contribute to the capacity of the system, while the pilot subcarriers and the CP contribute to overhead. Further, note that we use the CP duration used at the receiver to estimate the capacity that would be achievable with such CP.

Finally, the effective capacity can be averaged over multiple channel realizations to yield an average capacity as follows

$$C_{\text{average}} \triangleq \frac{1}{L} \sum_{j=0}^{L-1} C_{n_j}^{\text{effective}}(\hat{d}_j, M_{p_j}, CP_j, N_j|_{\mathbf{A}_j,\mathbf{B}_{\text{pre}_j},\mathbf{B}_{\text{next}_j}}) \quad (4.53)$$

where $\{\hat{d}_j, M_{p_j}, CP_j, N_j\}$ represent the cognitive parameters used for the j^{th} channel realization and where $C_{n_j}^{\text{effective}}(\hat{d}_j, M_{p_j}, CP_j, N_j|_{\mathbf{A}_j,\mathbf{B}_{\text{pre}_j},\mathbf{B}_{\text{next}_j}})$ is the effective capacity averaged across data subcarriers for the j^{th} channel realization.

4.6 Analyses and Simulations

The maximization set forth in the previous Section entails a 4-dimensional optimization. In order to make the problem tractable in practice, we set a sequence in the optimization process. Therefore, for a given transmission, the first optimization that we

perform is to find the optimal DFT window placement, i.e., determine $\hat{d}_{\text{opt}}$.

Once the optimal DFT window placement is found, we optimize the pilot structure for the given channel realization and operating SNR regime.

When the optimal pilot structure is identified, we compute the optimal CP duration for the identified optimal DFT window placement and pilot density.

The OFDM symbol duration can then be optimized. Note that since for a given system bandwidth, a change of the OFDM symbol duration entails a change in the sub-carrier spacing, the pilot structure can be revisited if the OFDM symbol duration has changed.

In practice, this optimization process can be iterative and the optimization can take other sequences.

4.6.1 DFT window

The placement of the DFT window consists of the time tracking at the OFDM receiver. We consider in this study a multi-hypothesis process where the SINR is computed for each of the candidate timing hypothesis. The optimization will select the OFDM symbol boundary providing the maximum projected capacity.

This multiple hypotheses are provided from the received waveform without any specific structure required, since the only difference is where the receiver starts discarding the CP and which sample is the first going to the DFT operation.

Figure 4.4 shows a toy example for a system with $N = 6$, $CP = 2$ and a channel span of 3 samples. As we see the chosen symbol boundary determines the DFT window.

Figure 4.5 shows the result of this optimization for different values of $\hat{d}$ for a channel realization of the UWB CM4, and for $N = 128$, M_p = 2, CP = 32 and Δf = 200kHz, at different operating SNRs. Note that most of the results in this chapter assume a residual frequency error of 200kHz which results from a transmit and receive

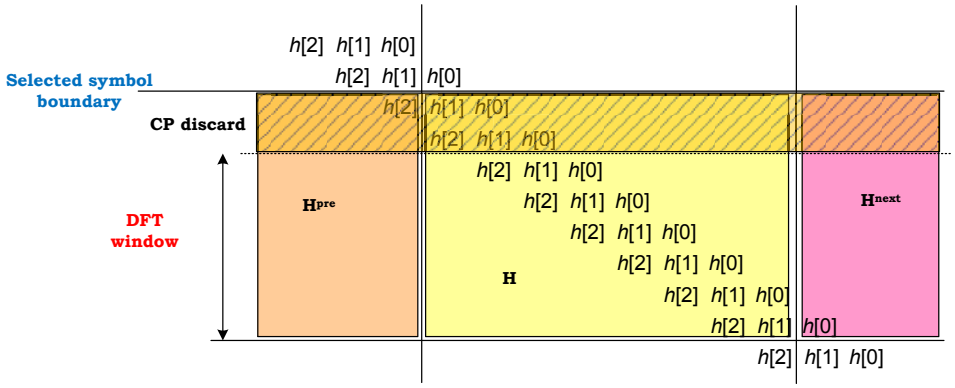

Figure 4.4 *DFT window placement example*

frequency tolerance of ± 20ppm, and we consider 5GHz operation. Further, note that this is the maximum expected residual frequency error in UWB systems and that this residual frequency error could be compensated for with frequency tracking mechanisms at the receiver.

For a given CP, the DFT window placement is robust against operating SNR as can be seen well in Figure 4.5. Indeed, this operation attempts to minimize the effect of the ISI from the previous and next OFDM symbols to find the best balance given the CP duration. Indeed, for channels decaying in time, the optimization process will yield to DFT window placements that minimize the ISI from the next OFDM symbol.

A value $\hat{d} = 1$ implies that the last sample of the channel realization is assumed to set the beginning of the DFT window - this choice causes ISI from the next OFDM symbol and does not exploit the available CP. In contrast, a value of $\hat{d} = 91$ in this example implies that the first sample of the channel realization sets the beginning of the DFT window. This is the point that we were denoting as $\tau = 0$ in [51].

Given that this particular channel realization incurs ISI (the CP duration is 32 samples, while the channel delay spread is 91 samples) we see that it is better to trade-off some ISI from the first 10 samples of the channel, and hence operate with ISI from the next OFDM symbol, to better use the protection offered by the CP from the previous OFDM symbol. Indeed, the filtering process at the transmitter and the receiver make the

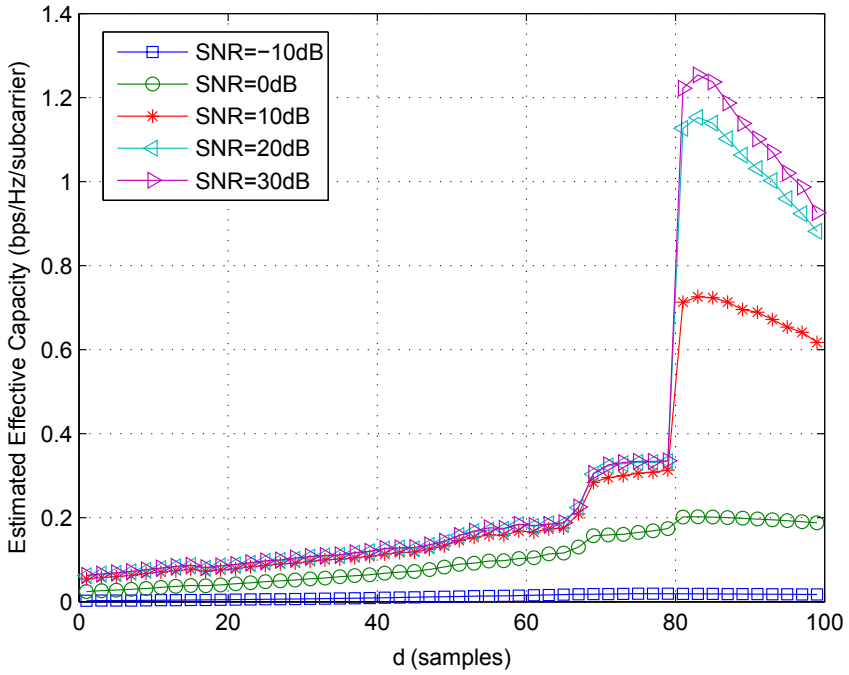

Figure 4.5 *$\hat{d}$ optimization for CM4 channel realization with a channel span of 91 samples and CP=32*

effective channel impulse response with some skirts around the channel taps.

Figure 4.6 shows the same Projected Capacity vs. $\hat{d}$ curve for a UWB CM2 channel realization. This channel realization has a channel span of 39 samples and the CP duration is 32 samples. The curve is obtained with M_p=2 and at different SNRs.

As we can see from Figure 4.5 and Figure 4.6, performance is very poor if the DFT window is placed at the end of the channel span. For this case, there is, obviously, no ISI from the previous OFDM symbol but all channel taps but one contribute to ISI from the next OFDM symbol. As one can see, for this case, the CP is of no use and is completely wasted.

The performance gradually improves for larger values of $\hat{d}$ with the effect that gradually more channel taps contribute to ISI from previous OFDM symbol and gradually less channel taps cause ISI from the next OFDM symbol. Note that channel taps contributing to ISI from the previous OFDM symbol get CP protection up to the CP

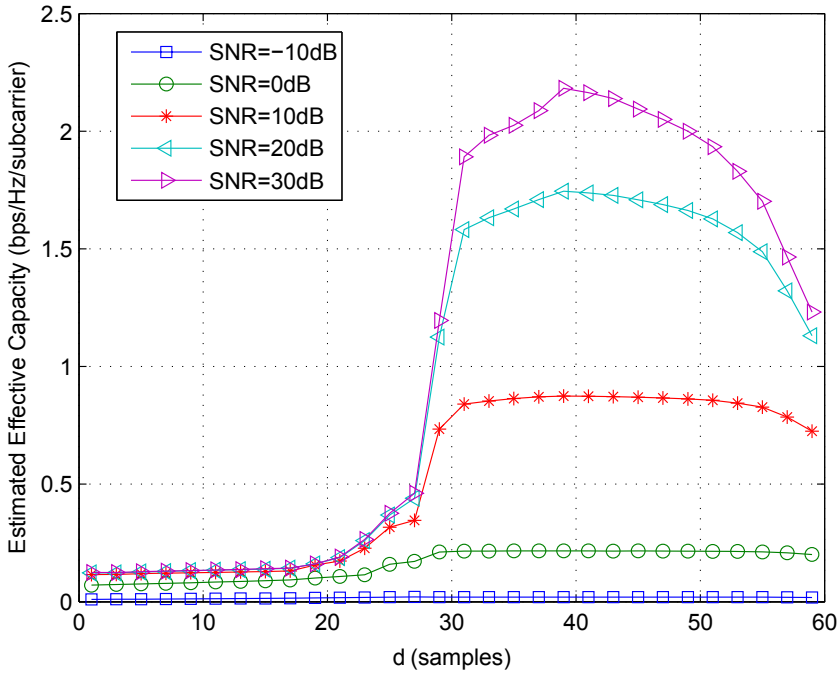

Figure 4.6 *$\hat{d}$ optimization for CM2 channel realization with a channel span of 39 samples and CP=32*

length. At some point there is an optimal balance between the CP protection removing ISI from the previous OFDM symbol and ISI from the next OFDM symbol. This point is usually where most of the ISI from the next OFDM symbol is removed. Given that the channel realizations are usually time-decaying, the ISI from the next OFDM symbol caused by the first channel taps is usually more severe than ISI from the previous OFDM symbol which is caused by the last channel taps.

4.6.2 Pilot structure

The pilot signal is transmitted to enable channel estimation at the receiver for coherent demodulation. The pilot structure that we consider is shown in Figure 4.3, where as can be seen, the same subcarriers are used for pilot transmission in every OFDM symbol. We consider the pilot signal itself to be pseudo-random and the evaluations assume a pseudo randomly generated QPSK signal.

We consider three different types of channel estimation algorithms. Channel estimation type I consists of frequency domain interpolation whereby the channel estimate at each data subcarrier is directly the receive signal at the closest pilot subcarrier. This channel estimation is highly inefficient since it uses only one pilot subcarrier for the estimation of the channel at each data subcarrier. Therefore, it does not perform any interpolation of pilot signals to derive the channel at data subcarriers nor performs any noise-and-interference averaging. Channel estimation type II consists of a linear frequency domain interpolation whereby the weighted average of the two closest pilot signals is used for the channel estimate of the data subcarriers. For data subcarriers at the edge of the band not falling between two pilot subcarriers, a direct extrapolation of the received signal at the closest pilot subcarrier is used as the channel estimation on those data subcarriers. Finally, channel estimation type III consists of a DFT-based channel estimation [52] where first, an IDFT of size N_p translates the estimation problem to the time domain. Then, the first N_h time-domain samples are retained while the others are truncated. These N_h samples get zero padded with $(N - N_h)$ additional samples and a DFT of size N is performed to transform back to the frequency domain. Note that this estimation is equivalent to a "discrete sinc" interpolation in the frequency domain as shown in Appendix B.2.

Figure 4.7, Figure 4.8 and Figure 4.9 show the estimated average capacity for different channel estimation types, and different pilot densities ranging from 1 pilot subcarrier every 2 subcarriers (M_p = 2) to 1 pilot subcarrier every 8 subcarriers (M_p = 8) averaged across 100 CM1 channel realizations. The results are obtained with SNR = 20dB, Δf = 200kHz, and the optimal DFT window placement for each of the realizations.

As can be seen from these figures, the DFT-based channel estimation is the best performing channel estimation method out of the three channel estimation algorithms that we investigate.

Figure 4.10 through Figure 4.12 show the same characterization for 100 realizations of UWB's CM2, CM3, and CM4, respectively, and using channel estimation type

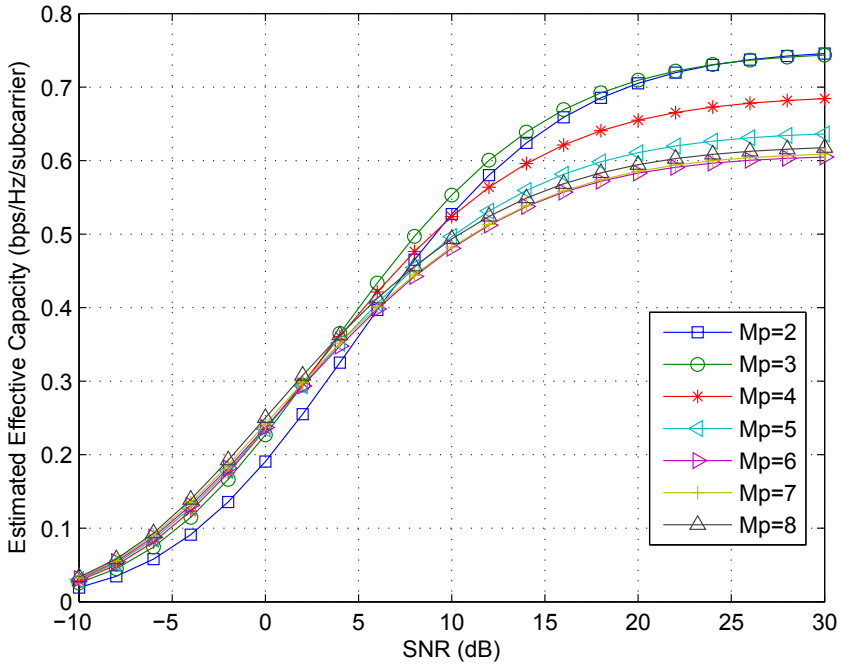

Figure 4.7 *Average estimated capacity vs. SNR for different pilot densities with channel estimation type I: CM1 channel realizations*

III (DFT-based channel estimation).

Note the interesting cross-overs of the different curves for different optimal values of M_p for different operating SNRs. A lower M_p value increases the channel estimation quality at the expense of reducing the number of effective (data) subcarriers, while a higher M_p value yields poorer channel estimates but with less pilot signal overhead.

Similar to the optimization of the DFT window placement, no special treatment in the transmit waveform is required to try different pilot densities hypotheses at the receiver as long as the hypothetical pilot densities are equal to or divide the original transmission pilot density. For example, if $M_p = 2$ is used as the nominal transmission, the receiver can try hypotheses $M_p = 2$, $M_p = 4$, $M_p = 8$ at the receiver.

A special case is the availability of pilot symbols where all the subcarriers carry pilot signal, i.e., TDM pilot. In this case, M_p = 1 and therefore the channel estimation can be performed assuming any value of M_p and is performed in the same way as it

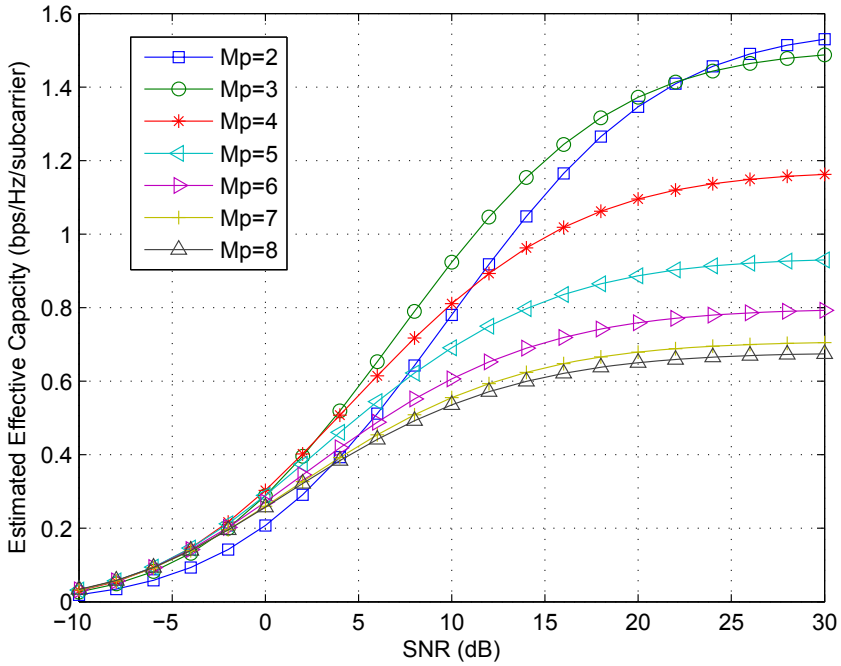

Figure 4.8 *Average estimated capacity vs. SNR for different pilot densities with channel estimation type II: CM1 channel realizations*

would be done for that particular pilot density. Provided that the pilot sequence itself is pseudo-random it will have the same effect as ICI as random data symbols.

4.6.3 CP duration

Once the optimal DFT window placement and pilot density are obtained, the receiver can optimize the CP duration. For this purpose we exploit the fact that the transmission over an OFDM symbol is circular considering the transmission of the CP. Indeed, the CP insertion circularly extends the OFDM symbol of length N samples to N_T samples. As a result, an OFDM receiver can perform partial CP discarding to test different CP duration hypotheses based on the same transmit OFDM symbol. In Section 4.4 we described the partial CP discarding operation in an OFDM system where the CP length inserted at the transmitter (CP_{tx}) may not be the same as the CP discarded at the receiver (CP_{rx}), i.e., $CP_{\text{tx}} \geq CP_{\text{rx}}$.

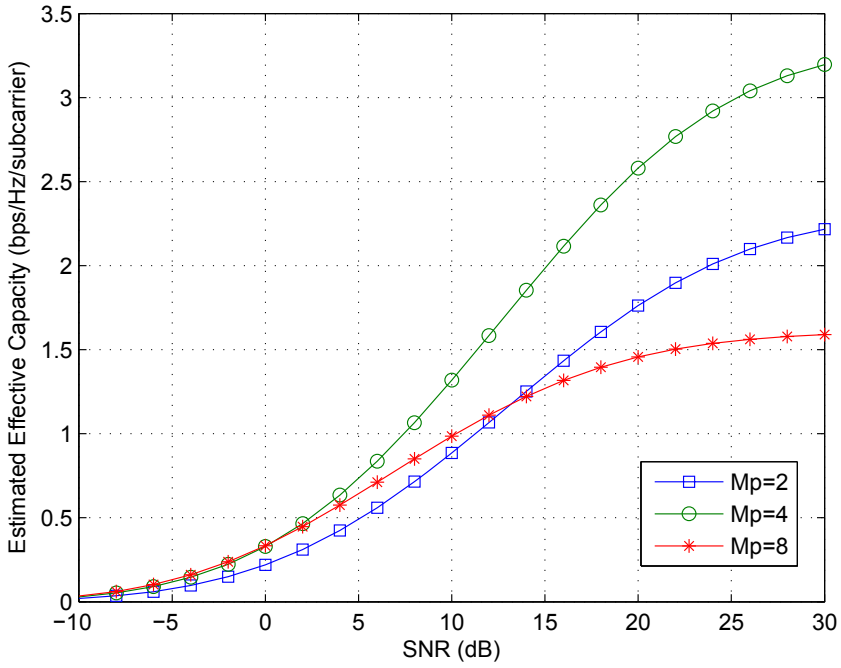

Figure 4.9 *Average estimated capacity vs. SNR for different pilot densities with channel estimation type III: CM1 channel realizations*

Consider a toy example as illustrated in Figure 4.13. For this example N = 6, $CP_{\text{tx}} = CP_{\text{rx}} = 3$ and the channel delay spread is 3 samples. We illustrate in the figure the channel matrices introduced in (4.12) with full CP discarding (3 samples). The effect of the CP discarding, matrix $\mathbf{R}_{\text{CP}}$ defined in (4.9), and CP insertion, matrix $\mathbf{T}_{\text{CP}}$ defined in (4.6), is graphically illustrated.

As we can see $\widetilde{\mathbf{H}}_{\text{pre}} = \widetilde{\mathbf{H}}_{\text{next}} = \mathbf{0}_{(N\times N)}$ and, therefore, there is no ISI. Also, $\widetilde{\mathbf{H}}$ is circulant and, therefore, $\mathbf{F}\widetilde{\mathbf{H}}\mathbf{F}^H = \mathbf{D}_H$ is diagonal. For the first case, the entries of the diagonal matrix $\mathbf{D}_H$ are the channel's frequency response evaluated at the subcarrier's frequencies, i.e., $g_m = \sum_{k=0}^{2} h_k \cdot e^{-j2\pi mk/6}, m = -3, -2, \ldots, 2$. The proof can be found as part of Appendix B.1.

Figure 4.14 illustrates the same toy example with partial CP discarding at the receiver of 2 samples, i.e., CP_{tx} = 3 and CP_{rx} = 2. This technique was introduced with the CP discarding matrix, $\mathbf{R}_{\text{CP}}$, defined in (4.9). Note that a third sample is discarded at

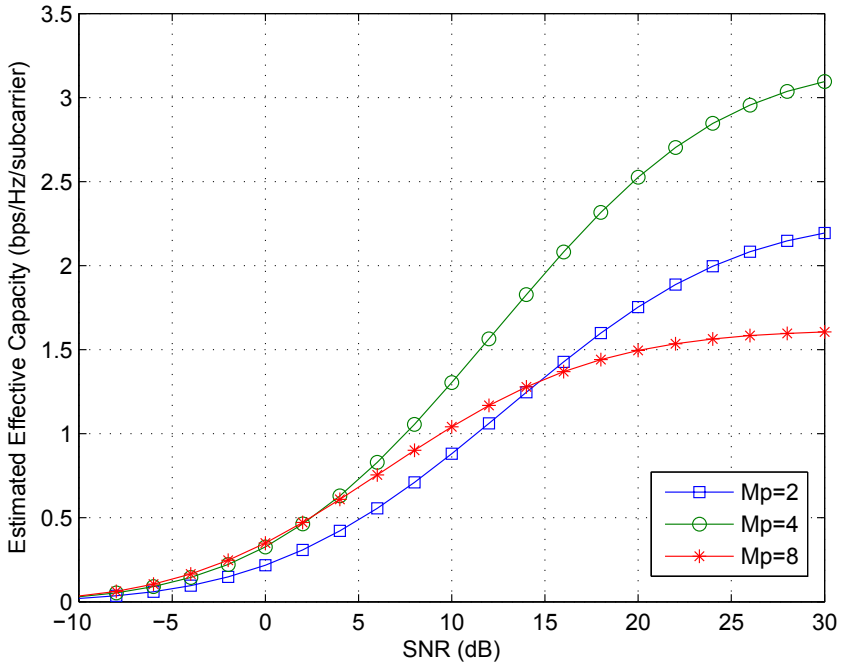

Figure 4.10 *Average estimated capacity vs. SNR for different pilot densities with channel estimation type III: CM2 channel realizations*

the end of the OFDM symbol as illustrated in the figure by the shaded band at the bottom of the figure so that the result of the CP discarding operation provides a vector of length N.

As we can see, for this example, the channel matrices $\widetilde{\mathbf{H}}'_{\text{pre}} = \widetilde{\mathbf{H}}'_{\text{next}} = \mathbf{0}_{(N\times N)}$ while the channel matrix $\widetilde{\mathbf{H}}'$ is circulant and, therefore, $\mathbf{F}\widetilde{\mathbf{H}}'\mathbf{F}^H = \mathbf{D}'_H$ is diagonal.

As shown in Appendix B.1, for the general case of partial CP discarding, the $(m,l)^{\text{th}}$ entry of the diagonal matrix $\mathbf{D}'_H$ is $D'_{H_{m,l}} = g_m \cdot e^{-j2\pi m(CP_{\text{tx}}-CP_{\text{rx}})/N} \cdot \delta_K(m-l)$.

Therefore, partial CP removal introduces a phase rotation of the effective channel gains at the OFDM receiver. This will have an effect in the interpolation methods used for channel estimation, especially because, as discussed in Appendix B.2, the magnitude of $(CP_{\text{tx}} - CP_{\text{rx}})$ can be large and even comparable to the number of subcarriers N.

As a result, for the purpose of channel estimation, whenever we perform partial

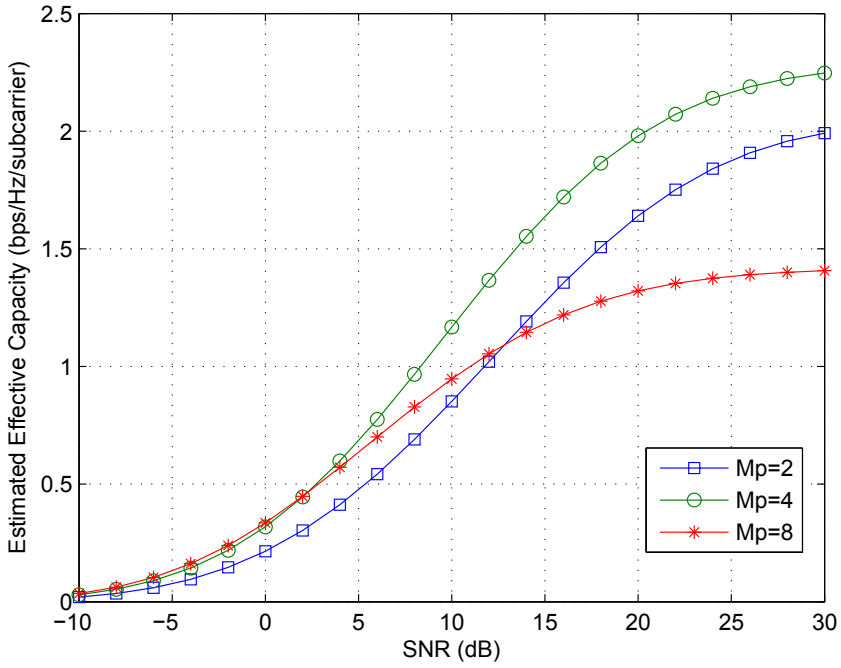

Figure 4.11 *Average estimated capacity vs. SNR for different pilot densities with channel estimation type III: CM3 channel realizations*

CP discard we will first de-rotate the pilot subcarriers according to the known phasor $e^{j2\pi m(CP_{\text{tx}}-CP_{\text{rx}})/N}$ depending on the subcarrier index. We will perform channel estimation as described in the previous Section and whenever the channel estimates at the data subcarriers are available we will apply again the rotation according to $e^{-j2\pi m(CP_{\text{tx}}-CP_{\text{rx}})/N}$. Appendix B.2 shows why the channel estimates without doing this de-rotation and subsequent rotation become very poor.

Figure 4.15 shows the estimated capacity averaged over 100 channel realizations of each of the UWB channel models CM1, CM2, CM3, and CM4 with realistic channel estimation. The channel estimation for Figure 4.15 is a DFT-based channel estimator with the parameter N_h (number of time-domain samples to estimate) set to the number of pilot subcarriers, N_p. All the results are obtained with SNR = 20dB, for the optimal DFT window placement and pilot density, M_p, for each of the realizations. In turn, Figure 4.16 shows the sensitivity analysis vs. CP duration averaged over 100 channel realizations

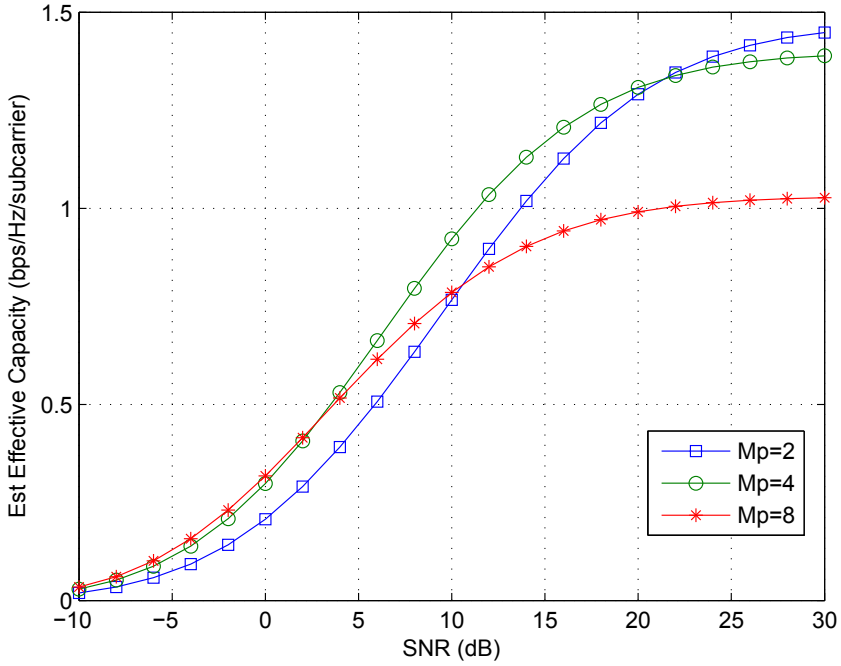

Figure 4.12 *Average estimated capacity vs. SNR for different pilot densities with channel estimation type III: CM4 channel realizations*

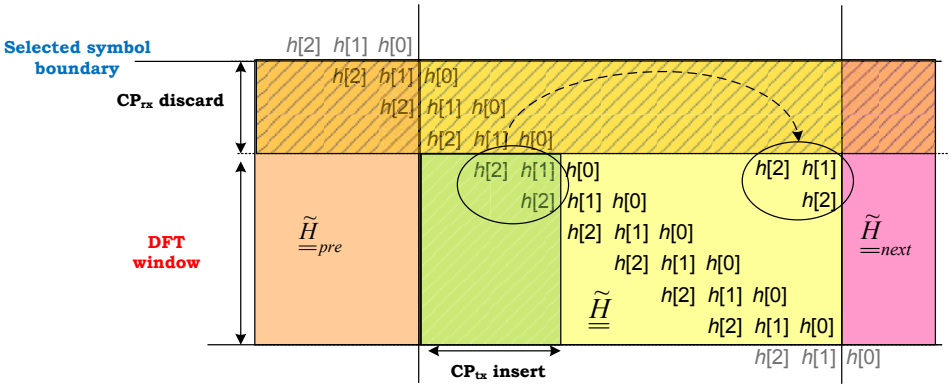

Figure 4.13 *Effect in channel matrices of CP insertion and full CP discarding*

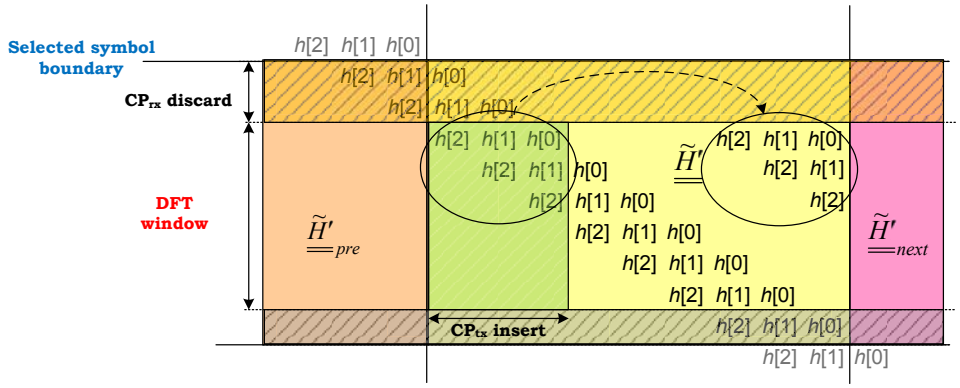

Figure 4.14 *Effect in channel matrices of CP insertion and partial CP discarding*

of CM1 and different operating SNRs. As can be seen from this figure the optimal CP duration depends on the operating SNR regime. For lower SNRs, the receiver can cope with more interference due to ISI with the benefit of a lower CP overhead, for higher SNRs, the receiver may become SINR limited unless the CP is not long enough.

As we can see from the figures, the capacity for each the channel models has a peak capacity at different CP durations. For small CP durations, the capacity is low due to low SINRs caused by the large ISI. For high CP durations, the capacity is also low due to the CP overhead. The cognitive-radio receiver will attempt to find the capacity peak for each situation.

As we have seen, there is no need of a special waveform structure to project the capacity for different CP durations provided that the hypothesis CP is of length equal to or less than the transmit CP, CP_{tx}. The receiver will need to compensate for the phase ramping of $e^{-j2\pi m(CP_{\text{tx}}-CP_{\text{rx}})/N}$ by de-rotating the pilot subcarrier prior to channel estimation, and rotating all the channel estimates according to the same ramping phasor.

4.6.4 OFDM symbol duration

The optimal OFDM symbol duration is related to the channel coherence time. The residual frequency error at the receiver may be seen as another contributor to the channel coherence time.

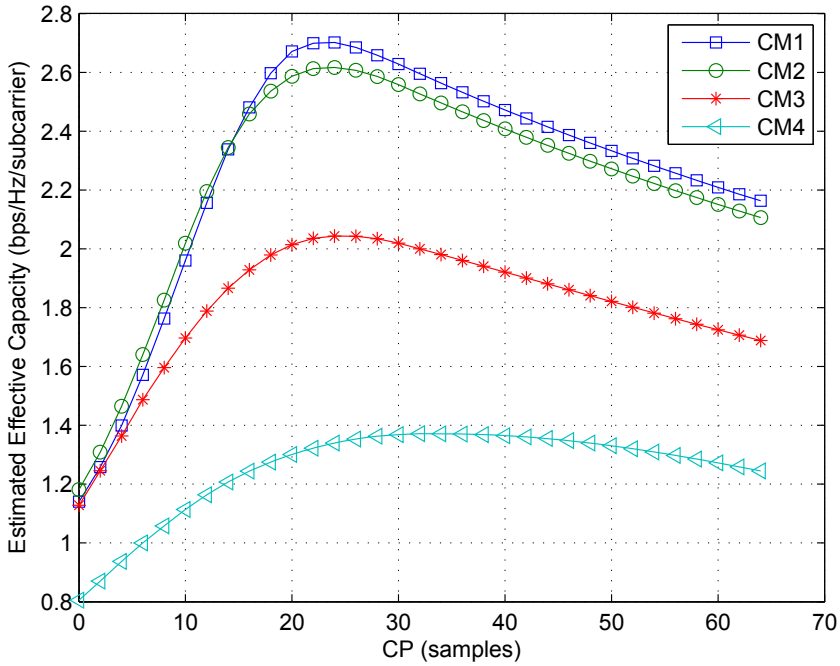

Figure 4.15 *Average estimated capacity of UWB channel models CM1, CM2, CM3, and CM4 vs. CP duration*

In order to realize the loss in subcarrier orthogonality incurred with a channel that varies within the OFDM symbol span we can compute the SINR for different OFDM symbol durations. Unlike the other optimizations $(\hat{d}, M_p, CP)$, this optimization requires the receiver to work on transmissions with different symbol durations T and estimate the effective capacity for each of them.

For the different values of the OFDM symbol duration, N, we can use the values found for the optimization of the DFT window, $\hat{d}$, the pilot structure, M_p, and the CP duration.

Figure 4.17 through Figure 4.20 show the estimated capacity for different values of N averaged across 100 channel realizations of each of the UWB channel models CM1, CM2, CM3, and CM4, respectively, and for various levels of SNR. The results assume a residual frequency error of 200kHz (maximum expected residual frequency error) and the optimal values found for the DFT window placement, the pilot structure and the CP

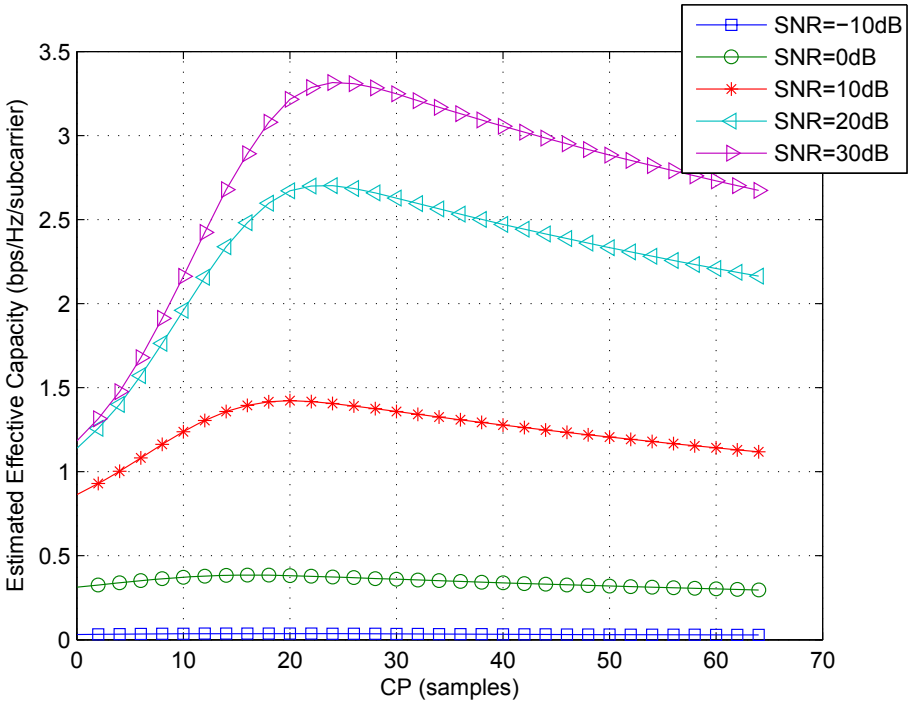

Figure 4.16 *Average estimated capacity of UWB channel model CM1 vs. CP duration for different SNR levels*

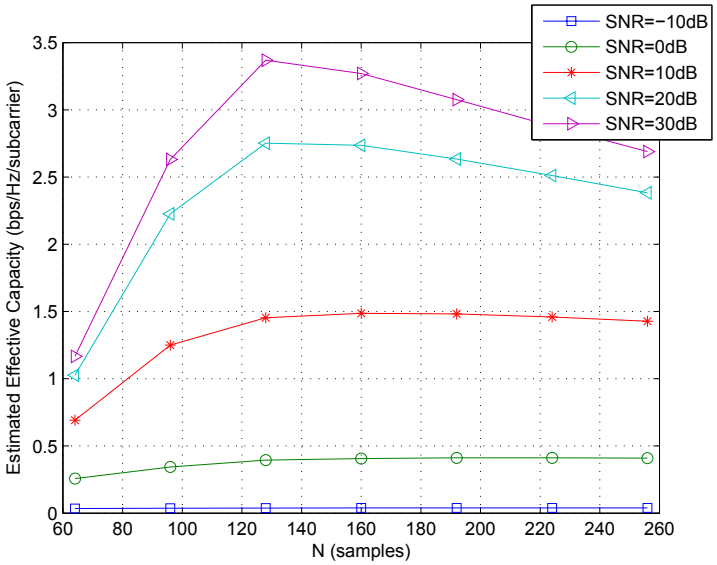

Figure 4.17 *Average estimated capacity for CM1 realizations vs. N: 200kHz residual frequency error*

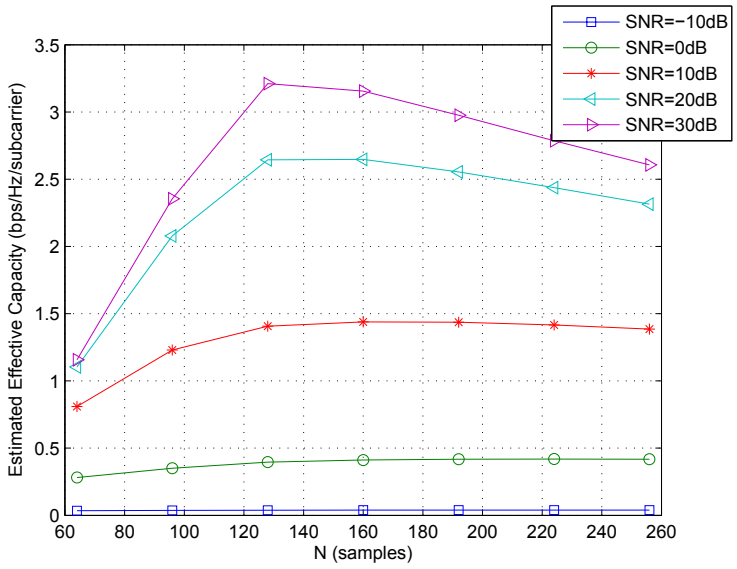

Figure 4.18 *Average estimated capacity for CM2 realizations vs. N: 200kHz residual frequency error*

duration for each of the channel realizations. As we can see, the optimal symbol duration depends on the channel model and on the operating SNR within a given channel model.

For lower SNR, there is less ICI impact since the thermal noise level is higher. Therefore, we can reduce the CP overhead by going to a longer OFDM symbol while improving on overall link efficiency.

In addition, the optimal OFDM symbol duration depends on the residual frequency error or Doppler frequency. Figure 4.21 is analogous to Figure 4.20 with the only difference that instead of 200kHz residual frequency error, there are 50kHz residual frequency error. As we can see comparing these two figures, the optimal OFDM symbol duration is sensitive to the residual frequency error. Also, we can see how this residual frequency error affects the estimated capacity, especially at high SNRs.

As we have seen, the optimization of the optimal OFDM symbol duration entails transmission with different OFDM symbol durations. As discussed before, the number of dimensions does not change with the OFDM symbol duration, and therefore the main benefit from a longer OFDM symbol is a lower CP overhead. Given the optimization of

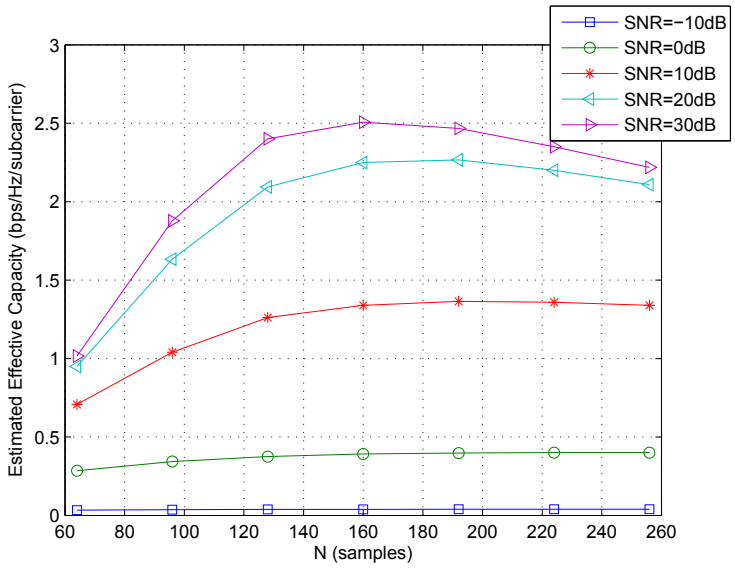

Figure 4.19 *Average estimated capacity for CM3 realizations vs. N: 200kHz residual frequency error*

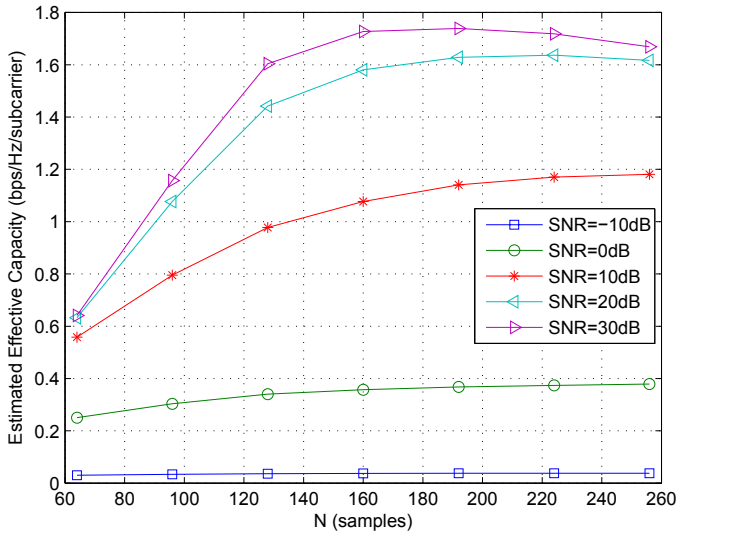

Figure 4.20 *Average estimated capacity for CM4 realizations vs. N: 200kHz residual frequency error*

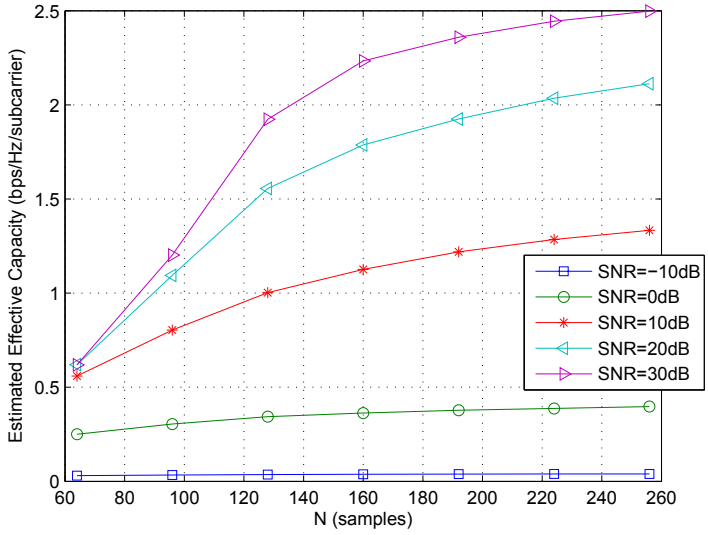

Figure 4.21 *Average estimated capacity for CM4 realizations vs. N: 50kHz residual frequency error*

the DFT/IDFT operations at the OFDM receiver/transmitter for FFT/IFFT implementations, this may set forth a constraint on the possible OFDM symbol duration values.

4.7 Conclusions

In this chapter we have discussed a cognitive OFDM system where the receiver performs an optimization process yielding parameter selections maximizing the communication link efficiency. We have considered an optimization entailing the DFT window placement, the pilot density, the CP duration, and the OFDM symbol duration. The optimization process at the receiver is based on a projection capacity function that resides at the receiver.

We have shown that the optimization of the DFT window placement, pilot density and CP duration do not require any special waveform treatment at the transmitter. The receiver can formulate multiple hypotheses based on the received waveform with its corresponding parameters.

The optimization of the OFDM symbol duration requires transmission of that duration for the receiver to derive the projected capacity.

4.8 Acknowledgements

The material of this chapter will be submitted for publication in *IEEE Transactions on Communications*. The dissertation author was the primary author and Prof. Laurence B. Milstein directed and supervised the research which forms the basis for this chapter.

CHAPTER 5

Conclusions

In this dissertation, we have studied the performance of OFDM with imperfections due to receiver non-idealities, such as residual timing error, residual frequency error and noisy channel estimates, as well as due to channel characteristics, such as Doppler and delay spread exceeding the OFDM symbol's CP. These non-ideal characterizations are key to be able to assess how well a cognitive receiver can work with different channel conditions. For example, at low SNRs, it may be better to operate with a lower CP overhead, since the performance is limited by thermal noise. Conversely, in very high SNR regimes, it may be better to incur more CP overhead and possibly pilot overhead to exploit the channel capacity at that regime by reducing the ISI/ICI and by improving the channel estimates.

More specifically, Chapter 2 has presented an OFDM model thoroughly characterizing the ISI and ICI terms. Different data detectors were formulated, and performance comparisons were presented. A performance study specialized on UWB systems has also been shown to characterize the sensitivity of an OFDM-based UWB system to key system parameters.

Note that the model in Chapter 2 can be used for other OFDM studies, e.g., in conjunction with channel estimation as done in Chapter 3, time and frequency correction, and multi-antenna techniques.

Chapter 3 analyzed the impact of realistic channel estimation in OFDM systems, accounting for imperfections such as residual time and frequency error, and a channel

delay spread larger than the CP. The impact of the pilot signal density on the data demodulation performance was also studied.

From the performance study at different levels of residual frequency error, the effect of ICI on channel estimation has been shown to be small. However, ISI can severely impact the quality of the channel estimates, and hence can yield a large (>2dB) data demodulation performance degradation when compared to ideal channel estimation.

The pilot signal density and the associated channel estimation algorithm were shown to be critical for the ISI cases. Note that ISI may be incurred by a channel delay spread larger than the CP, or by timing errors at the terminal receiver (late sampling), irrespective of the channel delay spread.

The large degradation in performance due to ISI emphasizes the importance of selecting an adequate CP length in OFDM systems, as also studied in Chapter 4. Further, channel estimation algorithms providing robust performance in the presence of ISI are critical for robust performance of OFDM systems.

Therefore, the framework presented in this work enables studies of various system trade-offs when designing OFDM systems, ranging from optimal values of OFDM system parameters such as, T, N, CP, pilot overhead, to robustness against different receiver impairments, such as time and frequency synchronization errors. We leverage from this in the cognitive-OFDM studies presented in Chapter 4.

Indeed, Chapter 4 presents a cognitive OFDM system where the receiver performs an optimization process yielding parameter selections maximizing the communication link efficiency. We consider an optimization entailing the DFT window placement, i.e., capacity maximizing timing synchronization, the pilot density in time and frequency, the CP duration, and the OFDM symbol duration. The optimization process at the receiver is based on an estimated capacity function conditioned on the channel realization and residing at the cognitive-OFDM receiver.

We have shown that the optimization of the DFT window placement, pilot den-

sity and CP duration do not require any special waveform design at the transmitter. Instead, the receiver can hypothesize different assumptions based on the transmit waveform and autonomously identify the best parameter setting. However, the optimization of the OFDM symbol duration requires transmission of that duration for the receiver to derive the projected capacity.

APPENDIX A

Cross-covariance between channel estimates and DFT outputs

This Appendix characterizes the cross-covariance between the channel estimates and the DFT outputs. We denote this cross-covariance at the *l*th subcarrier by

$$\begin{aligned}\rho_{y\hat{g}}(n_1, n_2; l) &\triangleq E\left\{(y_{n_1,l} - E\{y_{n_1,l}\}) \cdot (\hat{g}_{n_2,l} - E\{\hat{g}_{n_2,l}\})^*|_{\psi_l}\right\}/2 \\ &= E\left\{w_{n_1,l} \cdot v^*_{n_2,l}|_{\psi_l}\right\}/2 \end{aligned} \tag{A.1}$$

Note that we condition the expectation in (A.1) on the channel realization. However, we will drop this conditioning from the notation in the rest of the Appendix to simplify notation. Further, we need to keep the notation generic so that it applies to both the TDM and the FDM pilot cases. The index n_2 in (3.36) and (A.1) points to the OFDM symbol used for channel estimation, while the index n_1 points to the OFDM symbol with the data subcarriers being detected. For the FDM pilot case, we assume that the channel estimates are constructed from the pilot signal in the same OFDM symbol as the data subcarriers being detected, i.e., $n_1 = n_2$. For the TDM pilot case, however, the pilot signal used for channel estimation is inevitably in a different OFDM symbol than the data subcarriers being detected with those channel estimates, i.e., $n_1 \neq n_2$. Note that data and/or pilot subcarriers may need to be stored in order to perform channel estimation based on the pilot signal, and subsequently, apply those estimates on the data subcarriers. Using the

definition of $v_{n,l}$ for the general linear channel estimator, we get

$$\begin{aligned}\rho_{y\hat{g}}(n_1, n_2; l) &= E\Big\{w_{n_1,l} \sum_{m\in P(n_2)} \Omega^*_{l,m} \cdot w^*_{n_2,m}/p^*_{n_2,m}\Big\}/2 \\ &= \sum_{m\in P(n_2)} \Omega^*_{l,m}/p^*_{n_2,m} \cdot E\{w_{n_1,l} \cdot w^*_{n_2,m}\}/2 \end{aligned} \tag{A.2}$$

Therefore, we need to characterize $E\{w_{n_1,l_1} \cdot w^*_{n_2,l_2}\}$, where $l_1 \in \{D(n_1)\}$ and $l_2 \in \{P(n_2)\}$. Using the definitions of $w_{n,l}$ in (3.14) and (3.15), we get

$$\begin{aligned}E\{w_{n_1,l_1} \cdot w^*_{n_2,l_2}\} = E\Bigg\{\Big(&\sum_{m_1\in\{D(n_1)\setminus l_1\}} A_{l_1,m_1} s_{n_1,m_1} + \sum_{m_1\in\{D(n_1-1)\}} B^{pre}_{l_1,m_1} s_{n_1-1,m_1} \\ &+ \sum_{m_1\in\{D(n_1+1)\}} B^{next}_{l_1,m_1} s_{n_1+1,m_1} + y^{noise}_{n_1,l_1}\Big) \cdot \Big(\sum_{m_2\in\{D(n_2)\}} A^*_{l_2,m_2} s^*_{n_2,m_2} \\ &+ \sum_{m_2\in\{D(n_2-1)\}} B^{pre*}_{l_2,m_2} s^*_{n_2-1,m_2} + \sum_{m_2\in\{D(n_2+1)\}} B^{next*}_{l_2,m_2} s^*_{n_2+1,m_2} + y^{noise*}_{n_2,l_2}\Big)\Bigg\}\end{aligned} \tag{A.3}$$

The noise term is independent of the modulation symbols and therefore can be treated separately.

As noted in Section 3.4 and shown in Equation (A.1), n_1 indexes the OFDM symbol for data demodulation and n_2 indexes the OFDM symbol for channel estimation. We assume that the channel estimates are constructed from the pilot signal in a single OFDM symbol, the n_2-th OFDM symbol.

For the FDM pilot case, we assume that the pilot subcarriers in the *n*th OFDM symbol are used to generate the channel estimates for the detection of the data subcarriers in the same OFDM symbol. Therefore, $n_2 = n_1$ is of relevance for this case.

For the TDM pilot case, in the absence of ISI and assuming white noise, there is no correlation of the noise across different OFDM symbols, and therefore the correlation of the channel estimation noise and the noise in the data subcarriers is zero. If we consider ISI, the relevant cases for possible correlation between the noise-and-interference in the channel estimates and the noise-and-interference in the data subcarriers will be those

where data symbols appearing in the OFDM symbol for channel estimation also appear in the OFDM symbol(s) for the data demodulation. Assuming that the ISI does not go beyond the adjacent OFDM symbols, the relevant cases are $n_2 = n_1 \pm 1$ and $n_2 = n_1 \pm 2$. For relative values outside of this range, there will be no correlation between the noise-and-interference in the channel estimate and the noise-and-interference in the data subcarriers.

Therefore, for all the mentioned cases we can compute the covariance in (A.3). We present here the computation for the cases where ($n_2 = n_1 = n$), and where ($n_1 = n$, $n_2 = (n-1)$). The derivations for the other cases listed above are analogous.

A.1 Case $n_2 = n_1 = n$

The expression in (A.3) for this case becomes

$$\begin{aligned} E\{w_{n,l_1} \cdot w^*_{n,l_2}\} &= \sum_{m_1 \in \{D(n) \backslash l_1\}} \sum_{m_2 \in \{D(n)\}} A_{l_1,m_1} A^*_{l_2,m_2} E\{s_{n,m_1} s^*_{n,m_2}\} \\ &+ \sum_{m_1 \in \{D(n-1)\}} \sum_{m_2 \in \{D(n-1)\}} B^{pre}_{l_1,m_1} B^{pre*}_{l_2,m_2} E\{s_{n-1,m_1} s^*_{n-1,m_2}\} \\ &+ \sum_{m_1 \in \{D(n+1)\}} \sum_{m_2 \in \{D(n+1)\}} B^{next}_{l_1,m_1} B^{next*}_{l_2,m_2} E\{s_{n+1,m_1} s^*_{n+1,m_2}\} + N_0 \cdot \delta_K(l_2 - l_1) \end{aligned} \tag{A.4}$$

where we have assumed independence of the data modulation symbols across OFDM symbols. Further, assuming independence of the data modulation symbols across data subcarriers and constant average power of the data subcarriers across OFDM symbols, i.e., $P_d \triangleq E\{|s_{n,m}|^2\}/2 = E\{|s_{n-1,m}|^2\}/2 = E\{|s_{n+1,m}|^2\}/2$, we can write $E\{w_{n_1,l_1} \cdot w^*_{n_2,l_2}\}/2$ as

$$\begin{aligned} E\{w_{n_1,l_1} \cdot w^*_{n_2,l_2}\}/2 = P_d \Big(& \sum_{m_1 \in \{D(n) \backslash l_1\}} \sum_{m_2 \in \{D(n)\}} A_{l_1,m_1} A^*_{l_2,m_2} \\ + & \sum_{m_1 \in \{D(n-1)\}} \sum_{m_2 \in \{D(n-1)\}} B^{pre}_{l_1,m_1} B^{pre*}_{l_2,m_2} + \sum_{m_1 \in \{D(n+1)\}} \sum_{m_2 \in \{D(n+1)\}} B^{next}_{l_1,m_1} B^{next*}_{l_2,m_2} \end{aligned}$$

$$+\frac{N_0}{P_d}\cdot\delta_K(l_2-l_1)\Big) \tag{A.5}$$

Note that we will keep these assumptions for the other cases. Further, note from (A.5) that the existence of ICI and ISI will make the noise-and-interference of the channel estimates correlated across different subcarriers. This correlation will also exist between the noise-and-interference of the channel estimate, $v_{n_2,l}$, and the noise-and-interference at the DFT output, $w_{n_1,l}$.

A.2 Case $n_1 = n$ and $n_2 = (n-1)$

The expression in (A.3) for this case becomes

$$\begin{aligned} E\{w_{n,l_1}\cdot w^*_{n-1,l_2}\} &= \sum_{m_1\in\{D(n)\backslash l_1\}}\sum_{m_2\in\{D(n)\}} A_{l_1,m_1}B^{next*}_{l_2,m_2}E\{s_{n,m_1}s^*_{n,m_2}\} \\ &+ \sum_{m_1\in\{D(n-1)\}}\sum_{m_2\in\{D(n-1)\}} B^{pre}_{l_1,m_1}A^*_{l_2,m_2}E\{s_{n-1,m_1}s^*_{n-1,m_2}\} \end{aligned} \tag{A.6}$$

However, $\{D(n-1)=\emptyset\}$ since $n_2=(n-1)$ is a pilot symbol by construction, and hence

$$E\{w_{n,l_1}\cdot w^*_{n-1,l_2}\}/2 = P_d\sum_{m\in\{D(n)\backslash l_1\}} A_{l_1,m}B^{next*}_{l_2,m} \tag{A.7}$$

Note that the existence of ISI from the next OFDM symbol will make the channel estimation noise-and-interference, $v_{n_2,l}$, correlated with the noise-and-interference at the DFT output, $w_{n_1,l}$. The expressions in (A.5) and (A.7) can be used to obtain $\rho_{y\hat{g}}(n_1,n_2;l)$. For the FDM case, i.e., $n_1=n_2=n$, (A.2) becomes

$$\rho^{FDMpilot}_{y\hat{g}}(n,n;l) = \sum_{m\in\{P(n)\}}\Omega^*_{l,m}/p^*_{n,l}\cdot E\{w_{n,l}\cdot w^*_{n,m}\}/2$$

$$= P_d \sum_{m\in\{P(n)\}} \Omega^*_{l,m}/p^*_{n,l} \cdot \Bigg[\sum_{\vartheta\in\{D(n)\setminus l\}} A_{l,\vartheta} A^*_{m,\vartheta} + \sum_{\vartheta\in\{D(n-1)\}} B^{pre}_{l,\vartheta} B^{pre*}_{m,\vartheta} \quad \text{(A.8)}$$

$$+ \sum_{\vartheta\in\{D(n+1)\}} B^{next}_{l,\vartheta} B^{next*}_{m,\vartheta} + \frac{N_0}{P_d} \cdot \delta_K(m-l) \Bigg]$$

Since m represents a pilot subcarrier and l represents a data subcarrier, the noise term above goes away and we can re-write the correlation as

$$\rho^{FDMpilot}_{y\hat{g}}(n,n;l) = P_d \sum_{m\in\{P(n)\}} \Omega^*_{l,m}/p^*_{n,l} \quad \text{(A.9)}$$

$$\cdot \Bigg[\sum_{\vartheta\in\{D(n)\setminus l\}} A_{l,\vartheta} A^*_{m,\vartheta} + \sum_{\vartheta\in\{D(n-1)\}} B^{pre}_{l,\vartheta} B^{pre*}_{m,\vartheta} + \sum_{\vartheta\in\{D(n+1)\}} B^{next}_{l,\vartheta} B^{next*}_{m,\vartheta} \Bigg]$$

APPENDIX **B**

Partial CP discarding

B.1 Effect of partial CP discarding

First consider the construction of the channel matrix $\widetilde{\mathbf{H}}$ for the case of $\tau = 0$, i.e., the first channel tap sets the OFDM symbol boundary. In this case, if there is no ISI, the channel matrix $\widetilde{\mathbf{H}}$ for an example of a channel delay spread of 3 samples takes the following form.

$$\widetilde{\mathbf{H}} = \begin{bmatrix} h_0 & 0 & 0 & 0 & \cdots & h_1 \\ h_1 & h_0 & 0 & 0 & \cdots & h_2 \\ h_2 & h_1 & h_0 & 0 & \cdots & 0 \\ 0 & h_2 & h_1 & h_0 & \cdots & 0 \\ \vdots & \vdots & \vdots & \vdots & \ddots & \vdots \\ 0 & 0 & 0 & 0 & \cdots & h_0 \end{bmatrix}$$

From observation of the above matrix we can express the $(k,l)^{\text{th}}$ element of $\widetilde{\mathbf{H}}$ as

$$\widetilde{\mathbf{H}}_{k,l} = \begin{cases} h_{k-l} \text{ for } k = l, l+1, \ldots, l+P-1 \\ 0 \text{ elsewhere} \end{cases} \tag{B.1}$$

where P denotes the channel delay spread in number of samples (P = 3 for this example). We split the operation $\mathbf{F}_N \widetilde{\mathbf{H}} \mathbf{F}_N^H$ into $\mathbf{\Theta} \triangleq \mathbf{F}_N \widetilde{\mathbf{H}}$ first and then on $\mathbf{\Theta}\mathbf{F}_N^H$. Without loss of generality, we will assume the matrix indices to range from 0 to $(N-1)$. The $(k,l)^{\text{th}}$

element of the DFT matrix, $\mathbf{F}_N$, is

$$F_{k,l} = \frac{1}{\sqrt{n}} e^{-j2\pi kl/N} \tag{B.2}$$

The $(k,l)^{\text{th}}$ element of the matrix $\mathbf{\Theta}$ is found to be

$$\mathbf{\Theta}_{k,l} = \sum_{\vartheta=0}^{N-1} F_{k,\vartheta} \cdot \widetilde{H}_{\vartheta,l} = \frac{1}{\sqrt{N}} \sum_{\vartheta=0}^{N-1} e^{-j2\pi k\vartheta/N} \cdot \widetilde{H}_{\vartheta,l} \tag{B.3}$$

which using (B.1) can be re-written as

$$\begin{aligned} \mathbf{\Theta}_{k,l} &= \frac{1}{\sqrt{N}} \sum_{\vartheta=l}^{l+P-1} h_{\vartheta-l} \cdot e^{-j2\pi k\vartheta/N} = \frac{1}{\sqrt{N}} \sum_{\zeta=0}^{P-1} h_{\zeta} \cdot e^{-j2\pi k(\zeta+l)/N} \\ &= \frac{1}{\sqrt{N}} \sum_{\zeta=0}^{P-1} h_{\zeta} \cdot e^{-j2\pi k\zeta/N} \cdot e^{-j2\pi kl/N} = \frac{1}{\sqrt{N}} \cdot g_k \cdot e^{-j2\pi kl/N}. \end{aligned} \tag{B.4}$$

where we have defined the frequency response of the channel at the k^{th} carrier as g_k.

The $(k,l)^{\text{th}}$ element in the matrix $\mathbf{D}_H$ is, therefore, found to be

$$\begin{aligned} D_{H_{k,l}} &= \sum_{\vartheta=0}^{N-1} \mathbf{\Theta}_{k,\vartheta} \cdot F^H_{\vartheta,l} = \frac{1}{N} \sum_{\vartheta=0}^{N-1} g_k \cdot e^{-j2\pi k\vartheta/N} \cdot e^{j2\pi l\vartheta/N} = g_k \cdot \frac{1}{N} \sum_{\vartheta=0}^{N-1} e^{-j2\pi(k-l)\vartheta/N} \\ &= g_k \cdot \delta_K(k-l) \end{aligned} \tag{B.5}$$

where $\delta_K(k)$ is the Kronecker delta defined to be 1 for $k = 0$ and 0 elsewhere. The result in (B.5) is the well known OFDM behavior for no ICI and no ISI, whereby the channel gain of the l^{th} subcarrier at the OFDM receiver is the channel's frequency response at the same subcarrier.

As seen from (4.12), the channel matrix $\widetilde{\mathbf{H}}$ is constructed as $\widetilde{\mathbf{H}} = \mathbf{R}_{\text{CP}} \cdot \mathbf{H} \cdot \mathbf{T}_{\text{CP}}$. Putting the channel matrix $\widetilde{\mathbf{H}}$ in the following form $\mathbf{H} = [\mathbf{H_2 H_1}]$, where $\mathbf{H_2}$ is a $(N_T \times CP)$ matrix corresponding to the first CP columns of $\mathbf{H}$ and the channel matrix $\mathbf{H_1}$ is a

$(N_T \times N)$ matrix corresponding to the last N columns of $\mathbf{H}$, then

$$\mathbf{H} \cdot \mathbf{T}_{\text{CP}} = [\mathbf{H_2 H_1}] \cdot \begin{bmatrix} \mathbf{0}_{CP_{\text{tx}} \times (N - CP_{\text{tx}})} & \mathbf{I}_{CP_{\text{tx}}} \\ & \mathbf{I}_N \end{bmatrix} = [\mathbf{0}_{(N_T \times (N-CP))} \mathbf{H_2}] + \mathbf{H_1}, \quad \text{(B.6)}$$

which indicates that $\mathbf{H} \cdot \mathbf{T}_{\text{CP}}$ is equal to the matrix $\mathbf{H_1}$ plus the matrix $\mathbf{H_2}$ added to the last CP columns of $\mathbf{H_1}$. Assuming for example,

$$\mathbf{H} = \begin{bmatrix} h_0 & 0 & 0 & 0 & 0 & 0 & 0 \\ h_1 & h_0 & 0 & 0 & 0 & 0 & 0 \\ h_2 & h_1 & h_0 & 0 & 0 & 0 & 0 \\ 0 & h_2 & h_1 & h_0 & 0 & 0 & 0 \\ 0 & 0 & h_2 & h_1 & h_0 & 0 & 0 \\ 0 & 0 & 0 & h_2 & h_1 & h_0 & 0 \\ 0 & 0 & 0 & 0 & h_2 & h_1 & h_0 \end{bmatrix}$$

and $CP_{\text{tx}} = 2$, then

$$\mathbf{H} \cdot \mathbf{T}_{CP} = \begin{bmatrix} 0 & 0 & 0 & h_0 & 0 \\ 0 & 0 & 0 & h_1 & h_0 \\ h_0 & 0 & 0 & h_2 & h_1 \\ h_1 & h_0 & 0 & 0 & h_2 \\ h_2 & h_1 & h_0 & 0 & 0 \\ 0 & h_2 & h_1 & h_0 & 0 \\ 0 & 0 & h_2 & h_1 & h_0 \end{bmatrix}$$

The matrix $\mathbf{R}_{\text{CP}}$ removes the first CP_{rx} and the last $\Delta CP \triangleq (CP_{\text{tx}} - CP_{\text{rx}})$ rows of $\mathbf{H} \cdot \mathbf{T}_{\text{CP}}$. Therefore, for the example above and assuming $CP_{\text{rx}} = 2$, i.e., total CP removal, yields

the effective channel matrix $\widetilde{\mathbf{H}}$ found to be

$$\widetilde{\mathbf{H}} = \begin{bmatrix} h_0 & 0 & 0 & h_2 & h_1 \\ h_1 & h_0 & 0 & 0 & h_2 \\ h_2 & h_1 & h_0 & 0 & 0 \\ 0 & h_2 & h_1 & h_0 & 0 \\ 0 & 0 & h_2 & h_1 & h_0 \end{bmatrix}$$

while for partial CP removal of $CP_{\text{rx}} = 1$ the effective channel matrix becomes $\widetilde{\mathbf{H}}'$ found to be

$$\widetilde{\mathbf{H}}' = \begin{bmatrix} 0 & 0 & 0 & h_1 & h_0 \\ h_0 & 0 & 0 & h_2 & h_1 \\ h_1 & h_0 & 0 & 0 & h_2 \\ h_2 & h_1 & h_0 & 0 & 0 \\ 0 & h_2 & h_1 & h_0 & 0 \end{bmatrix}$$

which is a circular shift downwards by ΔCP rows of the rows of the channel matrix with total CP removal $\widetilde{\mathbf{H}}$. Note that this is true as long as the result of total and partial CP removal incurs no ISI, i.e., the matrices $\widetilde{\mathbf{H}}$ and $\widetilde{\mathbf{H}}'$ are both circulant. If the partial CP removal incurs ISI the matrix $\widetilde{\mathbf{H}}'$ is no longer circulant.

For the ISI free case, we can express the $(k,l)^{\text{th}}$ element of the matrix $\widetilde{\mathbf{H}}'$ as

$$\widetilde{\mathbf{H}}'_{k,l} = \begin{cases} h_{k-l-\Delta CP} \text{ for } k = l + \Delta CP, l + \Delta CP + 1, \ldots, l + \Delta CP + P - 1 \\ 0 \text{ elsewhere} \end{cases} \tag{B.7}$$

As a result, the $(k,l)^{\text{th}}$ element of the matrix $\mathbf{\Theta}' \triangleq \mathbf{F}_N \widetilde{\mathbf{H}}'$ takes the following form

$$\begin{aligned} \mathbf{\Theta}'_{k,l} &= \sum_{\vartheta=0}^{N-1} F_{k,\vartheta} \widetilde{H}'_{\vartheta,l} = \frac{1}{\sqrt{N}} \sum_{\vartheta=0}^{N-1} e^{-j2\pi k\vartheta/N} \widetilde{H}'_{\vartheta,l} \\ &= \frac{1}{\sqrt{N}} \sum_{\vartheta=l+\Delta CP}^{l+\Delta CP+P-1} e^{-j2\pi k\vartheta/N} h_{\vartheta-l-\Delta CP} = \frac{1}{\sqrt{N}} \sum_{\zeta=0}^{P-1} h_\zeta e^{-j2\pi k(\zeta+l+\Delta CP)/N} \end{aligned}$$

$$= \frac{1}{\sqrt{N}} \sum_{\zeta=0}^{P-1} h_\zeta e^{-j2\pi k\zeta/N} e^{-j2\pi kl/N} e^{-j2\pi k\Delta CP/N}$$
$$= \frac{1}{\sqrt{N}} g_k e^{-j2\pi kl/N} e^{-j2\pi k\Delta CP/N} \quad \text{(B.8)}$$

and therefore, the $(k,l)^{\text{th}}$ element of the matrix $\mathbf{D}'_H \triangleq \mathbf{\Theta}'\mathbf{F}_N^H$ takes the following form

$$D'_{H_{k,l}} = \sum_{\vartheta=0}^{N-1} \mathbf{\Theta}'_{k,\vartheta} \cdot F^H_{\vartheta,l} = \frac{1}{N} \sum_{\vartheta=0}^{N-1} g_k \cdot e^{-j2\pi k\vartheta/N} \cdot e^{-j2\pi k\Delta CP/N} \cdot e^{j2\pi l\vartheta/N}$$
$$= g_k \cdot e^{-j2\pi k\Delta CP/N} \frac{1}{N} \sum_{\vartheta=0}^{N-1} e^{-j2\pi(k-l)\vartheta/N} = g_k \cdot e^{-j2\pi k\Delta CP/N} \cdot \delta_K(k-l) \quad \text{(B.9)}$$

where $\delta_K(k)$ is the Kronecker delta, and which shows that $\mathbf{D}'_H$ is also diagonal but also shows that the channel frequency response gets weighted by a 'phase ramp' of value $e^{-j2\pi k\Delta CP/N}$, where 'k' is the subcarrier index.

This phase ramping of the channel's frequency response will have an effect in the estimation of the channel. Note that the same phase ramping effect is encountered if the symbol boundary is such that the first tap of the channel does not correspond to the first entry in the first column of the matrix $\widetilde{\mathbf{H}}$ and therefore we will have a matrix with diagonal entries equal to $g_m \cdot e^{-j2\pi m\tau/N}$, where τ is the transmit-receive timing error with late sampling for positive values of τ and early sampling for negative values of τ. Note, on the other hand, that $\tau << N$ is expected, in general, while ΔCP could get close to the value of N.

B.2 Channel estimation with partial partial CP discarding

Consider the linear interpolator (channel estimation type II) with M_p = 2. For this case, the channel estimate at the m^{th} subcarrier is obtained as follows:

$$\hat{\psi}_{n,m} = \frac{1}{\sqrt{2}}(\psi_{n,m-1} + \psi_{n,m+1}) \quad \text{(B.10)}$$

Table B.1 *Effect of phase ramping into channel interpolator*

CP	ΔCP	α
0	64	-1.41
8	56	-1.31
16	48	-1
24	40	-0.54
32	32	0
40	24	0.54
48	16	1
56	8	1.31
64	0	1.41

Assuming no ISI and no ICI, and ignoring the noise effect, from (B.9), the channel gain at the $(m-1)^{\text{th}}$ and $(m+1)^{\text{th}}$ subcarriers is given by $\psi_{n,m-1} = g_{n,m-1} \cdot e^{-j2\pi(m-1)\Delta CP/N}$ and $\psi_{n,m+1} = g_{n,m+1} \cdot e^{-j2\pi(m+1)\Delta CP/N}$, respectively. Therefore,

$$\hat{\psi}_{n,m} = \frac{1}{\sqrt{2}}\big(g_{n,m-1} \cdot e^{-j2\pi(m-1)\Delta CP/N} + g_{n,m+1} \cdot e^{-j2\pi(m+1)\Delta CP/N}\big) \tag{B.11}$$

while we would like to have

$$\hat{\psi}'_{n,m} = \frac{1}{\sqrt{2}}(g_{n,m-1} + g_{n,m+1}) \cdot e^{-j2\pi m\Delta CP/N} \tag{B.12}$$

Assuming $g_{n,m-1} = g_{n,m+1}$ to see the effect of the phase ramping we see that

$$\begin{aligned} \hat{\psi}_{n,m} &= \frac{1}{\sqrt{2}} g_{n,m-1} \cdot e^{-j2\pi m\Delta CP/N} \cdot (e^{-j2\pi\Delta CP/N} + e^{j2\pi\Delta CP/N}) \\ &= \sqrt{2} g_{n,m-1} \cdot e^{-j2\pi m\Delta CP/N} \cdot cos(2\pi\Delta CP/N) \end{aligned} \tag{B.13}$$

which has the weighting by $\alpha \triangleq cos(2\pi\Delta CP/N)$. Table B.1 shows the effect of this weight for the evaluations conducted in the corresponding CP optimization subsection.

As we can see, the channel gain can be weighted by negative values (swapping

the sign of the channel estimate) or even can be zero-ed.

For DFT-based channel estimators, we start with the IDFT operation over the pilot subcarriers to get $\hat{h}_k$. Assuming no ISI, no ICI and considering the noise-free case, we have

$$\hat{h}_k = \frac{1}{N_p} \sum_{m=0}^{N_p-1} \psi_{M_p m} \cdot e^{j2\pi M_p mk/N} \tag{B.14}$$

where we have dropped the time indices to shorten notation, where $\psi_m = g_m \cdot e^{-j2\pi m\Delta CP/N}$ and where $g_m = \sum_{\vartheta=0}^{P-1} h_\vartheta \cdot e^{-j2\pi m\vartheta/N}$. Therefore,

$$\begin{aligned} \hat{h}_k &= \frac{1}{N_p} \sum_{m=0}^{N_p-1} \sum_{\vartheta=0}^{P-1} h_\vartheta \cdot e^{-j2\pi M_p m\vartheta/N} \cdot e^{-j2\pi m M_p \Delta CP/N} \cdot e^{j2\pi M_p mk/N} \\ &= \frac{1}{N_p} \sum_{\vartheta=0}^{P-1} h_\vartheta \sum_{m=0}^{N_p-1} e^{-j2\pi M_p m(\vartheta+\Delta CP-k)/N}, k = 0 \ldots N_p - 1 \end{aligned} \tag{B.15}$$

Note that if $\Delta CP = 0$, $N/M_p = N_p$ and $N_p \geq P$, then $\hat{h}_k = h_k$, since the summation over m becomes

$$\frac{1}{N_p} \sum_{m=0}^{N_p-1} e^{-j2\pi m(\vartheta-k)/N_p} = \delta_K(\vartheta - k) \tag{B.16}$$

Further, note that if M_p does not divide N, there will be an interference effect as the function $\frac{1}{N_p} \sum_{m=0}^{N_p-1} e^{-j2\pi M_p m(\vartheta+\Delta CP)/N}$ is no longer a 'delta' function. The condition $N_p \geq P$ is required to avoid aliasing of channel taps in the transformation from frequency to time domain.

The DFT-based channel estimator may truncate $\hat{h}_k$ to N_h samples, then pad with $(N - N_h)$ zeros and perform a DFT of size N. We will consider $N_h = N_p$ in this example. Therefore,

$$\hat{\psi}_m = \sum_{k=0}^{N_p-1} \hat{h}_k \cdot e^{-j2\pi mk/N} = \frac{1}{N_p} \sum_{k=0}^{N_p-1} \sum_{\vartheta=0}^{P-1} h_\vartheta \sum_{l=0}^{N_p-1} e^{-j2\pi M_p l(\vartheta+\Delta CP-k)/N} \cdot e^{-j2\pi mk/N}$$

$$= \sum_{l=0}^{N_p-1} e^{-j2\pi M_p l\Delta CP/N} \frac{1}{N_p} \sum_{k=0}^{N_p-1} e^{-j2\pi(m-M_p l)k/N} \sum_{\vartheta=0}^{P-1} h_\vartheta e^{-j2\pi M_p l\vartheta/N}$$

$$= \sum_{l=0}^{N_p-1} g_{Mpl} e^{-j2\pi M_p l \Delta CP/N} \frac{1}{N_p} \sum_{k=0}^{N_p-1} e^{-j2\pi(m-M_p l)k/N}$$
$$= \sum_{l=0}^{N_p-1} g_{Mpl} e^{-j2\pi M_p l \Delta CP/N} \frac{1}{N_p} \frac{sin(\pi(m-M_p l)N_p/N)}{sin(\pi(m-M_p l)/N)} \cdot e^{-j\pi(m-M_p l)(N_p-1)/N} \quad \text{(B.17)}$$

which is a discrete 'sinc' interpolation in the frequency domain of the channel gains at the pilot subcarriers. Note that we would like to have the $e^{-j2\pi m \Delta CP/N}$ weighting outside of the 'sinc' interpolation of the channel gains at the pilot subcarriers g_{Mpl}.

REFERENCES

[1] J.G. Proakis, *Digital Communications*, Third Edition, McGraw Hill, 1995.

[2] J.-J. van de Beek, O. Edfors, M. Sandell, S. K. Wilson, and P. O. Börjesson, "On channel estimation in OFDM systems," in *Proc. IEEE Veh. Technol. Conf. (VTC)*, vol. 2, pp. 815-819, July 1995.

[3] M. Russel and G. L. Stüber, "Interchannel interference analysis of OFDM in a mobile environment," in *Proc. IEEE Veh. Technol. Conf. (VTC)*, vol. 2, pp. 820-824, July 1995.

[4] E. Viterbo and K. Fazel, "How to combat long echoes in OFDM transmission schemes: Sub-channel equalization and more powerful channel coding," in *Proc. IEEE GLOBECOM 1995*, Singapore, vol. 3, pp. 2069-2074, November 1995.

[5] M. Sandell, S. K. Wilson and P. O. Börjesson, "Performance analysis of coded OFDM on fading channel with non-ideal interleaving and channel knowledge," in *Proc. IEEE Veh. Technol. Conf. (VTC)*, vol. 3, pp. 1380-1384, May 1997.

[6] J. L. Seoane, S. K. Wilson and S. Gelfand, "Analysis of Intertone and Interblock Interference in OFDM when the length of the Cyclic Prefix is shorter than the length of the Impulse Response of the channel," in *Proc. IEEE GLOBECOM 1997*, Pheonix AZ, vol. 1, pp. 32-36, November 1997.

[7] M-H. Hsieh and C-H. Wei, "Channel estimation for OFDM systems based on comb-type pilot arrangement in frequency selective fading channels," *IEEE Trans. Consumer Electron.*, vol. 44, no. 1, pp. 217-225, February 1998.

[8] Y. Li, L. J. Cimini and N. R. Sollenberg, "Robust channel estimation for OFDM systems with rapid dispersive fading channels," *IEEE Trans. Commun.*, vol. 46, no. 7, pp. 902-915, July 1998.

[9] O. Edfors, M. Sandell, J. J. van de Beek, S. K. Wilson, and P. O. Börjesson, "OFDM channel estimation by singular value decomposition," *IEEE Trans. Commun.*, vol. 46, no. 7, pp. 931-939, July 1998.

[10] R. Negi and J. Cioffi, "Pilot tone selection for channel estimation in a mobile OFDM system," *IEEE Trans. Consumer Electron.*, vol. 44, no. 3, pp. 1122-1128, August 1998.

[11] D. Kim and G. L. Stüber, "Residual ISI Cancellation for OFDM with Applications to HDTV Broadcasting," *IEEE J. Sel. Areas Commun.*, vol. 16, no. 8, pp. 1590-1599, October 1998.

[12] Y. H. Kim, I. Song, H. G. Kim, T. Chang, and H. M. Kim, "Performance analysis of coded OFDM systems in time-varying multipath Rayleigh fading channels," *IEEE Trans. Veh. Technol.*, vol. 48, no. 5, pp. 1610-1615, September 1999.

[13] H. Steendam and M. Moeneclaey, "Analysis and Optimization of the Performance of OFDM on Frequency-Selective Time-Selective Fading Channels," *IEEE Trans. Commun.*, vol. 47, no. 12, pp. 1811-1819, December 1999.

[14] O. Edfors, M. Sandell, J.-J. van de Beek, S.K. Wilson, and P.O. Börjesson, *Analysis of DFT-based Channel Estimators for OFDM*, Personal Wireless Communication, Kluwer Academic Publishers, vol.12, no. 1, January 2000.

[15] L. Wan and V. K. Dubey, "Performance of Frequency and Time Domain Coded OFDM over Fast Fading LEO Channels," in *Proc. IEEE EUROCOMM '2000*, pp. 179-183, May 2000.

[16] Y. Li, "Pilot-symbol-aided channel estimation for OFDM in wireless systems," *IEEE Trans. Veh. Technol.*, vol. 49, no. 4, pp. 1207-1215, July 2000.

[17] Y. Li and L. J. Cimini, "Bounds on the intercarrier interference of OFDM in time-varying impairments," *IEEE Trans. Commun.*, vol. 49, no. 3, pp. 401-404, March 2001.

[18] B. Yang, K. B. Letaief, R. S. Cheng, and Z. Cao, "Channel estimation for OFDM transmission in multipath fading channels based on parametric channel modeling," *IEEE Trans. Commun.*, vol. 49, no. 3, pp. 467-478, March 2001.

[19] K. Sathananthan and C. Tellambura, "Probability of error calculation of OFDM systems with frequency offset," *IEEE Trans. Commun.*, vol. 49, no. 11, pp. 1884-1888, November 2001.

[20] S. Celebi, "Interblock Interference (IBI) and Time of Reference (TOR) Computation in OFDM Systems," *IEEE Trans. Commun.*, vol. 49, no. 11, pp. 1895-1900, November 2001.

[21] M. Morelli and U. Mengali, "A comparison of pilot-aided channel estimation methods for OFDM systems," *IEEE Trans. Signal Process.*, vol. 49, no. 12, pp. 3065-3073, December 2001.

[22] Y. Li, "Simplified channel estimation for OFDM systems with multiple transmit antennas," *IEEE Trans. Wireless Commun.*, vol. 1, no. 1, pp. 67-75, January 2002.

[23] W. Henkel, G. Taubock, P. Odling, P. Borjesson, N. Petersson, and A. Johansson, "The Cyclic Prefix of OFDM/DMT - An Analysis," in *Proc. 2002 International Zurich Seminar on Broadband Communications*, ETH Zurich, Switzerland, pp. 22.1-22.3, February 2002.

[24] H. S. Cheon and D. S. Hong, "Effect of channel estimation error in OFDM-based WLAN," *IEEE Commun. Lett.*, vol. 6, no. 5, pp. 190-192, May 2002.

[25] V. D. Nguyen and H. Kuchenbecker, "Intercarrier and Intersymbol Interference Analysis of OFDM Systems on Time-Invariant Channels," in *Proc. IEEE International Symposium on Personal, Indoor and Mobile Radio Communications (PIMRC)*, vol. 4, pp. 1482-1487, September 2002.

[26] S. Coleri, M. Ergen, A. Puri, and A. Bahai, "A study of channel estimation in OFDM systems," in *Proc. IEEE Veh. Technol. Conf. (VTC)*, vol. 2, pp. 894-898, September 2002.

[27] S. Coleri, M. Ergen, A. Puri, and A. Bahai, "Channel estimation techniques based on pilot arrangement in OFDM systems," *IEEE Trans. Broadcasting*, vol. 48, no. 3, pp. 223-229, September 2002.

[28] M-X. Chang and Y. T. Su, "Performance analysis of equalized OFDM systems in Rayleigh fading," *IEEE Trans. Wireless Commun.*, vol. 1, no. 4, pp. 721-732, October 2002.

[29] J. Foerster, Ed., "Channel modeling sub-committee report final," IEEE, Document IEEE P802.15-02/490r1-SG3a, February 2003.

[30] G. D. Pantos, A. G. Kanatas and P. Constantinou, "Performance Evaluation of OFDM Transmission Over a Challenging Urban Propagation Environment," *IEEE Trans. Broadcast.*, vol. 49, no. 1, pp. 78-96, March 2003.

[31] W. Lee, "On Channel Estimation for OFDM Systems in Multipath Environments with Relatively Large Delay Spread," in *Proc. IEEE Veh. Technol. Conf. (VTC)*, vol. 2, pp. 1303-1307, April 2003.

[32] X. Cai and G. B. Giannakis, "Error probability minimizing pilots for OFDM with M-PSK modulation over Rayleigh-fading channels," *IEEE Trans. Veh. Technol.*, vol. 53, no. 1, pp. 146-154, January 2004.

[33] V. D. Nguyen, K. Kyamakya and G. Gelle, "SER of Uncoded OFDM Systems with Insufficient Guard Interval Length and on Time-Varying Channels," in *Proc. IEEE Veh. Technol. Conf. (VTC)*, vol. 4, pp. 1897-1901, May 2004.

[34] A. Batra, J. Balakrishnan, G. R. Aiello, J. R. Foerster, and A. Dabak, "Design of a Multiband OFDM System for Realistic UWB Channel Environments," *IEEE Trans. Microw. Theory Tech.*, vol. 52, no. 9, pp. 2123-2138, September 2004.

[35] M. Batariere, K. Baum and T. P. Krauss, "Cyclic Prefix Length Analysis for 4G OFDM Systems," in *Proc. IEEE Veh. Technol. Conf. (VTC)*, vol. 1, pp. 543-547, September 2004.

[36] T. (Ronald) Wang, J. G. Proakis and J. R. Zeidler, "Techniques for Suppression of Intercarrier Interference in OFDM Systems," *IEEE Wireless Communications and Networking Conference*, vol. 1, pp. 39-44, March 2005.

[37] S. Takaoka, H. Gacanin and F. Adachi, "Impact of Imperfect Channel Estimation on OFDM/TDM Performance," in *Proc. IEEE Veh. Technol. Conf. (VTC)*, vol. 1, pp. 442-446, May 2005.

[38] W. Chan, W. Wu, C. Wang, M. Chiu, and C. Chao, "Application of Space-Time Codes to OFDM UWB Systems with Under-Sampled Receivers," in *Proc. IEEE Veh. Technol. Conf. (VTC)*, vol. 2, pp. 1191-1195, May-June 2005.

[39] X. Fan, B. Leng and G. Bi, "An Improved Channel Estimation Algorithm for OFDM UWB," in *Proc. IEEE International Conference on Wireless Communications, Networking and Mobile Computing*, vol. 1, pp. 173-176, September 2005.

[40] J. Wang, G. Zhu and J. Jin, "Optimal Power Allocation for Space-time Coded OFDM UWB Systems," in *Proc. IEEE International Conference on Wireless Communications, Networking and Mobile Computing*, vol. 1, pp. 189-192, September 2005.

[41] W. P. Siriwongpairat, W. Su, M. Olfat, and K. J. R. Liu, "Multiband-OFDM MIMO Coding Framework for UWB Communication Systems," *IEEE Trans. Signal Process.*, vol. 54, no. 1, pp. 214-224, January 2006.

[42] W. P. Siriwongpairat, W. Su and K. J. R. Liu, "Characterizing Performance of Multiband UWB Systems using Poisson cluster arriving fading paths," *IEEE Journal of Selected Areas in Communications*, Special Issue on Ultra-Wideband Communications, vol. 24, no. 4, pp. 745-751, April 2006.

[43] T. (Ronald) Wang, J. G. Proakis, E. Masry, and J. R. Zeidler, "Performance degradation of OFDM systems due to Doppler spreading," *IEEE Trans. Wireless Commun.*, vol. 5, no. 6, pp. 1422-1432, June 2006.

[44] J. Park, J. Kim, M. Park, K. Ko, C. Kang, and D. Hong, "Performance analysis of channel estimation for OFDM systems with residual timing offset," *IEEE Trans. Wilreless Commun.*, vol. 5, no. 7, pp. 1622-1625, July 2006.

[45] T. Cui and C. Tellambura, "Analysis and optimization of pilot symbol-assisted rake receivers for DS-CDMA systems," *IEEE Trans. Vehic. Technol.*, vol. 55, no. 4, pp. 1159-1170, July 2006.

[46] Y. G. Li, A. F. Molisch and J. Zhang, "Practical Approaches to Channel Estimation and Interference Suppression for OFDM-based UWB Communications," *IEEE Trans. Wireless Commun.*, vol. 5, pp. 2317-2320, September 2006.

[47] W. Lee and C. S. Curry, "A performance analysis of OFDM systems in excessively dispersive multipath channels," *KICS/IEEE Journal of Communications and Networks*, vol. 8, no. 3, pp. 323-329, September 2006.

[48] G. E. Bottomley and C. Cozzo, "Rake reception with channel estimation error," *IEEE Trans. Vehic. Technol.*, vol. 55, no. 6, pp. 1923-1926, November 2006.

[49] H.Q. Lai, W.P. Siriwongpairat and K. J. R. Liu, "Performance analysis of multiband OFDM UWB system with imperfect synchronization and intersymbol interference," *IEEE Journal of Selected Topic on Signal Processing*, Special Issue on Performance Limits of Ultra-Wideband Systems, vol. 1, no. 3, pp. 521-534, October 2007.

[50] A. S. Ling and L. B. Milstein, "Trade-Off Between Diversity and Channel Estimation Errors in Asynchronous MC-DS-CDMA and MC-CDMA," *IEEE Trans. Commun.*, vol. 56, no. 4, pp. 584-597, April 2008.

[51] J. I. Montojo and L. B. Milstein, "Effects of Imperfections on the Performance of OFDM Systems," Accepted for publication in *IEEE Trans. Commun*.

[52] J. I. Montojo and L. B. Milstein, "Channel Estimation for Non-Ideal OFDM Systems," Accepted for publication in *IEEE Trans. Commun*.